



DISSERTATION

## **A Comprehensive Analytical and Process-Technological Toolbox for Improved Penicillin Production**

ausgeführt zum Zwecke der Erlangung des akademischen Grades einer Doktorin der  
technischen Wissenschaften unter der Leitung von

Prof. Dr. Christoph Herwig

Institut 166/4

Institut für Verfahrenstechnik, Umwelttechnik und Technischen Biowissenschaften

eingereicht an der Technischen Universität Wien

Fakultät für Technische Chemie

von

Daniela Ehgartner

0611497

Pazmanitengasse 15/27, 1020 Wien

---

Wien, am

---

Eigenhändige Unterschrift



## **Acknowledgements**

My gratitude goes to everybody who supported me in the last three years.

Especially I thank Prof. Christoph Herwig for the possibility to do this interesting project and for his guidance during my PhD. I really liked the atmosphere in his working group and the possibility to acquire skills going beyond scientific work.

Further I thank Jens Fricke for the excellent collaboration. There was always the possibility to be supported in no matter what situation – was it for questions concerning experimental planning, interpretation of results or just substantial discussions. It was a pleasure, working with you!

Also, a big thank you to my colleagues. Especially I want to thank the CD laboratory team Paul Kroll, Matthias Brunner, Wieland Reichelt and Tobias Klein as well as members of the “fungi group” Alexandra Hofer, Aydin Golabgir, Lukas Veiter and Julian Kager. Further, it was a great pleasure to share the office with David Wurm, Paul Kroll and Thomas Gundinger. My gratitude also goes to Vanessa Karabetian for support in organizational belongings and Barbara Mahlberg supporting analytics.

Really important were also all the students accompanying my project. Special thanks to the master students Bernhard Seyer, Andreas Schröder, Manuela Frank, Sarah Heinzl and Thomas Hartmann.

In addition, I want to thank the Austrian Federal Ministry of Science, Research and Economy in course of the Christian Doppler Laboratory for funding and Sandoz GmbH for their collaboration and scientific discussions.

Finally, a big thankyou to my parents Hildegard and Michael, my brothers Markus and Johannes, my sister Julia and all my friends. Without your support, all this would never have been possible.

## Abstract

Biosynthesis of one of the most important antibiotics – penicillin - depends on various process parameters and morphological parameters. In several studies, a link between the specific growth rate ( $\mu$ ) and the specific penicillin production rate ( $q_p$ ) is described. Depending on the process, the link between  $\mu$  and  $q_p$  differs. Furthermore, penicillin producing bioprocesses exhibit highly dynamic  $q_p$ 's. Thus, a simple link between  $\mu$  and  $q_p$  cannot be described. Therefore, an extended set of process parameters needs to be considered in order to gain predictive and robust bioprocess performance.

This thesis aims providing an analytical and process-technological toolbox, enabling detailed investigation of  $\mu$ - $q_p$ -relations. Moreover, the control of process parameters to achieve optimal penicillin productivity in industrial fed-batch processes is in focus. Thereby, the complexity of filamentous bioprocesses ought to be considered: Fungal morphology varies in relation to process parameters like spore inoculum concentration and power input. Via broth viscosity and mass transfer the morphology affects process performance. Furthermore, biomass segregation occurs. Especially fungal pellets (dense hyphal aggregates) are concerned. Thus, viable biomass measurements in non-disperse growing cultures are important.

An analytical and process-technological toolbox for the investigation of morphology and biomass segregation, applicable in all process phases, was developed consisting of:

- At first, this toolbox allows the at-line determination of spore sub-populations and the measurement of the viable spore concentration via spore germination monitoring. Thereby, reproducible starting conditions of fed-batch cultures, which are based on comparable batch processes, should be achievable.
- Secondly, one of the methodologies provided in the toolbox enables the online control of the specific growth rate based on viable biomass measurements. This tool is able to cope with physiological and morphological changes of filamentous fungi. Furthermore, the control strategy adapts to changing biomass yields, which is an important issue in the here presented bioprocess for penicillin production.
- The last tool at-line analyses fungal morphology to evaluate morphological parameters as a central variable in filamentous processes.

Using this toolbox, the  $\mu$ - $q_p$ -relation for a penicillin V producing and pellet growing *Penicillium chrysogenum* process with highly dynamic  $q_p$ -trajectories was described. Thereby, the consumed glucose

was found to be an important factor concerning the influence of  $\mu$  on  $q_p$ . This contribution highlights the importance and applicability of the presented analytical and process-technological toolbox for scientific investigations as well as for the conduction of robust and reproducible processes. A methodology for the analysis of  $\mu$ - $q_p$ -interactions and other interfering mechanisms was hence created.

Combining knowledge about  $\mu$ - $q_p$ -relations with the presented tools provides the basis for the experimental design and the process control for the improvement of penicillin producing bioprocesses towards optimal  $q_p$ -trajectories. Apart from process robustness via reproducible starting conditions and the control of the specific growth rate based on viable biomass measurements, at-line monitoring of fungal morphology provides an additional tool for process control.

## Zusammenfassung

Die Biosynthese von Penicillin, noch immer eines der wichtigsten Antibiotika, ist ein komplexer Prozess der von verschiedensten Mechanismen beeinflusst wird. Mehrere Studien zeigten den Einfluss der spezifischen Wachstumsrate ( $\mu$ ) auf die spezifische Produktionsrate ( $q_p$ ). Diese Studien beschreiben unterschiedliche  $\mu$ - $q_p$ -Zusammenhänge. Außerdem ist  $q_p$  im hier verwendeten Penicillin-Produktionsprozess trotz konstantem  $\mu$  dynamisch und verändert sich im Laufe des Prozesses. Daher scheint die Herstellung eines simplen Links ohne die Einbeziehung zusätzlicher Variablen nicht möglich. Zusätzliche Prozessparameter müssen miteinbezogen werden, um eine vorhersagbare, robuste Prozessperformanz zu erhalten.

Das Ziel dieser Dissertation war es, eine analytische und prozesstechnologische Toolbox zu entwickeln, welche es ermöglicht, den Zusammenhang von  $\mu$  und  $q_p$  auch für dynamische  $q_p$ -Trajektorien zu zeigen und weitere Einflussgrößen zu evaluieren. Dabei muss die Komplexität filamentöser Bioprozesse berücksichtigt werden: Die Morphologie der Pilze steht in engem Zusammenhang zu Prozessparametern wie Sporenkonzentration und Rührgeschwindigkeit. Über Viskosität und Massentransfer beeinflusst die Morphologie die Prozessleistung. Biomassensegregation tritt im Laufe der Kultivierung auf, wobei vor allem Pellets (dichte Hyphenaggregate) betroffen sind. Daher ist die Bestimmung der Lebendbiomasse speziell in nicht-dispers wachsende Kulturen wichtig.

Eine analytische und prozesstechnologische Toolbox wurde entwickelt, welche die Messung von Biomassensegregation und Morphologie zu allen Prozesszeitpunkten ermöglicht. Diese besteht aus folgenden Methoden:

- Die Toolbox ermöglicht die Unterscheidung von unterschiedlichen Subpopulationen der Sporen sowie die Konzentrationsmessung lebender Sporen durch die Erfassung der Sporenkeimung. Dadurch werden reproduzierbare Startbedingungen für Fed-Batch-Kulturen geschaffen, die auf vergleichbaren Batchprozessen basieren.
- Weitere Methoden der Toolbox ermöglichen die Onlinekontrolle der spezifischen Wachstumsrate basierend auf der Messung lebender Biomasse. Dieses Tool ist unabhängig von physiologischen und morphologischen Veränderungen der Pilze und adaptiert die Kontrolle automatisch wenn Biomasse yields sich verändern.
- Der letzte durch die Toolbox abgedeckte Bereich, ist die Analyse der Pilzmorphologie, welche eine zentrale Variable im Bioprozess mit filamentösen Pilzen darstellt.

Die Verwendung der Toolbox ermöglichte die Beschreibung von  $\mu$ - $q_p$ -Zusammenhängen in einem Penicillin-Produktionsprozess mit dynamischen  $q_p$ -Trajektorien. Die von den Pilzen konsumierte Glucose wurde als wichtiger Faktor in der  $q_p$ -Dynamik identifiziert. Diese Studie unterstreicht die Wichtigkeit und Anwendung der hier präsentierten analytischen und prozesstechnologischen Toolbox für wissenschaftliche Untersuchungen aber auch für robuste, reproduzierbare Bioprozesse für den Einsatz im industriellen Umfeld.

Die Kombination aus der inhaltlichen Studie zu  $\mu$ - $q_p$ -Zusammenhängen und den Methoden der Toolbox legen die Basis für experimentelles Design und Prozesskontrolle, um Penicillin-Produktionsprozesse zu optimieren. Neben Prozessrobustheit durch reproduzierbare Startbedingungen und der Kontrolle der spezifischen Wachstumsrate, stellt die morphologische Analyse ein zusätzliches Tool zur Prozesskontrolle dar.

## Table of content

Acknowledgements .....	i
Abstract.....	ii
Zusammenfassung .....	iv
Table of content .....	vi
1 Introduction .....	1
1.1 Background .....	1
1.1.1 Penicillin: Historical introduction.....	1
1.1.2 Penicillin synthesis .....	1
1.1.3 Fungal morphology .....	2
1.1.4 Influence of $\mu$ on penicillin production .....	7
1.2 Motivation and goal .....	7
1.3 Summary and scientific contribution to the manuscripts .....	9
1.3.1 Spore-tools (Tool I & tool II) .....	10
1.3.2 Measuring morphology using a large particle flow cytometer (Tool III & tool IV) .....	11
1.3.3 Online control of fungal growth (Tool V) .....	12
1.3.4 Connecting specific growth rate and penicillin productivity.....	13
1.4 References .....	14
2 Manuscripts .....	18
At-line determination of spore inoculum quality in <i>Penicillium chrysogenum</i> bioprocesses .....	19
At-line determining spore germination of <i>Penicillium chrysogenum</i> bioprocesses in complex media ..	34
Imaging Flow Cytometry and High-Throughput Microscopy .....	45
Morphological analysis of filamentous fungi using flow cytometry – the fast alternative to microscopy and image analysis .....	56
Controlling the specific growth rate via biomass trend regulation in filamentous fungi bioprocesses .	86

Table of content

---

Production rate dynamics at constant growth conditions in a penicillin production process.....	115
3 Conclusions & future perspectives .....	139

# 1 Introduction

## 1.1 Background

### 1.1.1 Penicillin: Historical introduction

Penicillin and its antibacterial effect was accidentally discovered by Alexander Fleming back in 1928. While working with *Staphylococcus*, agar plates contaminated with mold. Bacteria growing near these mold colonies started to lyse. Fleming identified the mold as *Penicillium rubrum* [1]. Later-on the fungus was re-identified to be *P. notatum*, subsequently known as *P. chrysogenum* [2]. Although some primary investigations on penicillin were conducted in the early 1930s, the real break-through of penicillin started 1940 with a study by Chain and Florey curing mice from bacterial diseases [3]. Henceforth, penicillin was produced in large amounts. Initially the crude extract was applied. However, under the concern of human safety the production of purified penicillin was started as soon as in 1945 [4].

Actual industrial strains derive from *P. chrysogenum* NRRL 1951 which was isolated 1943. This initial strain yielded up to 150 µg/ml penicillin in submerged cultures. After several rounds of mutagenesis and strain improvement programs, today's industrial strains yield more than 50 mg/ml [5].

Already in the 1940s first resistances of bacteria against penicillin were observed [6]. Nowadays, resistances of pathogen bacteria occur to most natural penicillins but also semi-synthetic penicillins. This issue concerns most antibiotics on the market [7]. Still, penicillin is one of the most important antibiotics and its productivity raised significantly within the last decades to reach a market volume of 5 billion dollar in 2003 [8].

### 1.1.2 Penicillin synthesis

Penicillins are  $\beta$ -lactam antibiotics with a penam as basic structure [9]. In the penicillin group, natural penicillins (like penicillin G), biosynthetic penicillin V and semisynthetic penicillin (amoxicillin, ampicillin, cloxacillin and peracillin) are distinguished [8]. Penicillin G (benzylpenicillin) and penicillin V (phenoxy-methylpenicillin) differ in their sidechain, attached to 6-aminopenicillanic acid (6-APA) at the end of the synthesis pathway. Therefore precursors from the medium are needed – phenylacetic acid respective phenoxyacetic acid [10]. For the production of semisynthetic penicillins, the sidechain is removed via penicillin acylase [8].

The biosynthesis of penicillin in *P. chrysogenum* is strongly interlinked with metabolic pathways and is conducted in different compartments of fungal cells [11]. The basis for penicillin formation are the three

amino acids L- $\alpha$ -amino adipic acid (L- $\alpha$ -AAA), L-cysteine and L-valine. The first mentioned originates from the amino adipate pathway, being an intermediate in lysine formation. These three amino acids are condensed to the tripeptide  $\delta$ -(L- $\alpha$ -amino adipyl)-L-cysteiny-D-valine (ACV), performed by the enzyme  $\delta$ -(L- $\alpha$ -amino adipyl)-L-cysteiny-D-valine synthetase. The linear ACV is in the next step transformed via oxidative ring closure into isopenicillin N, catalyzed by the enzyme isopenicillin N synthase. Isopenicillin N is the first bioactive intermediate in the process of penicillin biosynthesis. Besides, it forms the basis for another class of antibiotics, the cephalosporins. The last step of biosynthesis is the exchange of the L- $\alpha$ -AAA sidechain for another sidechain depending on the supplied precursor. This reaction is catalyzed by the acyl coenzyme A:isopenicillin N acyltransferase. This step involves 6-APA as intermediate [9].

Penicillin production is a highly complex mechanism depending on the process environment. Excess of glucose showed to repress penicillin production. Thus, the production phase is conducted under C-limited conditions. The C-source influences penicillin production via transcriptional and post-transcriptional regulation of biosynthesis genes. Further it was shown, that the flux from L- $\alpha$ -AAA to ACV was impacted. In addition to the availability of C-source, also the C-source itself is crucial. Higher product titers were achieved when applying lactose. Apart from C-source, other process conditions as for example the pH crucially influence penicillin production, whereby a higher pH is favored [9]. Comparing a Wisconsin 54-1255 strain to a high producing strain yielded insight into the diversity of regulation levels of penicillin biosynthesis. It starts with growth and metabolism concerning nutrients and precursors, the synthesis of penicillin from the precursors, number of peroxisomes (important cell location for penicillin biosynthesis), leads over penicillin secretion to cell differentiation and morphology [12].

### 1.1.3 Fungal morphology

#### 1.1.3.1 *From spores to pellets*

Filamentous bioprocesses like the penicillin production process using *Penicillium chrysogenum* start by inoculating spores into the bioreactor [13, 14]. These fungal spores are initially in a dormant state, hence showing low metabolic activity. In process environment with access to nutrients, the spores quit the dormant state by water uptake and hence swelling as well as starting to be metabolically active [15, 16]. In this step, spore size increases significantly [14, 16].

Further, a germ tube is built to start growth of hyphae (namely spore germination) [17]. A spore was defined to be germinated when the hyphae is at least as long as the diameter of the actual spore [18]. These hyphae elongate and eventually branch. Germination was reported to be influenced by a variety of parameters as the spore age [19], the medium composition [17, 19, 20], the spore concentration [17,

20], the temperature [17], the pH [17] and the storage conditions of the spore inoculum [16]. In addition, not all spores which swell, necessarily are able to germinate [21].

Hyphae can grow/build entanglements and aggregates leading to various morphological forms. The largest elements are the so-called pellets with a dense hyphal core. Latter is a central dark region in the center of the aggregate, which is typical for pellets. The core is surrounded by a brighter outer mycelial region, the “hairy” annular region. Pellets have the size of several hundred micrometer to more than one millimeter [21, 22].

Most common morphological classifications distinguish between freely dispersed mycelia and aggregates. Freely dispersed mycelia include hyphae, which are long and can have branches [22]. Simple clumps, also called small clumps or entanglements, are larger freely dispersed mycelia where the main hypha is not identifiable. These are often referred as “artificially overlapping hyphae” [21-23]. A further dispersed morphological class are clumps, also called large clumps [21-23]. These consist of aggregated or clumped hyphae [22]. Large clumps are distinguished from so-called pellets by the missing of a dense core [21, 22].

These steps in morphological development are interlinked. As already mentioned, the concentration of spores influences spore germination [17, 20]. Furthermore, initial spore concentration has an impact on later morphology [24-26]. Thus, initial spore concentrations ought to be the same to yield reproducible morphologies in later process phases. Studies of spore concentrations impacting later morphology revealed that at higher spore concentrations, pellet building takes longer. Hence, pellets were smaller in early process phases leading to longer stability of the pellets (vs. pellet breakage) [24].

### *1.1.3.2 Importance of the morphology*

An important parameter in filamentous bioreactor cultivations is the morphology of the fungi, because the morphology and the productivity are highly interlinked and depend on process conditions [27]. Filamentous fungi in submerged culture exhibit a large variety of morphological forms, as already described above. Depending on the aimed product, different characteristics of the morphology are favorable [27]. However, it is not just that the productivity is directly linked to the morphology, but also the process is affected. Several studies were conducted investigating the connection of morphology and viscosity. The latter is linked to mass transfer and energy input [28-30]. As a general trend, it can be stated that filamentous growth with high amounts of hyphae causes increased viscosity [31]. Furthermore, a high fraction of pellets results in better mass and heat transfer, and lower power input levels needed for mixing [32]. Various factors build a complex system of interactions. Operation

---

conditions influence growth, product formation and morphology. In addition, filamentous growth directly influences the morphology, which, consequently, further changes the viscosity and which in turn has an impact on the operation conditions [31].

Concerning the morphology in penicillin producing processes, different models/approaches have been published. Paul and Thomas (1998) distinguished four parts of hyphae based on the activities of these four compartments. Discriminated were the tips of hyphae, the so-called actively growing regions, non-growing cytoplasm, vacuolized hyphae and metabolically inactive/degenerated regions [33]. Growth takes place only in actively growing regions, while penicillin is produced by the non-growing cytoplasm. New actively growing (apical) regions emerge by the building of branches from the non-growing region. Via growth, actively growing regions become non-growing regions. The older a compartment is, the more vacuoles are built, hence a development towards vacuolized region takes place. High amounts of vacuoles in a compartment lead to autolysis or degeneration [33]. An equivalent approach is the distinction of apical, subapical and hyphal cells in hyphae. Due to this model, only subapical cells are able to produce penicillin [34].

Other approaches focus on larger morphological structures than single hyphae. Wittler et al. (1986) suggested the differentiation of four layers within one pellet. The outer layer is the active one, containing high quantities of cytoplasm. The second layer shows a decreased cytoplasm content. In the center of the pellet, the hyphal structure is already degenerated. In-between this inner layer and the second one, another layer ought to exist in hollow pellets. This third layer contains cytoplasm, as the outer layer does [35].

What all these models have in common is, that the youngest hyphal regions (in hyphae and pellets) are defined to be active and growing. The older hyphae are (the more the center of the pellet is approached), the more the hyphal structure and cytoplasm are lost and vacuolization and degeneration occurs. In large aggregates like pellets, degeneration and loss of hyphal structure ought further be linked to decreased oxygen and nutrient levels due to limitations in mass transfer within the pellet [36].

### *1.1.3.3 Analyzing morphology*

In recent decades, investigation of fungal morphology in submerged bioreactor cultures had been a central issue. Microscopy in combination with image analysis is the most common method [21-23, 37]. Automated image recording and automated analysis of images allows a high-throughput, statistically verified morphological analysis [23]. Furthermore, online methods for image analysis exist like quantification of morphology in flowthrough cells. These last mentioned online analyses focused only on

hyphal morphology. The flow cell with a height of 40  $\mu\text{m}$  limits the tools to dispersed growing cultures [38, 39].

Although flow cytometry has often been applied for the morphological description of microorganisms as for example bacteria [40, 41], investigations of filamentous organisms apart from the spore stadium [42] are scarce. Main reason for that, is the size limitation of common flow cytometers. Hyphal aggregates risk to clog the tubing [43]. Only large-particle flow cytometers ought to cope with pellets of several hundred micrometers diameter. So far, investigations of filamentous fungi in pellet stadium focused on size, density and fluorescence measurement but did not go more into detail concerning morphology [44, 45].

#### *1.1.3.4 Biomass segregation and viability*

Typical segregation of biomass concerns the viability or fitness of cells. Previously, viability was defined to be the capability of performing all cell functions which are necessary for survival under current conditions. Elementary for viable cells is the intactness of the cytoplasmic membrane being the barrier between the cytoplasm and the extracellular environment. Furthermore, the generation of energy for the maintenance of the metabolism and the biosynthesis of building blocks and other elements is required. In addition, DNA transcription and RNA translation is of utter importance. As a last eventual point, growth and multiplication are mentioned [46]. For the assessment of viability, these requirements need to be approached [46].

One approach for viability assessment is the use of fluorogenic substrates, tailored to a specific enzyme class. Naturally, the substrate should be cheap and react with enzymes that are of broad abundance in the cell system to be investigated. A well-known example is fluorescein diacetate (FDA), which is often combined with propidium iodide (PI) for a control [47, 48]. FDA is converted to a fluorescent product via esterases and hence reflects the metabolic activity of cells [49]. PI fluorescence originates from the intercalation into the DNA in cells with compromised membrane integrity, and should thus act as a dead cell stain [47].

In this thesis biomass segregation and viability is distinguished in two different morphological phases: First, the viability of spores is investigated, and, secondly, biomass segregation in the main cultures containing hyphae and hyphal aggregates. During spore germination, fungal cell wall undergoes substantial changes in its chemical and structural configuration [50-52], hampering the development of a protocol that is universally applicable to different bioprocess setups and across different process phases.

The most widely applied method for investigating spore viability is colony forming unit (CFU) determination [24, 25]. This method, however, is often inaccurate, time intensive and not applicable in real-time. Spores are plated on agar at least one week prior to the start of the fermentation to serve as an input parameter for concentration adjustment of viable spores in the inoculum. Thus, the spore concentration in these cases is equal to so-called viable spores, respective spores germinating on agar plates. Hence, spores growing on agar plates are assumed to as well germinate in the liquid environment of a bioreactor.

A common technology to assess cell viability in different biotechnological applications is the combination of flow cytometry and fluorescence-based viability stains. There have been studies using flow cytometry for biomass segregation in processes with bacteria [40, 53], mammals [54], yeasts [55] and algae [56]. For fungal bioprocesses the combination of flow cytometry and viability staining has not yet been applied, although this combination has been used in other fields like disinfection studies [42].

Biomass segregation of hyphae and hyphal aggregates was reported to be investigated using the combination of viability staining and microscopy. The information content provided by different fluorescence stains is high [57], and in case image analysis is applied, quantitative data are achieved [22, 58].

The investigation of biomass segregation in pellets revealed dead biomass (detection of impaired cytoplasmic membrane via PI) in the core of the bacterial pellet and viable biomass in the outer layer [59]. These findings go in line with fluorescence staining of fungal pellets: protein synthesis, localized via mRNA staining with Acridine Orange, was found to occur in young hyphae, subapical and branching zones. However, in pellet cores – especially of larger pellets – no protein synthesis could be found. The same effect was detected for replicating DNA visualized by the uptake of the thymidine analog bromo deoxyuridine [60].

A classical tool for the online evaluation of viable biomass concentration is dielectric spectroscopy. In filamentous fungi bioprocesses a growth phase and a decline phase (at the end of cultivation) is differentiated. For growth phase biomass prediction via dielectric spectroscopy is reported to be highly applicable. However, the biomass prediction in the decline phase still shows very error-prone results [61-63].

#### 1.1.4 Influence of $\mu$ on penicillin production

In penicillin production, several studies identified the specific growth rate  $\mu$  as crucial variable influencing the specific production rate  $q_p$  [64-69]. This was shown for chemostat [64, 67, 68] as well as fed-batch cultures [64, 69]. At low  $\mu$ -values, a positive correlation between  $\mu$  and  $q_p$  was found [64, 65, 67-69]. Which level of specific growth rate revealed the maximal  $q_p$ , depended on the investigation. Van Gulik et al. (2000) published a maximal  $q_p$  of penicillin G at a specific growth rate of  $0.03 \text{ h}^{-1}$  for continuous cultures [68]. Contrary, the maximum  $q_p$  in the fed-batch cultures described by Ryu and Hospodka (1980) were reached at a  $\mu$  of  $0.015 \text{ h}^{-1}$  [67]. The maximum  $q_p$  found in fed-batch cultures conducted by Wittler and Schügerl (1992) was at a specific growth rate of  $0.018 \text{ h}^{-1}$  [69]. The highest  $\mu$ -value investigated in the last-mentioned study was the one with maximal  $q_p$  ( $\mu=0.018 \text{ h}^{-1}$ ), and thus the maximal  $q_p$  ought to be found at higher growth rates. Nonetheless, the value of  $\mu = 0.018 \text{ h}^{-1}$  as the optimal point for penicillin production fits well with the findings of another study investigating fed-batches. Douma et al. (2010) described the maximal  $q_p$  in fed-batch cultures to be at approximately  $0.02 \text{ h}^{-1}$  [64, 69]. Concerning the trend of  $q_p$  at specific growth rates higher than where the maximum  $q_p$  was found, is divisive. While Douma et al. (2010) and van Gulik et al. (2000) found a negative correlation between  $\mu$  and  $q_p$  for chemostat and fed-batch cultures [64, 68], other investigations stated  $q_p$  to be independent of  $\mu$  [66, 67]. The two studies describing cultivations for penicillin V production (versus penicillin G in the other studies) did not investigate growth rates exceeding  $0.018 \text{ h}^{-1}$  [69] respective  $0.009 \text{ h}^{-1}$  [65].

Data for the description of  $\mu$ - $q_p$ -curves derived from different approaches: When continuous cultures were investigated, each steady state yielded one pair of  $\mu$  and  $q_p$  [66, 68]. Pirt and Righelato (1967) calculated the mean  $q_p$  of each steady state [66]. Contrary, van Gulik et al. (2000) used the maximal  $q_p$  in case the steady state was not stable [68]. Also, the results for fed-batch processes resulted from different approaches: either each cultivation revealed one  $\mu$ - $q_p$ -pair [69] or several  $\mu$ - $q_p$ -pairs [64].

## 1.2 Motivation and goal

The description of the current knowledge about the penicillin production process via *Penicillium chrysogenum* reveals the complexity of the system. Various variables/parameters influence the biosynthesis of the secondary metabolite. One parameter repeatedly investigated in the last 50 years was the specific growth rate.

Process monitoring and control are crucial factors for the examination of interacting process parameters, especially in such a complex system, containing variables like fungal morphology. However, process monitoring and process control are not only a necessity in research but also in industrial environment, when knowledge concerning inter alia the specific growth rate is implemented.

The link of  $\mu$  and  $q_p$  as well as the complexity of the penicillin production process described by previous contributions, and further, the dynamic  $q_p$ -trajectories of the here applied *Penicillium chrysogenum* strain, are the basis for the following hypothesis which was chosen to be investigated within this thesis: *The application of an analytical and process-technological toolbox enables the description of  $\mu$ - $q_p$ -trajectories and thus provides the basis for robust bioprocesses with optimized penicillin production.*

Deriving from this hypothesis, the main goal can be defined as follows: *Development of an analytical and process-technological toolbox and its application for the description of  $\mu$ - $q_p$ -interlinks in processes with dynamic  $q_p$ -trajectories to provide the basis for robust bioprocesses with optimized penicillin production.*

The toolbox ought to include methodologies meeting the following requirements:

1. A fast method for viable spore concentration measurement, enabling a common starting point for all cultivations by analogous initial spore concentrations in the bioreactor. So-called viable spores are defined as spores able to germinate in liquid process environment (Tools I&II).
2. A fast, at-line applicable method for the investigation of fungal morphology (Tools III&IV).
3. A tool for online  $\mu$ -control based on viable biomass (Tool V).

These tools ought to set the base for the description of  $\mu$ - $q_p$ -trajectories and further variables influencing penicillin production as shown in Figure 1.1. Therefore common starting points of the cultivations should be provided, the specific growth rate controlled and morphology analyzed.

The knowledge about the exact  $\mu$ - $q_p$ -interlinks and the interference of further variables can then be used in combination with the toolbox to design and conduct controlled processes achieving robust and optimized penicillin production (see Figure 1.1).

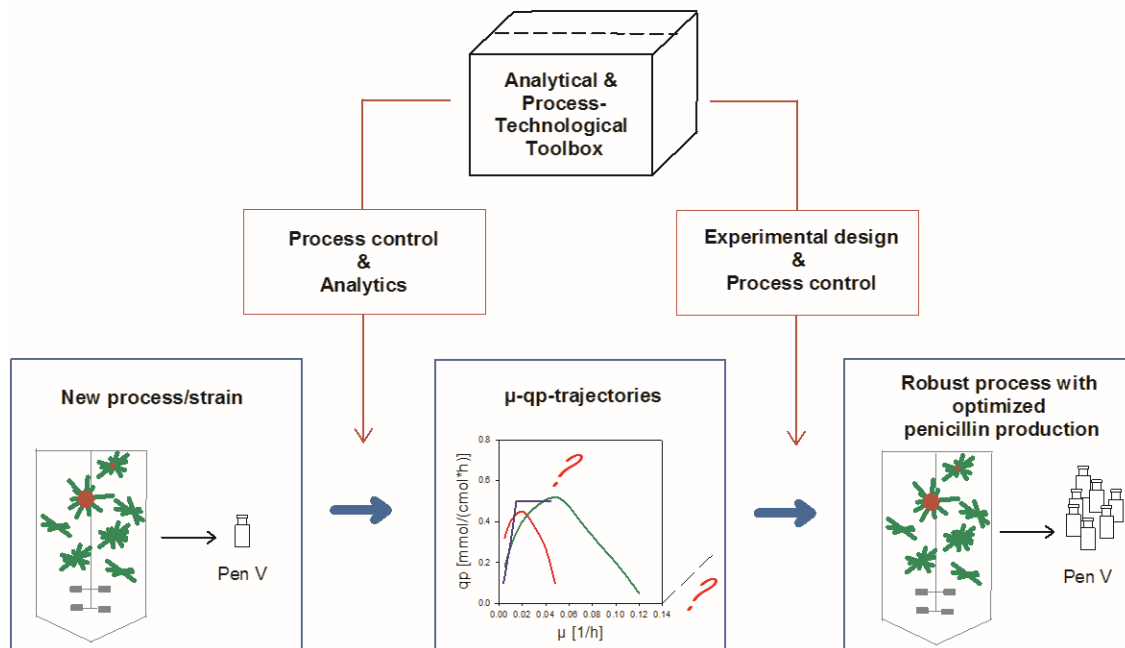


Figure 1.1: The impact of the analytical and process-technological toolbox on the investigation of a new strain or bioprocess, and the application of the thereby yielding knowledge about  $\mu$ - $q_p$ -trajectories. Last mentioned can be used in combination with the toolbox to design experiments and control the process towards optimized penicillin production processes.

For the achievement of the goal and clarification of the hypothesis, this thesis presents the development of five methodologies providing the analytical and process-technological toolbox. In a final study  $\mu$ - $q_p$ -interlinks and further variables influencing the specific penicillin production rate for a process with dynamic  $q_p$ -trajectories are described. This last contribution should underline the importance of the toolbox and provide the basis for experimental design towards improved penicillin production.

### 1.3 Summary and scientific contribution to the manuscripts

This thesis contains six manuscripts, whereof five describe methods for process monitoring and process control, forming the analytical and process-technological toolbox. The final and sixth manuscript describes  $\mu$ - $q_p$ -relations and investigates mechanisms behind  $q_p$ -trajectories. Fed-batch processes described in this final study are paradigmatic cultivations where the toolbox could find its application.

### 1.3.1 Spore-tools (Tool I & tool II)

#### 1.3.1.1 *Spore quality: description of spore sub-populations (Tool I)*

**Manuscript citation:**

**Ehgartner, D.**, Herwig, C., & Neutsch, L. (2016). At-line determination of spore inoculum quality in *Penicillium chrysogenum* bioprocesses. *Applied microbiology and biotechnology*, 100(12), 5363-5373.

**Summary:**

For the determination of spore inoculum quality, the first manuscript focuses on the development of a viability staining combination applicable for *Penicillium chrysogenum* spores in complex cultivation media. Challenges which had to be faced were the high medium background and similar staining targets found in complex medium particles and spores (DNA, sugars etc.). The combination of fluorescein diacetate, propidium iodide and scatter properties of the cells measured with the flow cytometer enabled not only the distinction of spores from media particles, but much more the classification of spores into four sub-populations: metabolically active (viable) spores, quiescent and dead spores, as well as so-called empty envelopes. Hence, it was not only possible to develop a faster at-line alternative to CFU, but to measure spore inoculum quality by investigating the spore sub-populations.

**My contribution:**

I planned and conducted all experiments including staining development, shake flask cultures, flow cytometric measurements and data treatment. Furthermore, I drafted and wrote the manuscript.

#### 1.3.1.2 *Viable spore concentration via spore germination (Tool II)*

**Manuscript citation:**

**Ehgartner, D.**, Fricke, J., Schröder, A., & Herwig, C. (2016). At-line determining spore germination of *Penicillium chrysogenum* bioprocesses in complex media. *Applied Microbiology and Biotechnology*, 100(20), 8923-8930.

**Summary:**

The contribution representing tool II focused on the metabolically active (viable) spore population. In addition to physiological variables like metabolic activity, the morphology of spores was investigated. Tool II enabled the at-line monitoring of spore germination, based on scatter data from the flow cytometer.

An important finding in combination with spore germination was, that not all metabolically active spores germinate in the bioreactor. Thus, the metabolically active spore population is not equal to the viable spore population. As a good correlation between the viable spore concentration based on CFU and the metabolically active spore population was shown, it was concluded that the CFU is not representative for the concentration of germinating (hence viable) spores in the bioreactor, especially not for older spore inocula. In fresh spore inocula, the majority of metabolically active spores showed to germinate.

**My contribution:**

I did experimental planning and gave hands-on in the lab. The practical work including bioreactor cultivations and flow cytometry measurements were conducted with the assistance of Andreas Schröder. My focus in this contribution was the development of the method for germination determination and data treatment of flow cytometric measurements. Further, I wrote the manuscript. The whole study was done under the supervision of Christoph Herwig and Jens Fricke.

**1.3.2 Measuring morphology using a large particle flow cytometer (Tool III & tool IV)**

**1.3.2.1 *Morphological investigation via image analysis (tool III)***

**Manuscript citation:**

Golabgir, A., **Ehgartner, D.**, Neusch, L., Posch, A. E., Sagmeister, P., & Herwig, C. (2014). Imaging Flow Cytometry and High-Throughput Microscopy. *Genetic Transformation Systems in Fungi*, 2, 201.

**Summary:**

Tool III uses the image in flow function of the flow cytometer, enabling picture taking of hyphae and hyphal aggregates in the flow cell. Those pictures are further processed using an image analysis method for microscopy developed by Posch et al. [23], resulting in the same morphological output variables as the equivalent microscopy method does.

**My contribution:**

This book chapter describing tool III is based on the image analysis method for microscopy developed by Andreas Posch. The image analysis method was adapted by Aydin Golabgir in order to apply and verify the computational routines of the methodology on pictures taken in the flow cell of the flow cytometer. My contribution was planning and conductance of the experiments with the flow cytometer. Further, I drafted the part of the manuscript concerning the flow cytometry method.

### 1.3.2.2 *Morphological investigation using scatter properties (tool IV)*

**Manuscript citation:**

**Ehgartner, D.**, Herwig, C., & Fricke, J. Morphological analysis of filamentous fungi using flow cytometry – the fast alternative to microscopy and image analysis. Applied Microbiology and Biotechnology, submitted.

**Summary:**

Tool IV describes the morphology based on scatter properties of the hyphae and hyphal aggregates. The same established approach of morphological classification and investigated morphological variables, as for tool III and beforehand published microscopy methods, was chosen [21-23]. Within the scientific contribution, tool III was compared to microscopy. Both methods yielded in comparable distinction of morphological sub-populations and described their morphology more in detail. In addition to the appropriate quantification of size parameters and the description of the hyphal region around pellets, tool IV revealed a novel compactness parameter for fungal pellets which is not accessible via image analysis.

**My contribution:**

My contribution to this manuscript was the experimental planning, conductance of the majority of the flow cytometric measurements, data treatment, method development and verification, as well as writing of the manuscript.

### 1.3.3 Online control of fungal growth (Tool V)

**Manuscript citation:**

**Ehgartner, D.**, Hartmann, T., Heinzl, S., Frank, M., Veiter, L., Kager, J., Herwig, C., & Fricke, J. Controlling the specific growth rate via biomass trend regulation in filamentous fungi bioprocesses. Chemical Engineering Science, submitted.

**Summary:**

In the study presented in this manuscript, we developed a control strategy for the specific growth rate based on online estimation of viable biomass via dielectric spectroscopy. The method was verified using an at-line staining method for viability measurement. The online viable biomass estimation is applicable in the growth and decline phase, coping with physiological and morphological changes of filamentous

fungi. Furthermore, the control strategy adapts to changing biomass yields which is a big issue in the here presented bioprocess for penicillin production.

Two application runs were conducted showing online viable biomass estimation and control of the specific growth rate at a constant level of  $0.012 \text{ h}^{-1}$ . We achieved biomass prediction with an average error of 1.5 g/l over the whole fed-batch process. In the decline phase, the control of the specific growth rate was not possible due to physiological constraints. However, in the growth phase, a total specific growth rate of  $0.013 \text{ h}^{-1}$  was achieved, which met the pre-defined acceptance criterion for this method.

The method is thus ready for viable biomass estimation in growth and decline phase of the penicillin production process. Furthermore, the method is applicable to control the specific growth rate during the growth phase.

**My contribution:**

My contribution to this scientific publication was the experimental planning, the method development, the process control and the writing of the manuscript. Furthermore, I participated in the conduction of bioreactor cultivations and data treatment, which were assisted by Thomas Hartmann, Sarah Heinzl, Manuela Frank and Lukas Veiter. The setup of process control was supported by Julian Kager. Jens Fricke and Christoph Herwig supervised the experiments and revised the manuscript.

1.3.4 Connecting the specific growth rate and the penicillin productivity

**Manuscript citation:**

**Ehgartner, D.**, Hartmann, T., Heinzl, S., Herwig, C., & Fricke, J. Production rate dynamics at constant growth conditions in a penicillin production process. Engineering in Life Sciences, submitted.

**Summary:**

The relation of  $\mu$  and  $q_p$  for highly dynamic  $q_p$ -trajectories at constant  $\mu$ -levels in fed-batch cultures was investigated. First,  $q_p$  started to increase until it reached a maximum, and decreased. Despite lacking constant  $q_p$ -phases, a connection between  $\mu$  and  $q_p$  could be described which fits results published earlier.  $\mu$ - $q_p$ -pairs for the description of this connection derived from maximal  $q_p$ -levels as well as after a certain amount of glucose was consumed. In addition, mean values of  $\mu$  and  $q_p$  resulted in the same conclusions.

Furthermore, it was found that the maximal  $q_p$  was reached after metabolizing a certain amount of glucose. Thus, the time needed to reach maximal  $q_p$  and hence the point of  $q_p$  decline, is a function of

the average  $\mu$  of the fed-batch. The increase of  $q_p$  was associated with an adaption effect to the actual specific growth rate. Decline of  $q_p$  was proposed to stand in relation with NADPH supply from the mannitol cycle.

The results enable the prediction of  $q_p$ -trajectories and thus are of use for the planning of fed-batch cultivations towards optimal penicillin production.

**My contribution:**

I planned the experiments and did the statistical analysis. Further, I participated in the practical part of the cultivations and supervised analysis and data treatment, which were conducted with the assistance of Thomas Hartmann and Sarah Heinzl. Finally, I wrote the manuscript which was revised by Jens Fricke and Christoph Herwig.

## 1.4 References

1. Flemming, A., On the Antibacterial Action of Cultures of a Penicillium, with Special Reference to Their Use in the Isolation of B. influenzae. *British journal of experimental pathology* 1929, 10, 226-236.
2. Houbraken, J., Frisvad, J.C., Samson, R.A., Fleming's penicillin producing strain is not Penicillium chrysogenum but P. rubens. *IMA Fungus* 2011, 2, 87-95.
3. Wainwright, M., Swan, H.T., C.G. Paine and the earliest surviving clinical records of penicillin therapy. *Med Hist* 1986, 30, 42-56.
4. Wainwright, M., The history of the therapeutic use of crude penicillin. *Med Hist* 1987, 31, 41-50.
5. Jami, M.S., Barreiro, C., Garcia-Estrada, C., Martin, J.F., Proteome analysis of the penicillin producer Penicillium chrysogenum: characterization of protein changes during the industrial strain improvement. *Mol Cell Proteomics* 2010, 9, 1182-98.
6. Abraham, E.P., Chain, E.B., An Enzyme from Bacteria able to Destroy Penicillin. *Nature* 1940, 146, 837.
7. Aminov, R.I., A brief history of the antibiotic era: lessons learned and challenges for the future. *Front Microbiol* 2010, 1, 134.
8. Ozcengiz, G., Demain, A.L., Recent advances in the biosynthesis of penicillins, cephalosporins and clavams and its regulation. *Biotechnol Adv* 2013, 31, 287-311.
9. Brakhage, A.A., Sprote, P., Al-Abdallah, Q., Gehrke, A., et al., Regulation of penicillin biosynthesis in filamentous fungi. *Adv Biochem Eng Biotechnol* 2004, 88, 45-90.
10. Prausse, M.T., Schauble, S., Guthke, R., Schuster, S., Computing the various pathways of penicillin synthesis and their molar yields. *Biotechnol Bioeng* 2016, 113, 173-81.
11. Evers, M.E., Trip, H., van den Berg, M.A., Bovenberg, R.A., et al., Compartmentalization and transport in beta-lactam antibiotics biosynthesis. *Adv Biochem Eng Biotechnol* 2004, 88, 111-35.
12. van den Berg, M.A., Albang, R., Albermann, K., Badger, J.H., et al., Genome sequencing and analysis of the filamentous fungus Penicillium chrysogenum. *Nat Biotechnol* 2008, 26, 1161-8.

13. Ehgartner, D., Fricke, J., Schroder, A., Herwig, C., At-line determining spore germination of *Penicillium chrysogenum* bioprocesses in complex media. *Appl Microbiol Biotechnol* 2016, 100, 8923-30.
14. Ehgartner, D., Herwig, C., Neutsch, L., At-line determination of spore inoculum quality in *Penicillium chrysogenum* bioprocesses. *Appl Microbiol Biotechnol* 2016.
15. d'Enfert, C., Fungal Spore Germination: Insights from the Molecular Genetics of *Aspergillus nidulans* and *Neurospora crassa*. *Fungal Gen Biol* 1997, 21, 163-172.
16. Gottlieb, D., The physiology of spore germination in fungi. *The Botanical Review* 1950, 16, 229-257.
17. Demming, S., Sommer, B., Llobera, A., Rasch, D., et al., Disposable parallel poly(dimethylsiloxane) microbio reactor with integrated readout grid for germination screening of *Aspergillus ochraceus*. *Biomicrofluidics* 2011, 5, 14104.
18. Dantigny, P., Bensoussan, M., Vasseur, V., Lebrihi, A., et al., Standardisation of methods for assessing mould germination: a workshop report. *Int J Food Microbiol* 2006, 108, 286-91.
19. Paul, G.C., Kent, C.A., Thomas, C.R., Viability testing and characterization of germination of fungal spores by automatic image analysis. *Biotechnol Bioeng* 1993, 42, 11-23.
20. Fletcher, J., Morton, G., Physiology of germination of *Penicillium griseofulvum* conidia. *T Brit Mycol Soc* 1970, 54, 65-81.
21. Paul, G.C., Thomas, C.R., Characterisation of mycelial morphology using image analysis. *Adv Biochem Eng Biotechnol* 1998, 60, 1-59.
22. Cox, P.W., Paul, G.C., Thomas, C.R., Image analysis of the morphology of filamentous microorganisms. *Microbiology* 1998, 144 ( Pt 4), 817-27.
23. Posch, A.E., Spadiut, O., Herwig, C., A novel method for fast and statistically verified morphological characterization of filamentous fungi. *Fungal Genet Biol* 2012, 49, 499-510.
24. Posch, A.E., Herwig, C., Physiological description of multivariate interdependencies between process parameters, morphology and physiology during fed-batch penicillin production. *Biotechnol Prog* 2014, 30, 689-99.
25. Posch, A.E., Koch, C., Helmelt, M., Marchetti-Deschmann, M., et al., Combining light microscopy, dielectric spectroscopy, MALDI intact cell mass spectrometry, FTIR spectromicroscopy and multivariate data mining for morphological and physiological bioprocess characterization of filamentous organisms. *Fungal Genet Biol* 2013, 51, 1-11.
26. Tucker, K.G., Thomas, C.R., Inoculum effects on fungal morphology: Shake flasks vs agitated bioreactors. *Biotechnology techniques* 1994, 8, 153-156.
27. Papagianni, M., Fungal morphology and metabolite production in submerged mycelial processes. *Biotechnol Adv* 2004, 22, 189-259.
28. Chain, E.B., Gualandi, G., Morisi, G., Aeration studies. IV. Aeration conditions in 3000-liter submerged fermentations with various microorganisms. *Biotechnology and Bioengineering* 1966, 8, 595-619.
29. Petersen, N., Stocks, S., Gernaey, K.V., Multivariate models for prediction of rheological characteristics of filamentous fermentation broth from the size distribution. *Biotechnol Bioeng* 2008, 100, 61-71.
30. Riley, G.L., Tucker, K.G., Paul, G.C., Thomas, C.R., Effect of biomass concentration and mycelial morphology on fermentation broth rheology. *Biotechnol Bioeng* 2000, 68, 160-72.
31. Quintanilla, D., Hagemann, T., Hansen, K., Gernaey, K.V., Fungal Morphology in Industrial Enzyme Production--Modelling and Monitoring. *Adv Biochem Eng Biotechnol* 2015, 149, 29-54.
32. Znidarsic, P., Pavko, A., The morphology of filamentous fungi in submerged cultivations as a bioprocess parameter. *Food Technology and Biotechnology* 2001, 39, 237-252.

33. Paul, G.C., Syddall, M.T., Kent, C.A., Thomas, C.R., A structured model for penicillin production on mixed substrates. *Biochemical Engineering Journal* 1998, 2, 11-21.
34. Zangirolami, T.C., Johansen, C.L., Nielsen, J., Jorgensen, S.B., Simulation of penicillin production in fed-batch cultivations using a morphologically structured model. *Biotechnol Bioeng* 1997, 56, 593-604.
35. Wittier, R., Baumgartl, H., Lubbers, D.W., Schugerl, K., Investigations of oxygen transfer into *Penicillium chrysogenum* pellets by microprobe measurements. *Biotechnol Bioeng* 1986, 28, 1024-36.
36. Hille, A., Neu, T.R., Hempel, D.C., Horn, H., Oxygen profiles and biomass distribution in biopellets of *Aspergillus niger*. *Biotechnol Bioeng* 2005, 92, 614-23.
37. Vanhoutte, B., Pons, M.N., Thomas, C.R., Louvel, L., et al., Characterization of *Penicillium chrysogenum* physiology in submerged cultures by color and monochrome image analysis. *Biotechnol Bioeng* 1995, 48, 1-11.
38. Christiansen, T., Spohr, A.B., Nielsen, J., On-line study of growth kinetics of single hyphae of *Aspergillus oryzae* in a flow-through cell. *Biotechnol Bioeng* 1999, 63, 147-53.
39. Spohr, A., Dam-Mikkelsen, C., Carlsen, M., Nielsen, J., et al., On-line study of fungal morphology during submerged growth in a small flow-through cell. *Biotechnol Bioeng* 1998, 58, 541-53.
40. Ehgartner, D., Sagmeister, P., Herwig, C., Wechselberger, P., A novel real-time method to estimate volumetric mass biodensity based on the combination of dielectric spectroscopy and soft-sensors. *J Chem Technol Biotechnol* 2015, 90, 262-272.
41. Langemann, T., Mayr, U.B., Meitz, A., Lubitz, W., et al., Multi-parameter flow cytometry as a process analytical technology (PAT) approach for the assessment of bacterial ghost production. *Appl Microbiol Biotechnol* 2016, 100, 409-18.
42. Mesquita, N., Portugal, A., Pinar, G., Loureiro, J., et al., Flow cytometry as a tool to assess the effects of gamma radiation on the viability, growth and metabolic activity of fungal spores. *Int Biodeter Biodegr* 2013, 84, 250-257.
43. Dubelaar, G.B.J., Gerritzen, P.L., CytoBuoy: a step forward towards using flow cytometry in operational oceanography. *Scientia Marina* 2000, 64, 255-265.
44. de Bekker, C., van Veluw, G.J., Vinck, A., Wiebenga, L.A., et al., Heterogeneity of *Aspergillus niger* microcolonies in liquid shaken cultures. *Appl Environ Microbiol* 2011, 77, 1263-7.
45. Delgado-Ramos, L., Marcos, A.T., Ramos-Guelfo, M.S., Sanchez-Barrionuevo, L., et al., Flow cytometry of microencapsulated colonies for genetics analysis of filamentous fungi. *G3 (Bethesda)* 2014, 4, 2271-8.
46. Breeuwer, P., Abee, T., Assessment of viability of microorganisms employing fluorescence techniques. *Int J Food Microbiol* 2000, 55, 193-200.
47. Brul, S., Nussbaum, J., Dielbandhoesing, S.K., Fluorescent probes for wall porosity and membrane integrity in filamentous fungi. *J Microbiol Methods* 1997, 28, 169-178.
48. Bunthof, C.J., van den Braak, S., Breeuwer, P., Rombouts, F.M., et al., Rapid fluorescence assessment of the viability of stressed *Lactococcus lactis*. *Appl Environ Microbiol* 1999, 65, 3681-9.
49. Rotman, B., Papermaster, B.W., Membrane properties of living mammalian cells as studied by enzymatic hydrolysis of fluorogenic esters. *Proc Natl Acad Sci U S A* 1966, 55, 134-41.
50. Allen, P.J., Metabolic aspects of spore germination in fungi. *Annu Rev Phytopathol* 1965, 3, 313-342.
51. Bartnicki-Garcia, S., Cell wall chemistry, morphogenesis, and taxonomy of fungi. *Annu Rev in Microbiol* 1968, 22, 87-108.
52. Martin, J.F., Nicolas, G., Villanueva, J.R., Chemical changes in the cell walls of conidia of *Penicillium notatum* during germination. *Can J Microbiol* 1973, 19, 789-96.

53. Langemann, T., Koller, V.J., Muhammad, A., Kudela, P., et al., The Bacterial Ghost platform system: production and applications. *Bioeng Bugs* 2010, 1, 326-36.
54. Kumar, N., Borth, N., Flow-cytometry and cell sorting: an efficient approach to investigate productivity and cell physiology in mammalian cell factories. *Methods* 2012, 56, 366-74.
55. Hyka, P., Zullig, T., Ruth, C., Looser, V., et al., Combined use of fluorescent dyes and flow cytometry to quantify the physiological state of *Pichia pastoris* during the production of heterologous proteins in high-cell-density fed-batch cultures. *Appl Environ Microbiol* 2010, 76, 4486-96.
56. Hyka, P., Lickova, S., Pribyl, P., Melzoch, K., et al., Flow cytometry for the development of biotechnological processes with microalgae. *Biotechnol Adv* 2013, 31, 2-16.
57. Hickey, P.C., Swift, S.R., Roca, M.G., Read, N.D., Live-cell Imaging of Filamentous Fungi Using Vital Fluorescent Dyes and Confocal Microscopy. *Methods in Microbiology* 2004, 34.
58. Bizukojc, M., Ledakowicz, S., The morphological and physiological evolution of *Aspergillus terreus* mycelium in the submerged culture and its relation to the formation of secondary metabolites. *World Journal of Microbiology and Biotechnology* 2010, 26, 41-54.
59. Nieminen, L., Webb, S., Smith, M.C., Hoskisson, P.A., A flexible mathematical model platform for studying branching networks: experimentally validated using the model actinomycete, *Streptomyces coelicolor*. *PLoS One* 2013, 8, e54316.
60. Schügerl, K., Gerlach, S.R., Siedenberg, D., *Influence of the process parameters on the morphology and enzyme production of Aspergilli*, in *Relation Between Morphology and Process Performances*, K. Schügerl, Editor. 1998, Springer Berlin Heidelberg: Berlin
61. Neves, A., Pereira, D., Vieira, L., Menezes, J., Real time monitoring biomass concentration in *Streptomyces clavuligerus* cultivations with industrial media using a capacitance probe. *Journal of Biotechnology* 2000, 84, 45-52.
62. Rønne, N.P., Stocks, S.M., Lantz, A.E., Gernaey, K.V., Introducing process analytical technology (PAT) in filamentous cultivation process development: comparison of advanced online sensors for biomass measurement. *Journal of industrial microbiology & biotechnology* 2011, 38, 1679-1690.
63. Sarra, M., Ison, A., Lilly, M., The relationships between biomass concentration, determined by a capacitance-based probe, rheology and morphology of *Saccharopolyspora erythraea* cultures. *Journal of Biotechnology* 1996, 51, 157-165.
64. Douma, R.D., Verheijen, P.J., de Laat, W.T., Heijnen, J.J., et al., Dynamic gene expression regulation model for growth and penicillin production in *Penicillium chrysogenum*. *Biotechnol Bioeng* 2010, 106, 608-18.
65. Kluge, M., Siegmund, D., Diekmann, H., Thoma, M., A model for penicillin production with and without temperature shift after the growth phase. *Appl Microbiol Biotechnol* 1992, 36, 446-51.
66. Pirt, S.J., Righelato, R.C., Effect of Growth Rate on the Synthesis of Penicillin by *Penicillium chrysogenum* in Batch and Chemostat Cultures. *Appl Microbiol* 1967, 15, 1284-90.
67. Ryu, D.D.Y., Hospodka, J., Quantitative Physiology of *Penicillium chrysogenum* in Penicillin Fermentation. *Biotechnol Bioeng* 1980, 22, 289-298.
68. van Gulik, W.M., de Laat, W.T., Vinke, J.L., Heijnen, J.J., Application of metabolic flux analysis for the identification of metabolic bottlenecks in the biosynthesis of penicillin-G. *Biotechnol Bioeng* 2000, 68, 602-18.
69. Wittler, R., Schügerl, K., Interrelation between penicillin productivity and growth rate. *Appl Microbiol Biotechnol* 1985, 21, 348-355.

## 2 Manuscripts

This chapter contains the six manuscripts. In addition, a title page was added to each manuscript depicting title, authors, journal, status of the publication and the key figure of the contribution.

### **Roadmap:**

- 1) Spore quality and spore germination

**Manuscript 1** (Tool I): At-line determination of spore inoculum quality in *Penicillium chrysogenum* bioprocesses

**Manuscript 2** (Tool II): At-line determining spore germination of *Penicillium chrysogenum* bioprocesses in complex media

- 2) Measuring morphology by using a large particle flow cytometer

**Manuscript 3** (Tool III): Imaging Flow Cytometry and High-Throughput Microscopy

**Manuscript 4** (Tool IV): Morphological analysis of filamentous fungi using flow cytometry – the fast alternative to microscopy and image analysis

- 3) Online control of fungal growth

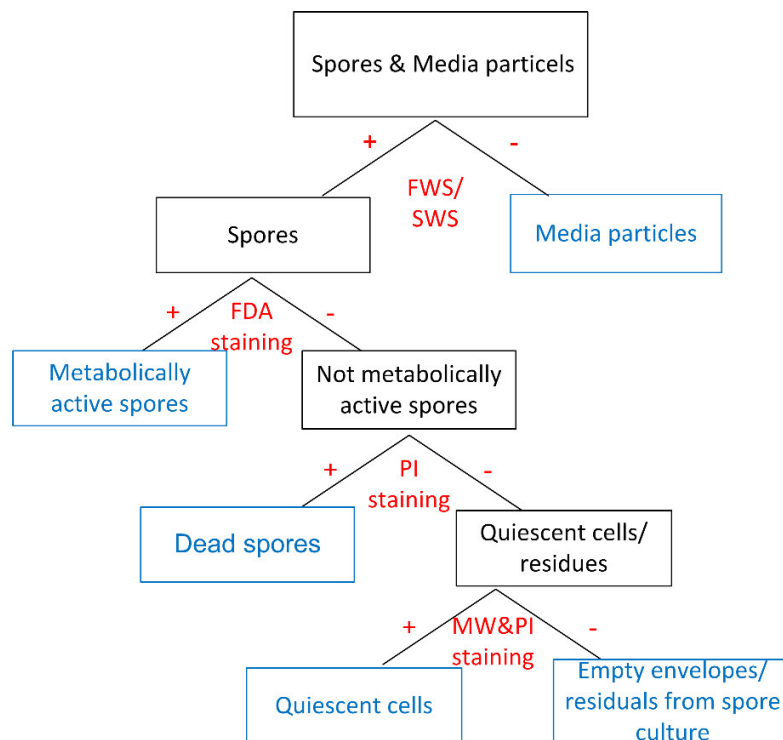
**Manuscript 5** (Tool V): Controlling the specific growth rate via biomass trend regulation in filamentous fungi bioprocesses

- 4) Connecting specific growth rate and penicillin productivity

**Manuscript 6:** Production rate dynamics at constant growth conditions in a penicillin production process

## At-line determination of spore inoculum quality in *Penicillium chrysogenum* bioprocesses

Ehgartner, D., Herwig, C., & Neutsch, L., Applied microbiology and biotechnology, 100(12), 5363-5373 (2016)





## At-line determination of spore inoculum quality in *Penicillium chrysogenum* bioprocesses

Daniela Ehgartner<sup>1,2</sup> · Christoph Herwig<sup>1,2</sup> · Lukas Neutsch<sup>2</sup>

Received: 28 September 2015 / Revised: 11 January 2016 / Accepted: 13 January 2016  
© Springer-Verlag Berlin Heidelberg 2016

**Abstract** Spore inoculum quality in filamentous bioprocesses is a critical parameter influencing pellet morphology and, consequently, process performance. It is essential to determine the concentration of viable spores before inoculation, to implement quality control and decrease batch-to-batch variability. The ability to assess the spore physiologic status with close-to-real time resolution would offer interesting perspectives enhanced process analytical technology (PAT) and quality by design (QbD) strategies. Up to now, the parameters contributing to spore inoculum quality are not clearly defined. The state-of-the-art method to investigate this variable is colony-forming unit (CFU) determination, which assesses the number of growing spores. This procedure is tedious, associated with significant inherent bias, and not applicable in real time.

Here, a novel method is presented, based on the combination of viability staining (propidium iodide and fluorescein diacetate) and large-particle flow cytometry. It is compatible with the complex medium background often observed in filamentous bioprocesses and allows for a classification of the

spores into different subpopulations. Next to viable spores with intact growth potential, dormant or inactive as well as physiologically compromised cells are accurately determined. Hence, a more holistic view on spore inoculum quality and early-phase biomass composition is provided, offering enhanced information content.

In an industrially relevant model bioprocess, good correlation to CFU counts was found. Morphological parameters (e.g. spore swelling) that are not accessible via standard monitoring tools were followed over the initial process phase with close temporal resolution.

**Keywords** Filamentous fungi · Flow cytometry · Viability staining · Spore quality · Bioprocess development

### Introduction

In fungal bioprocesses, the amount of germinating spores influences pellet morphology and hence process performance and product titer (Posch and Herwig 2014). Therefore, the determination of spore inoculum quality is of primary importance.

The most widely applied method for investigating spore inoculum quality is colony-forming unit (CFU) determination. This method, however, is often inaccurate, time intensive and not applicable in real time. Spores have to be plated on agar at least 1 week prior to the start of the fermentation to serve as an input parameter for concentration adjustment of viable spores in the inoculum. Alternative faster methods would be required to carry out this important process step in at-line mode and, moreover, offer capability to use spore viability as a parameter in process monitoring.

A common technology to assess cell viability in different biotechnological applications is the combination of flow

**Electronic supplementary material** The online version of this article (doi:10.1007/s00253-016-7319-9) contains supplementary material, which is available to authorized users.

✉ Christoph Herwig  
christoph.herwig@tuwien.ac.at

<sup>1</sup> CD Laboratory on Mechanistic and Physiological Methods for Improved Bioprocesses, Vienna University of Technology, Gumpendorferstrasse 1a/166, 1060 Vienna, Austria

<sup>2</sup> Research Area Biochemical Engineering, Institute of Chemical Engineering, Vienna University of Technology, Gumpendorferstrasse 1a/166, 1060 Vienna, Austria

cytometry (FCM) and fluorescence-based viability stains. There have been studies using FCM for biomass segregation in processes with bacteria (Ehgartner et al. 2015; Kell et al. 1998; Langemann et al. 2010; Quiros et al. 2007; Sundstrom et al. 2004), mammals (Kumar and Borth 2012; Vermes et al. 2000), yeasts (Hyka et al. 2010; Quiros et al. 2007) and algae (Hyka et al. 2013). The higher information content on biomass properties allowed for enhanced process control and more detailed assessment of process performance (Diaz et al. 2010). However, application examples of FCM to bioprocesses with filamentous fungi are scarce, which may be due to inherent challenges associated with such setups.

Historically, filamentous bioprocesses with hosts such as *Penicillium chrysogenum* for penicillin production use complex and relatively undefined media, containing non-solubilized particles of 50  $\mu\text{m}$  and more in size (Posch et al. 2012). This hampers flow cytometric analysis, particularly because of the inherent difficulty in discriminating between spores and media particles, which reside in the same size class. Also, large particles from the medium can lead to clogging in fluid lines, valves, etc. Therefore, most common flow cytometers are not suitable for operation in complex media. The CytoSense flow cytometer (CytoBuoy, Netherlands) is a device especially designed for analysis of particles up to a size of 1 mm, owing to its main designated area of use in aquatic research (Hashemi et al. 2011). It is here first used for flow cytometric analysis of filamentous fungi in cultivations with complex media.

Viability stain combinations for FCM have been developed and successfully applied for a wide range of host organisms of biotechnological relevance (Deere et al. 1998; Langemann et al. 2010; Mesquita et al. 2013; O'Brien and Bolton 1995; Vermes et al. 2000). However, most conventional products and protocols are tailored to mammalian, yeast and microbial cells, which are characterized by cell membranes that are relatively easy to permeize by, e.g. chemical treatment (Rieseberg et al. 2001). In contrast, fungal spores feature a resistive cell wall that is designed by nature for maximum stability also in adverse environments (Prigione and Filipello Marchisio 2004). It is for this reason that most standard FCM protocols do not give satisfying results for spore cell analysis.

Moreover, the fungal cell wall undergoes substantial changes in its chemical and structural configuration during spore germination (Allen 1965; Bartnicki-Garcia 1968; Martin et al. 1973), hampering the development of a protocol that is universally applicable to different bioprocess setups and across different process phases. In the background of complex media such as corn steep liquor, which themselves contain significant amounts of DNA, sugars, proteins and lipids, it is difficult to identify a suitable biological target for reliable discrimination between media particles and fungal cells.

One approach for viability assessment with higher selectivity than the typical dye-exclusion principle is the use of fluorogenic substrates, tailored to a specific enzyme class. Naturally, the substrate should be cheap and reacts with enzymes that are of broad abundance in the cell system to be investigated. A well-known example is fluorescein diacetate (FDA), which is often combined with propidium iodide (PI) for a control (Brul et al. 1997; Bunthof et al. 1999; Jones and Senft 1985). FDA is converted to a fluorescent product via esterases and hence reflects the metabolic activity of cells (Rotman and Papermaster 1966). PI fluorescence originates from the intercalation into the DNA in cells with compromised membrane integrity and should thus act as a dead cell stain (Brul et al. 1997). Both are common dyes used for viability assessment (Binder et al. 2010; Brul et al. 1997; Hua et al. 2011) but have not been applied to filamentous fungi cultured in a bioprocess environment.

This study describes a novel method for spore inoculum quality monitoring in biotechnological production, based on the combination of the FDA/PI viability staining and flow cytometric detection. Due to special instrumentation, the method is fully compatible with the complex environment in filamentous bioprocesses and provides multiparametric data on spore physiology and morphology in a previously unmatched degree of detail.

The goal of this study was to find a fast alternative to CFU which in addition serves a higher information content concerning biomass segregation. Thereby, parameters contributing to spore inoculum quality ought to be better defined. The improved means of describing biomass status and growth especially in early process phases will further deepen the general understanding of critical parameters and as such is in direct line with the main objective of the emerging quality by design (QbD) initiative.

## Materials and methods

### Strain, medium and cultivation system

Spore suspensions of the P-14 *P. chrysogenum* candidate strain for penicillin production descending from the P-2 *P. chrysogenum* candidate strain (American Type Culture Collection with the access number ATCC 48271) (Lein 1986) were provided by Sandoz GmbH (Kundl, Austria) and used for all experiments.

One hundred milliliters of an autoclaved complex culture medium (sucrose 18 g/l, glucose 3 g/l, corn steep liquor 26 g/l and 3.8 g/l  $\text{CaCO}_3$ ) in a 500-ml shake flask were inoculated using  $1 \times 10^9$  spores/ml

and cultivated in an Infors HT Multitron shaker (Infors, Bottmingen, Switzerland) at 25 °C at 280 rpm.

### Sample preparation

Samples from shake flasks including culture broth were diluted 1:10 into dH<sub>2</sub>O and stained with PI (Sigma-Aldrich, MO, USA; 20 mM stock dissolved in DMSO, diluted to a final concentration of 20 µM). After incubation for 30 min, FDA (Sigma-Aldrich, St. Louis, MO, USA; stock solution of 5 g/l dissolved in acetone) was added to a final concentration of 5 mg/l. After addition of FDA, the sample was further diluted (1:10 in the same buffer) for flow cytometric analysis.

To prepare a positive control for membrane-compromised cells (PI positive), 5 ml of cultivation broth (diluted 1:5 in dH<sub>2</sub>O) was pipetted into a 100-ml Erlenmeyer flask and heated for 30 s at 940 W in a M510 microwave oven (Philips, Amsterdam, Netherlands). After microwaving, the suspension was further diluted in dH<sub>2</sub>O to a total dilution of 1:10. The staining procedure was carried out as described above.

Next to the FDA/PI combination, other dyes were investigated in parallels with regard to their discrimination potential between fungal spores and media particles. If not stated otherwise, spores from shake flask cultures were investigated. SYTO9 (final concentration 3.34 µM, incubation time 15–30 min) was taken from the LIVE/DEAD® FungaLight Yeast Viability Kit (Molecular Probes, Eugene, OR, USA), calcofluor (the 1 g/l solution was added to sample in a ratio 1:2; no incubation; Sigma-Aldrich, St. Louis, MO, USA), FM464 (final concentration 0.5 mg/l), Hoechst 33342 (H33342; final concentration 20 mg/l) and 4',6-diamidino-2-phenylindole (DAPI; final concentration 20 mg/l). The latter three dyes were obtained from Life Technologies (Carlsbad, CA, USA). Various fluorescence-labeled lectins were tested to stain fungal cell wall carbohydrates, including *Lens culinaris* agglutinin (fLCA; final concentration 100 mg/l), *Galanthus nivalis* lectin (fGNL; final concentration 40 mg/l), *Solanum tuberosum* lectin (fSTL; final concentration 40 mg/l) and wheat germ agglutinin (fWGA; final concentration 100 mg/l) from *Triticum vulgare*. All were used as the FITC conjugate obtained from the supplier (Vector Laboratories, Burlingame, CA, USA). If not stated otherwise, incubation of stains was conducted in the dark at room temperature and several incubation times between 0–120 min were investigated.

### CFU determination

For CFU determination, the shake flask samples were diluted in a sterile solution of 8.5 g/l sodium chloride and 1 ml/l Tween 80 and plated. The agar plates used, were prepared of a medium resembling to the one used for shake flask cultivations and included 25 g/l agar agar.

### Microscopy

Fluorescence staining was investigated using a Zeiss Epifluorescence Axio Observer. Z1 deconvolution microscopy system (Carl Zeiss, Oberkochen, Germany) equipped with LD Plan-Neofluar 63x objective (+ ×10 ocular) and the LED illumination system Colibri®. Exposure wavelengths and filter sets for the two stains were chosen with reference to the individual stains (FDA: ex/em 485/525; PI: ex/em 535/600). Exposure time and illumination parameters were adjusted individually for optimal visibility.

### Flow cytometry

A CytoSense flow cytometer (CytoBuoy, Woerden, Netherlands) with two forward scatter (FWS), one sideward scatter (SWS) and three fluorescence channels (yellow, orange, red) was used for single cell analysis. The implemented laser had a wavelength of 488 nm. The configuration of the filter set was 515–562 ± 5 nm for the green/yellow fluorescence channel (used for FDA) and 605–720 ± 5 nm for the red fluorescence channel (used for PI). The device was equipped with a PixeLINK PL-B741 1.3-MP monochrome camera for inflow image acquisition. For data treatment, the software CytoClus (CytoBuoy, Woerden, Netherlands) and a custom-programmed Matlab 2009a script (MathWorks, Natick, MA, USA) were used.

## Results

### Screening for a viability stain combination

As mentioned above, there is a high similarity of media particles and spores concerning the sides interacting with the stain. Therefore, differences in staining targets for media particles and spores needed to be investigated to choose the stains for microscopy. Spores as well as media particles are expected to contain glycans, lipids and DNA. While glycans and lipids are supposed to be easily accessible in both, the DNA in spores is enclosed by the cell wall and therefore not directly accessible for the stain. The difference of viable from non-viable spores is the less intact cell membrane of the second, which increases accessibility of stain targets in the cell. Furthermore, viable spores contain active enzymes in contrast to non-viable spores and media particles. Table S1 in the supplementary material gives an overview about staining targets of viable and non-viable spores as well as medium particles.

The fact that spores and medium deliver similar targets for stains and that the cell wall of the fungus has a high resistance hampered the finding of an appropriate viability stain combination. As depicted in Table S2 in the supplementary material, dyes intercalating into DNA as DAPI, SYTO9 and H33342

stained spores, but also medium. Furthermore, stains targeting different carbohydrate epitopes were investigated to be able to distinguish between spores and medium particles. Nonetheless, all of these dyes stained the medium (fGNL, fSTL, fWGA, fLCA and calcofluor), and some of them did not even target spores (fGNL and fLCA). FM464, reported to interact with lipids (Walther et al. 2006), did not stain spores (although hyphae did) and was therefore not further investigated. Exemplary images of the staining development are shown in Fig. S1–S3 in the supplementary material.

The combination of PI/FDA was found to be suitable. Due to the dormant state of spores in fresh spore inoculum, FDA staining was low or undetectable (Fig. 1d–f). But FDA allowed staining big part of spores in untreated shake flask samples after short cultivation suggesting metabolic activity in these spores (Fig. 1a–c). In addition, some spores in untreated samples were PI positive—possibly dead cells (Fig. 1a–c).

The microwave-treated samples consisted of cells with compromised membrane integrity as indicated by PI staining as well as unstained spores, while no FDA-positive spores were found (Fig. 2).

No double staining occurred. Hence, each spore was only stained either by FDA or by PI, although some spores were found to neither fluorescence red nor green when stained with both fluorescence stains.

As medium particles were neither stained by FDA nor PI (see Fig. 1a–c), the viability stain combination fulfilled apart from the differentiation of spore subpopulations also in segregating spores from media particles and was therefore applied for FCM.

#### Differentiation of spores and media particles via forward and sideward scatter

The first measurements after an applicable viability stain combination had been found were to measure diluted and stained

spore samples from shake flask cultivations. These measurements were used to evaluate the segregation of media particles and spores with FCM. Therefore, the scatter channels were applied because staining development had introduced spores which were stained by neither of the two stains and thus were not expected to be separated from media particles via viability staining.

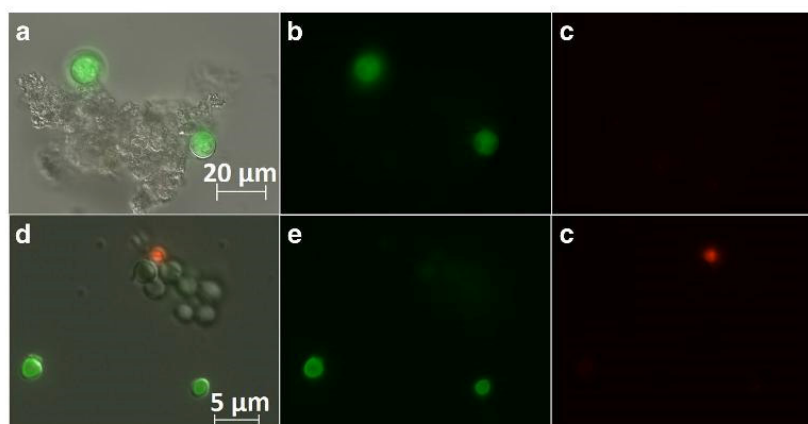
Hence, the method to distinguish spores from media particles is a segregation performed via FWS and SWS and therefore based on particle size (FWS) and particle complexity (SWS). Further information about the principle of FWS and SWS can be found in Díaz et al. (2010). In Fig. 3a, the measurement of a shake flask sample after 8 h of cultivation time is plotted over total FWS and SWS. Two clusters of particles appear which are separated via gate setting. This separation line was set to distinguish media particles from spores. For separation line definition measurements of pure medium, untreated pure spore inoculum as well as microwave-treated and PI-stained fresh spores were conducted.

It is not possible to conduct this segregation neither with FWS alone nor with SWS. The combination of these two scatter signals in order to calculate their ratio is crucial for the distinction.

#### Classification according to membrane permeability and enzymatic activity

The cluster containing spores—determined via light scattering—was plotted over green and red fluorescence to show the effect of PI and FDA staining. This was done for an untreated sample (see Fig. 3b) and a microwave-treated sample (Fig. 3d). A part of spores were found to have high fluorescence either in the green or in the red channel. Spores were classified as PI positive or FDA positive when their fluorescence exceeded the one of the cluster where medium particles were found.

**Fig. 1** Staining spores with FDA and PI. **a–c** Spores after 24 h cultivation in complex medium. **d–f** Spore inoculum. **a, d** Overlay image; **b, e** green fluorescence channel; **c, f** red fluorescence channel



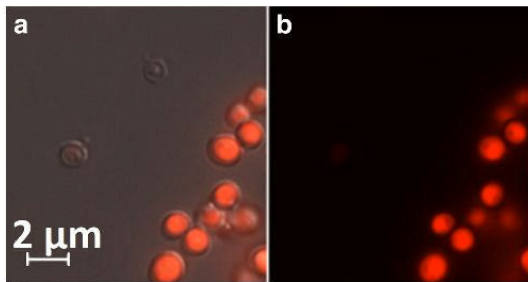


**Fig. 2** Microwave-treated spores. **a** Overlay image; **b** red fluorescence

Apart from PI-positive and FDA-positive spores, there was a PI-negative/FDA-negative population in the untreated and in the microwave-treated samples. This fact had already been suspected after staining development.

The shake flask sample after 8 h cultivation time was measured in triplicate, whereas one measurement is exemplarily shown in Fig. 3. The total spore concentration measured for the untreated and the microwave-treated samples was the same ( $101 \pm 12$  particles/ $\mu\text{l}$  vs.  $108 \pm 11$  particles/ $\mu\text{l}$ ). This total spore population could be divided into three different combinations of FDA positive/negative and PI positive/negative as Table 1 depicts. For the untreated as well as the microwave-

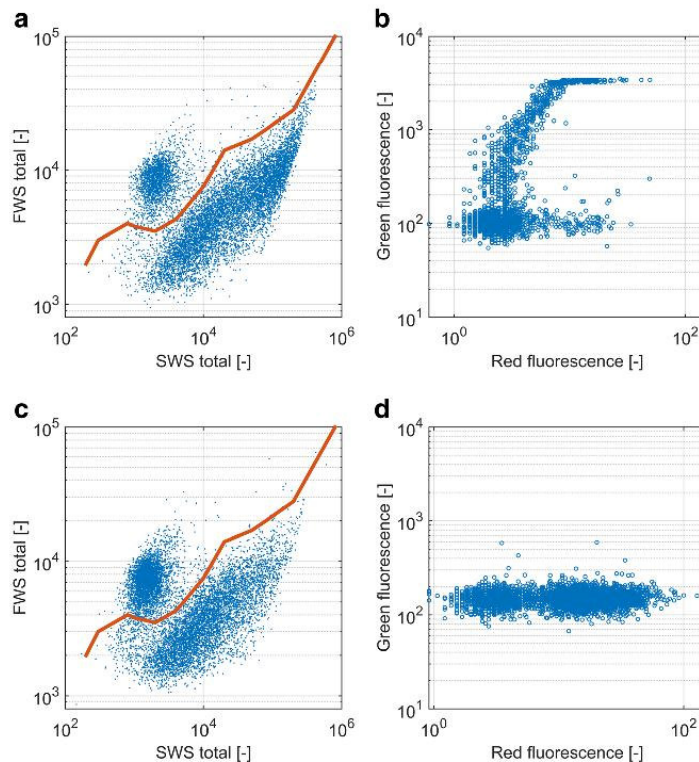
treated samples, the big population, neither stained by FDA nor PI, is apparent. In the untreated sample, the majority of spores is sorted into this group, whereas in the microwave-treated samples, most spores are PI positive.

**Dividing the fungal cells into four subpopulations**

Applying the above-described method on a combination of untreated and microwave-treated samples, a decision tree was established as shown in Fig. 4. With each step, the distinction of the spore population becomes more detailed. The analysis starts with a separation of spores and media particles/background via FWS/SWS. Furthermore, only particles classified as spores are investigated.

In a second step, the distinction between FDA-positive and FDA-negative spores is emphasized and classified as metabolically active or not metabolically active spores. The latter are investigated whether they are PI positive or PI negative. PI-positive spores are determined to be dead spores. The PI-negative subpopulation is further divided into quiescent spores and empty envelopes/residuals from spore inoculum depending on whether they are PI positive after microwaving or not.

**Fig. 3** Scatter plots of a FDA/PI-stained 8-h shake flask culture. An untreated sample is shown over total FWS vs. total SWS (**a**). The same can be seen for a microwave-treated sample (**c**). In the untreated sample (**b**) and microwave-treated sample (**d**), only particles shown above the line in **a** and **c** are shown



**Verification II: correlation of FDA-positive spores and CFU assay**

The common method to determine viable spores in spore inoculum is the CFU assay. A correlation of colony-forming units to metabolically active cells measured with the here presented method was almost 1 (see Fig. 6). The  $R^2$  of this linear fit was 0.8033.

**Kinetics of FDA**

FDA is known to show staining kinetics as the FDA is converted to fluorescein via esterases (Schnürer and Rosswall 1982). Hence, the green fluorescence is supposed to increase in metabolically active spores as more and more FDA is converted to fluorescein. This is shown in Fig. 7 where the development of green fluorescence level of 5 h-cultivated and FDA-stained spores over 19 min of FDA incubation is monitored. Green fluorescence levels increase with longer FDA incubation, and especially the number of spores at low fluorescence levels decreases.

This kinetic represents the conversion of FDA to fluorescein via esterase and therefore shows the activity of the enzyme. For a single measurement, incubation times of FDA should be held constant on a level of minutes as due to these developments in green fluorescence intensity during stain incubation, the comparability of measurements ought to be decreased.

**Further applications: monitoring of spore swelling**

The above-described method enables monitoring of the activation of spores from a dormant state and spore swelling in the first hours of cultivation. Figure 8 shows exemplarily a shake flask culture how metabolically active cells shift in total FWS and SWS signals to higher values. This reflects changes in spore size and surface character within the first hours of

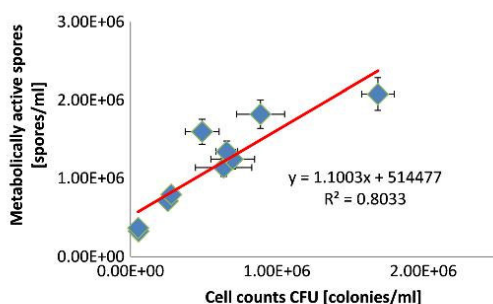


Fig. 6 Correlation of culturable cells determined via CFU and metabolically active cells measured using the flow cytometer

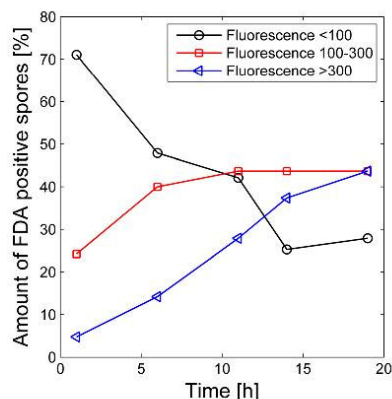


Fig. 7 Cell counts for different intensities in the green fluorescence channel for FDA-positive cells of a 5-h shake flask sample after 1 to 19 min incubation with FDA. Fluorescence lower than 100 is shown in black circles, fluorescence 100 to 300 units with red squares and higher 300 in blue triangles

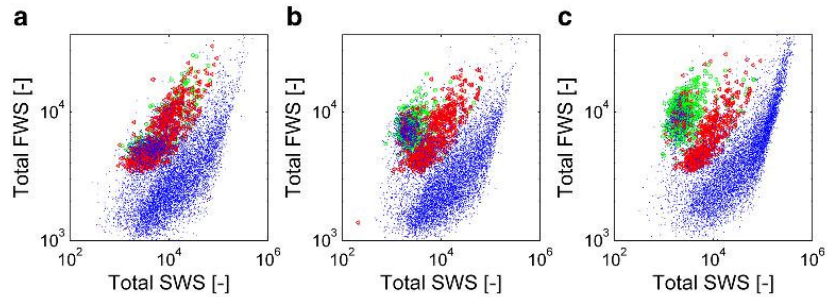
cultivation. Opposed to this, there is no change in total FWS and SWS for cells with compromised membrane integrity. While, at the beginning of the cultivation, both subpopulations have the same intensity in the FWS ( $7.44 \times 10^3 \pm 4.03 \times 10^3$  for metabolically active spores vs.  $7.05 \times 10^3 \pm 3.70 \times 10^3$  for dead spores), the average of metabolically active spores rises already after 2 h ( $7.76 \times 10^3 \pm 2.05 \times 10^3$ ) and even more after 7 h ( $1.02 \times 10^4 \pm 3.11 \times 10^3$ ).

Furthermore, parts of FDA-negative/PI-negative spores in untreated samples (quiescent population) increase in size similar to metabolically active spores. This can be seen in Fig. 8 where a part of the unstained population is overlaid by the cluster of FDA-positive spores. In contrast, FDA-negative/PI-negative spores do not change over time. This means that the quiescent subpopulation, which per se could not be plotted as its numbers are calculated (see Eq. 1), changes its size over cultivation time, meaning that the activation of metabolic activity is not necessarily crucial for spore swelling.

The sample shown in Fig. 8 shows a lot of FDA-negative/PI-positive spores. This is because half of spore inoculum was microwave treated before inoculation in order to artificially produce a culture with a high amount of dead spores.

Not only the mean size (mean FWS) changes for metabolically active cells but also the size distribution looks different for several samples in the first hours of cultivation. Figure 9 shows the distribution of metabolically active spores over the FWS for the same shake flask culture as presented in Fig. 8, just including an additional time point after 11 h. At the start of the cultivation, there are two peaks in the FWS plot in Fig. 9, which may represent two populations of metabolically active

**Fig. 8** The plot shows how spores swell over the first 7 h of cultivation. The green population (green rings) consists of metabolically active cells while dead cells are shown as red triangles. The blue dotted population equals particles not classified as spores and spores neither stained by FDA nor PI. **a** 0 h, **b** 1 h and **c** 7 h of cultivation



spores which are possibly single spores and two spores sticking together. After 2 h, all spores should be single as *Penicillium* is from the non-coagulating type (Metz and Kossen 1977) and start to swell which is reflected by one single population which has a higher FWS than the sample at 0 h. In the next hours until 11 h cultivation time, this population increases in the FWS and becomes less homogenous.

Homogeneity of spore swelling as a quality criterion could be extracted from a plot like it is shown in Fig. 9. The narrower the peak after some hours of swelling is, the more homogenous the spore size is. Homogenous spore size means a more parallel swelling of all spores in contrast to consecutive swelling.

**Discussion**

**Distinction of viable spores from non-viable subpopulations**

In most cases, biomass can be segregated in more subpopulations than simply the distinction of viable and non-viable cells

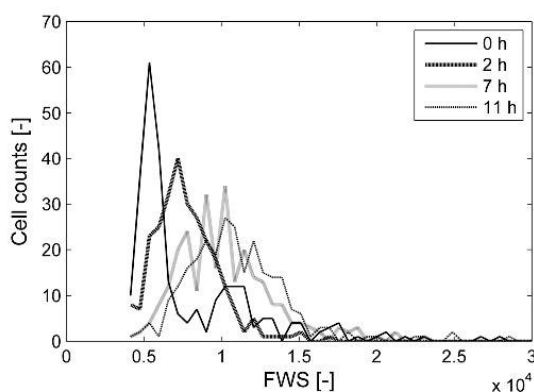


**Fig. 9** Distribution of FWS signal of metabolically active spores during spore swelling (0 h, 1 h, 7 h and 11 h)

(Bemey et al. 2007; Quiros et al. 2007; Ueckert et al. 1995). Also, it is not clearly defined which parameter in regard to viability is the most relevant for process performance. Is membrane permeability, which is measured via PI staining, crucial for the distinction of viable versus non-viable? In this case, structurally intact but not metabolically active cells which here are described by the quiescent subpopulation as well as the population of envelopes would be counted as viable. Thus, these two subpopulations would apart from metabolically active spores be relevant for process performance. Or is metabolic activity measured via FDA crucial for a cell to reproduce/germinate?

Due to the correlation of FDA-positive spores to CFU assay with a slope of approximately 1, the metabolic active subpopulation of spores is the only one which germinates—at least on agar plates. This means that esterase activity stands for germination potential, while swelling, which is reported to be a prior step to germination (d’Enfert 1997) and which could be detected via the combination of FWS and SWS, is not an indication for it. Hence, the big quiescent subpopulation which is swelling as well over time is not assumed to germinate.

**Quiescent or viable non-culturable?**

For multiple organisms, there exist publications about viable non-culturable populations which are defined as not growing on agar (Liao et al. 1999; Ueckert et al. 1995) but as metabolically active (Davis 2014; Ueckert et al. 1995). To our knowledge, such a subpopulation has not yet been described for filamentous fungi, although it has been mentioned for yeast (Hyka et al. 2010; Quiros et al. 2007). The population here referred to as “quiescent” does not fulfill all criteria of viable non-culturable cells as defined by Ueckert et al. (1995) and Davis (2014). This subpopulation is FDA negative and hence not metabolically active or—as actually measured via FDA—at least without esterase activity (Davis 2014; Ueckert et al. 1995). But for the other criterion concerning growth on agar (Liao et al. 1999; Ueckert et al. 1995), the here presented

quiescent population of spores could be defined as viable non-culturable.

Much more than categorizing the quiescent subpopulation to viable non-culturable cells, this spore subpopulation could simply be in a dormant state. Dormant spores are not metabolically active and are just activated when exposed to nutrients (Allen 1965; Gottlieb 1950). As described above, the quiescent spore subpopulations increases in FWS over the first hours of cultivation, as FDA-positive spores do. Spore swelling is seen as a step prior to spore germination itself. In this phase, the spore absorbs water to increase its inner water content (d'Enfert 1997; Fletcher and Morton 1970; Nielsen 1992), but also numerous metabolic activities are resumed (d'Enfert 1997; Nielsen 1992). The spores of the quiescent subpopulation might not yet be metabolically active enough to be highlighted via FDA staining, but are still swelling. But there needs to be another difference between FDA-positive and quiescent cells, as the latter do not seem to grow on agar plates.

When talking of this “quiescent population”, it has to be kept in mind that it is one of the four subpopulations which cannot be directly measured but is a population of spores deriving from the comparison of untreated and microwave-treated samples. Although both approaches for calculation for this subpopulation lead to the same numbers of size of this subpopulation, only cell sorting could definitely approve and describe this spore population.

#### Ratio of spore subpopulations and its relevance for the process

The extent of the four subpopulations is not as someone would expect. In context to the other four spore subpopulations, PI-positive cells are rather a small part of all spores. But the number of these spores with compromised membrane integrity increases with the age of the spore inoculum. Therefore, the amount of PI-positive spores per total spores can be seen as an additional marker for spore inoculum quality.

Another surprisingly small subpopulation includes the metabolically active spores. This is the case especially in contrast to the quiescent subpopulation and envelopes/residues. The definition of FDA-positive cells could be a factor for that. Gate setting for the distinction of FDA-positive from FDA-negative cells was done by using the cluster of medium particles as a limit. Decreasing this limit to a signal of the green fluorescence channel, which is not exceeded by microwave treated spores, would be an alternative, as dead cells should not display metabolic activity and could therefore be used as negative control. This would diminish the “quiescent population” albeit no clustering of cells is visible at this threshold. Furthermore, the metabolically active subpopulation correlated to CFU.

The last subpopulation which is neither staining FDA nor PI after microwave treatment was called envelopes/residues, as it is supposed to consist of a combination of DNA free cell envelopes and residues from conidiophores. This population makes a major proportion of the spores, and as these cells contain neither DNA nor esterase, the question arose whether it should be counted as spore subpopulation or if it would be better to exclude it as these cells do not seem to have any impact on process performance.

The knowledge on subpopulations is required to, e.g. discriminate between (temporarily) dormant and (durably) compromised spores. This information on the individual fractions is useful for, e.g. indicating high spore inoculum age or wrong storage conditions. Spore inocula of higher age germinate slower (Paul et al. 1993), which is also visible in a retarded transition from dormant to metabolically active state. This transition kinetics can be followed via repeated analysis with the flow cytometric FDA method over time.

#### Replacing CFU assay by the flow cytometric method

The here-developed method aims to be a faster and more informative alternative to the actual standard tool to determine spore inoculum quality—the CFU assay. The CFU targets the viable cell population (Brecuwer and Abec 2000) which is the process-relevant spore subpopulation (Posch and Herwig 2014). Usually, determining the number of non-viable spores in the sample is not part of conventional CFU assays, since this would require initial analysis of the spore inoculum suspension in a cell or particle counter (also most conventional devices would fail in performing this task due to the background of undissolved media particles). Typically, only the number of viable spores (colonies on agar) per milliliter of suspension is determined, and the inoculum concentration is adjusted to the intended value. The additional information on the fraction of dead spores, which may be an interesting quality parameter reflecting the “history” of the sample, is lost.

The information about dead spore concentration could also be provided by other methods than the FCM, for example microscopy in combination with viability stains. But microscopy is more tedious, more labour-intensive and commonly takes more time than FCM to access the same amount of cells (Veal et al. 2000).

The also labour-intensive CFU determination takes several days, while the here presented FCM method can be used in high throughput and provides results within hours—the measurement including incubation times of the stains only takes half an hour. The spores should be cultured for some hours in medium to quit the dormant state and hence to show metabolic activity which is accessible for FDA staining (Brul et al. 1997; Mesquita et al. 2013). Besides only measuring the amount of metabolically active cells after spores quitted the dormant state, the here presented method offers further information.

A big advantage is the possibility to monitor this process of metabolic activity activation and further spore swelling.

Furthermore, the growth behaviour in liquid cultures differs from growth on solid medium (Budde and Rasch 2001; Quiros et al. 2007). Therefore, a spore which might germinate in a bioreactor might not grow to hyphae when plated on agar—a further advantage of the here presented method compared to CFU.

Previous studies investigating the combination of FDA and FCM for spores of filamentous fungi could not find a connection of FDA staining to CFU (Brul et al. 1997). In contrast to this study, this correlation was found here for FDA-positive cells and viable cells determined via CFU. The difference in Brul et al. (1997) to the here presented study may be due to differences in gate setting, the use of fresh (not cultivated/activated) spores and the incubation time of FDA. Especially gate setting to distinguish FDA-positive and FDA-negative cells as well as the FDA incubation time may differ depending on the organism investigated. Thus, the transferability of the here-developed method to strains of some other filamentous fungi species has to be evaluated on a case-by-case basis. Still, viability staining in combination with FCM is seen as the more accurate method to determine the amount of growing cells than CFU (Budde and Rasch 2001; Quiros et al. 2007).

Altogether, the here-developed method does enable to re-define the term of spore inoculum quality. Spore inoculum quality now is not only the concentration of viable spores but also the amount of other subpopulations indicating the quality of the spore inoculum. Further, the definition of spore inoculum quality is extended to additional information about the viable cell population as spore swelling over process time and the activeness of esterases (increase of green fluorescence in a certain time period). The here-developed method enables the investigations of all these spore inoculum quality attributes on process performance.

#### Applicability of the method in process environment

The here presented method could be applied as a tool to measure and control the amount of viable spores which is inoculated in real time in the bioreactor. Furthermore, it could be used as an at-line tool to monitor spore swelling (size distribution of cells) and spore activation (metabolic activity) when awakening from the dormant state in the first hours of cultivation. Spore germination, whereof spore swelling is an essential step (d'Enfert 1997), influences process performance, as for example simultaneous germination showed to lead to narrow pellet size distribution (Meyerhoff and Bellgardt 1995). Therefore, the here presented method could be a promising process analytical tool (PAT) due to the initiatives of the food and drug administration, especially because there are already applications of FCM as an online method (Broger et al. 2011). Furthermore, information about spore

subpopulations, kinetics in spores quitting the dormant state and in spore swelling, may not only be monitored but also used for process control.

What this all amounts to is that the here-developed method which combines viability staining and FCM for filamentous fungi cultures in complex medium is a fast and easy tool which enables investigation and monitoring of spore inoculum quality. This is done at-line, in high throughput, and may be implemented as process analytical tool or could even be used for process control. In contrast to conventional methods for spore inoculum quality determination, it does not only provide information about the amount of viable spores but also yields much more in the description of spore subpopulations and the kinetics of spore swelling. Therefore, morphological information gained by multiparametric data from the CytoSense flow cytometer is combined to a metabolic activity investigated via FDA staining. The imaging tool in the flow cell may be used to evaluate this method.

#### Compliance with ethical standards

**Conflict of interest** The authors declare that they have no competing interests.

**Funding** This study was funded by the Christian Doppler Gesellschaft (grant number 171).

**Ethical approval** This article does not contain any studies with human participants or animals performed by any of the authors.

#### References

- Allen PJ (1965) Metabolic aspects of spore germination in fungi. *Annu Rev Phytopathol* 3:313–342
- Bartnicki-Garcia S (1968) Cell wall chemistry, morphogenesis, and taxonomy of fungi. *Annu Rev Microbiol* 22:87–108
- Berney M, Hammes F, Bosshard F, Weilenmann HU, Egli T (2007) Assessment and interpretation of bacterial viability by using the LIVE/DEAD BacLight Kit in combination with flow cytometry. *Appl Environ Microbiol* 73:3283–3290. doi:10.1128/AEM.02750-06
- Binder U, Chu M, Read ND, Marx F (2010) The antifungal activity of the *Penicillium chrysogenum* protein PAF disrupts calcium homeostasis in *Neurospora crassa*. *Eukaryot Cell* 9:1374–1382. doi:10.1128/EC.00050-10
- Breeuwer P, Abec T (2000) Assessment of viability of microorganisms employing fluorescence techniques. *Int J Food Microbiol* 55:193–200
- Broger T, Odermatt RP, Huber P, Sonnleitner B (2011) Real-time on-line flow cytometry for bioprocess monitoring. *J Biotechnol* 154:240–247. doi:10.1016/j.jbiotec.2011.05.003
- Brul S, Nussbaum J, Diebandhoesing SK (1997) Fluorescent probes for wall porosity and membrane integrity in filamentous fungi. *J Microbiol Methods* 28:169–178
- Budde BB, Rasch M (2001) A comparative study on the use of flow cytometry and colony forming units for assessment of the antibacterial effect of bacteriocins. *Int J Food Microbiol* 63:65–72

- Bunthof CJ, van den Braak S, Breeuwer P, Rombouts FM, Abec T (1999) Rapid fluorescence assessment of the viability of stressed *Lactococcus lactis*. *Appl Environ Microbiol* 65:3681–3689
- d'Enfert C (1997) Fungal spore germination: insights from the molecular genetics of *Aspergillus nidulans* and *Neurospora crassa*. *Fungal Genet Biol* 21:163–172
- Davis C (2014) Enumeration of probiotic strains: review of culture-dependent and alternative techniques to quantify viable bacteria. *J Microbiol Methods* 103:9–17. doi:10.1016/j.mimet.2014.04.012
- Deere D, Shen J, Vesey G, Bell P, Bissinger P, Veal D (1998) Flow cytometry and cell sorting for yeast viability assessment and cell selection. *Yeast* 14:147–160. doi:10.1002/(SICI)1097-0061(19980130)14:2<147::AID-YEA207>3.0.CO;2-L
- Diaz M, Herrero M, García LA, Quirós C (2010) Application of flow cytometry to industrial microbial bioprocesses. *Biochem Eng J* 48:385–407
- Ehgartner D, Sagmeister P, Herwig C, Wechselberger P (2015) A novel real-time method to estimate volumetric mass biodecay based on the combination of dielectric spectroscopy and soft-sensors. *J Chem Technol Biotechnol* 90:262–272
- Fletcher J, Morton G (1970) Physiology of germination of *Penicillium griseofulvum* conidia. *Trans Brit Mycol Soc* 54:65–81
- Gottlieb D (1950) The physiology of spore germination in fungi. *Bot Rev* 16:229–257
- Hashemi N, Erickson JS, Golden JP, Jackson KM, Ligler FS (2011) Microflow cytometer for optical analysis of phytoplankton. *Biosens Bioelectron* 26:4263–4269. doi:10.1016/j.bios.2011.03.042
- Hua SS, Brandt MT, Hemlem B, Eng JG, Sarreal SB (2011) Fluorescent viability stains to probe the metabolic status of aflatoxigenic fungus in dual culture of *Aspergillus flavus* and *Pichia anomala*. *Mycopathologia* 171:133–138. doi:10.1007/s11046-010-9352-z
- Hyka P, Züllig T, Ruth C, Looser V, Meier C, Klein J, Melzoch K, Meyer HP, Glieder A, Kovar K (2010) Combined use of fluorescent dyes and flow cytometry to quantify the physiological state of *Pichia pastoris* during the production of heterologous proteins in high-cell-density fed-batch cultures. *Appl Environ Microbiol* 76:4486–4496. doi:10.1128/AEM.02475-09
- Hyka P, Lickova S, Pribyl P, Melzoch K, Kovar K (2013) Flow cytometry for the development of biotechnological processes with microalgae. *Biotechnol Adv* 31:2–16. doi:10.1016/j.biotechadv.2012.04.007
- Jones KH, Senft JA (1985) An improved method to determine cell viability by simultaneous staining with fluorescein diacetate-propidium iodide. *J Histochem Cytochem* 33:77–79
- Kell DB, Kaprelyants AS, Weichart DH, Harwood CR, Barer MR (1998) Viability and activity in readily culturable bacteria: a review and discussion of the practical issues. *Antonie Van Leeuwenhoek* 73:169–187
- Kumar N, Borth N (2012) Flow-cytometry and cell sorting: an efficient approach to investigate productivity and cell physiology in mammalian cell factories. *Methods* 56:366–374. doi:10.1016/j.ymeth.2012.03.004
- Langemann T, Koller VJ, Muhammad A, Kudela P, Mayr UB, Lubitz W (2010) The bacterial ghost platform system: production and applications. *Bioengineered bugs* 1:326–336. doi:10.4161/bbug.1.5.12540
- Lein J (1986) The Panlabs penicillin strain improvement program. In: Vanek Z, Hostalek Z (eds) Overproduction of microbial metabolites. Butterworths, Boston, pp 105–139
- Liao RS, Rennie RP, Talbot JA (1999) Assessment of the effect of amphotericin B on the vitality of *Candida albicans*. *Antimicrob Agents Chemother* 43:1034–1041
- Martin JF, Nicolas G, Villanueva JR (1973) Chemical changes in the cell walls of conidia of *Penicillium notatum* during germination. *Can J Microbiol* 19:789–796
- Mesquita N, Portugal A, Pinar G, Loureiro J, Coutinho AP, Trovao J, Nunes I, Botelho ML, Freitas H (2013) Flow cytometry as a tool to assess the effects of gamma radiation on the viability, growth and metabolic activity of fungal spores. *Int Biodeter Biodegr* 84:250–257
- Metz B, Kossen NWF (1977) The growth of molds in the form of pellets—a literature review. *Biotechnol Bioeng* 19:781–799
- Meyerhoff J, Bellgardt K (1995) A morphology-based model for fed-batch cultivations of *Penicillium chrysogenum* growing in pellet form. *J Biotechnol* 38:201–217
- Nielsen J (1992) Modelling the growth of filamentous fungi. *Adv Biochem Eng Biotechnol* 46:187–223
- O'Brien MC, Bolton WE (1995) Comparison of cell viability probes compatible with fixation and permeabilization for combined surface and intracellular staining in flow cytometry. *Cytometry* 19:243–255. doi:10.1002/cyto.990190308
- Paul GC, Kent CA, Thomas CR (1993) Viability testing and characterization of germination of fungal spores by automatic image analysis. *Biotechnol Bioeng* 42:11–23
- Posch AE, Herwig C (2014) Physiological description of multivariate interdependencies between process parameters, morphology and physiology during fed-batch penicillin production. *Biotechnol Prog* 30:689–699. doi:10.1002/btpr.1901
- Posch AE, Spadiut O, Herwig C (2012) Switching industrial production processes from complex to defined media: method development and case study using the example of *Penicillium chrysogenum*. *Microb Cell Fact* 11:88. doi:10.1186/1475-2859-11-88
- Prigione V, Filippello Marchisio V (2004) Methods to maximise the staining of fungal propagules with fluorescent dyes. *J Microbiol Methods* 59:371–379. doi:10.1016/j.mimet.2004.07.016
- Quiros C, Herrero M, García LA, Diaz M (2007) Application of flow cytometry to segregated kinetic modeling based on the physiological states of microorganisms. *Appl Env Microbiol* 73:3993–4000. doi:10.1128/AEM.00171-07
- Rieseberg M, Kasper C, Reardon KF, Scheper T (2001) Flow cytometry in biotechnology. *Appl Microbiol Biotechnol* 56:350–360
- Rotman B, Papermaster BW (1966) Membrane properties of living mammalian cells as studied by enzymatic hydrolysis of fluorogenic esters. *Proc Natl Acad Sci U S A* 55:134–141
- Schnürer J, Rosswall T (1982) Fluorescein diacetate hydrolysis as a measure of total microbial activity in soil and litter. *Appl Env Microbiol* 43:1256–1261
- Sundstrom H, Wallberg F, Ledung E, Norrman B, Hewitt CJ, Enfors SO (2004) Segregation to non-dividing cells in recombinant *Escherichia coli* fed-batch fermentation processes. *Biotechnol Lett* 26:1533–1539. doi:10.1023/B:BILE.0000044458.29147.75
- Ueckert J, Breeuwer P, Abec T, Stephens P, von Caron GN, ter Steeg PF (1995) Flow cytometry applications in physiological study and detection of foodborne microorganisms. *Int J Food Microbiol* 28:317–326
- Veal DA, Deere D, Ferrari B, Piper J, Attfield PV (2000) Fluorescence staining and flow cytometry for monitoring microbial cells. *J Immunol Methods* 243:191–210
- Vermes I, Haanen C, Reutelingsperger C (2000) Flow cytometry of apoptotic cell death. *J Immunol Methods* 243:167–190
- Walther TC, Brickner JH, Aguilar PS, Bernaldes S, Pantoja C, Walter P (2006) Eisosomes mark static sites of endocytosis. *Nature* 439:998–1003. doi:10.1038/nature04472

**Supplementary Material**

**At-line determination of spore inoculum quality in *Penicillium chrysogenum* bioprocesses**

Daniela Ehartner<sup>1,2</sup>, Christoph Herwig<sup>1,2\*</sup> and Lukas Neutsch<sup>2</sup>

\*to whom the correspondence should be addressed to

<sup>1</sup> CD Laboratory on Mechanistic and Physiological Methods for Improved Bioprocesses, TU Wien,  
Gumpendorferstrasse 1a/166, 1060 Vienna, Austria

<sup>2</sup> Research Area Biochemical Engineering, Institute of Chemical Engineering, TU Wien, Gumpendorferstrasse  
1a/166, 1060 Vienna, Austria

Corresponding author:

christoph.herwig@tuwien.ac.at

Tel (Office): +43 1 58801 166400

Fax: +43 1 58801 166980

Table S1: Overview over targets of investigated fluorescence stains and whether medium particles, viable and non-viable spores contain these targets

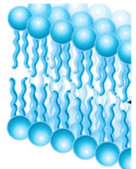
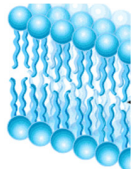
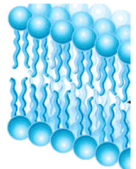
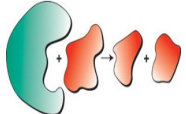
	SPORES (viable)	SPORES (non-viable)	MEDIUM PARTICLES
DNA			
Glycans			
Lipids			
Enzymes			

Table S2: Staining performance of investigated stains. (x does not stain at all, o partially staining according to viability, ✓ staining, N.A. not investigated)

Stain	Untreated spores	Microwaved cells	Medium
DAPI	✓	✓	✓
H 33342	✓	✓	✓
Lectines	fGNL	N.A.	✓
	fSTL	N.A.	✓
	fWGA	N.A.	✓
	fLCA	N.A.	✓
SYTO9	✓	✓	✓
FM 464	x	N.A.	N.A.
Calcofluor	✓	N.A.	✓
PI	o	✓	x
Metabolic stain	o	x	x

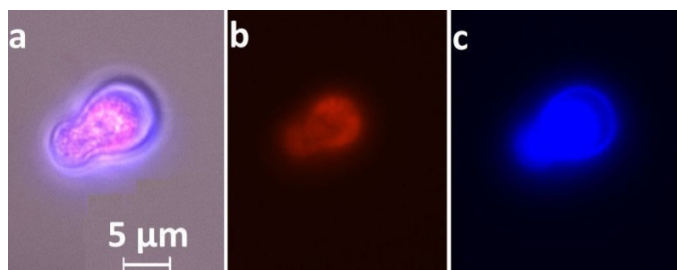


Figure S1: Spore stained with PI and DAPI. a) overlay image, b) red fluorescence, c) blue fluorescence

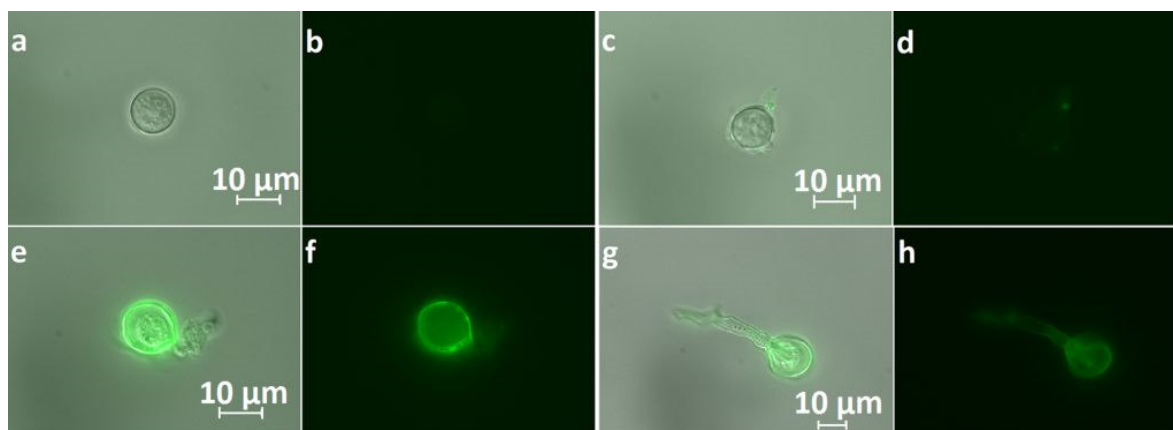


Figure S2: Lectin staining: LCA (a, b), GNL (c, d), STL (e, f) and WGA (g, h). a, c, e and g are overlay pictures while b, d, f and h show green fluorescence

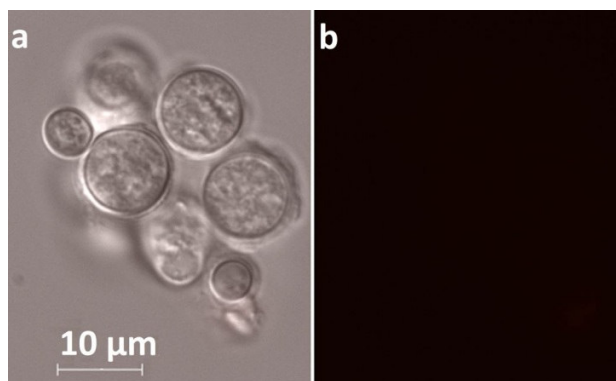


Figure S3: Spores stained with FM464. a) overlay image, b) red fluorescence

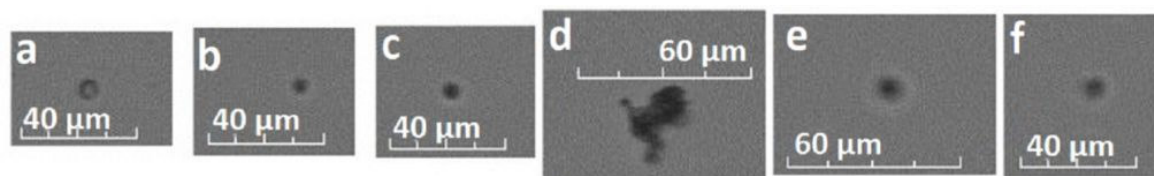
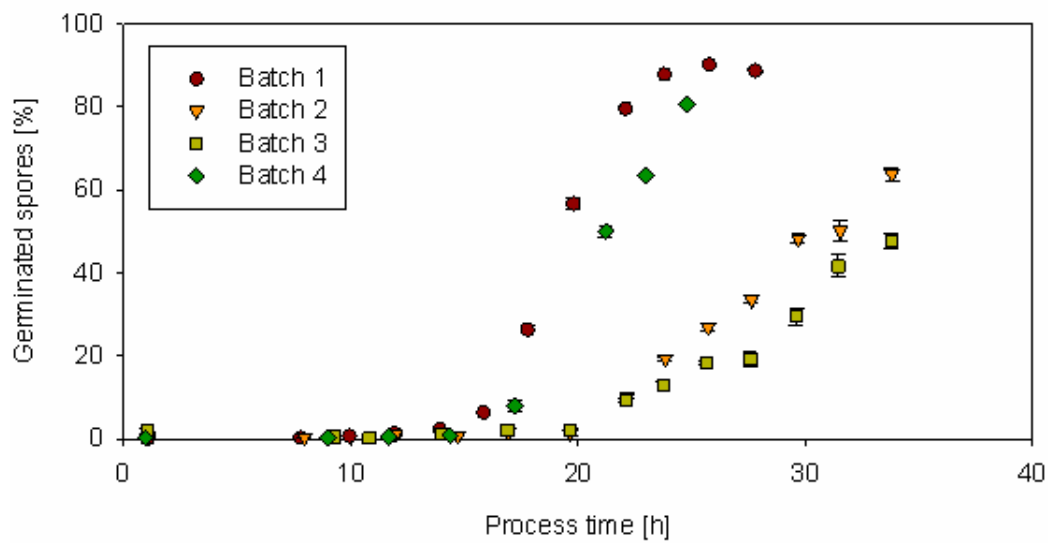


Figure S4: Pictures taken in the flow cell of the flow cytometer while measuring the 8h shake flask culture shown in Figure 3. While a-d were pictures from an untreated sample, e-f origin from a sample after microwave treatment: a) FDA positive spore, b) PI positive spore, c) spore FDA/PI negative, d) medium particle, e) PI positive spore, f) spore FDA/PI negative

## At-line determining spore germination of *Penicillium chrysogenum* bioprocesses in complex media

Ehgartner, D., Fricke, J., Schröder, A., & Herwig, C., Applied microbiology and biotechnology, 100(20), 8923-8930 (2016)





## At-line determining spore germination of *Penicillium chrysogenum* bioprocesses in complex media

Daniela Ehgartner<sup>1,2</sup> · Jens Fricke<sup>1,2</sup> · Andreas Schröder<sup>1,2</sup> · Christoph Herwig<sup>1,2</sup>

Received: 7 April 2016 / Revised: 28 July 2016 / Accepted: 3 August 2016 / Published online: 24 August 2016  
© The Author(s) 2016. This article is published with open access at Springerlink.com

**Abstract** Spore inoculum quality in filamentous bioprocesses is a critical parameter associated with viable spore concentration (1) and spore germination (2). It influences pellet morphology and, consequently, process performance. The state-of-the-art method to measure viable spore concentration is tedious, associated with significant inherent bias, and not applicable in real-time. Therefore, it is not usable as process analytical technology (PAT). Spore germination has so far been monitored using image analysis, which is hampered by complex medium background often observed in filamentous bioprocesses. The method presented here is based on the combination of viability staining and large-particle flow cytometry which enables measurements in real-time and hence aims to be applicable as a PAT tool. It is compatible with the complex media background and allows the quantification of metabolically active spores and the monitoring of spore germination. A distinction of germinated spores and not germinated spores was based on logistic regression, using multiparametric data from flow cytometry. In a first step, a significant correlation between colony-forming unit (CFU) counts and viable spore concentration (1) in an industrially relevant model bioprocess was found. Spore germination (2)

was followed over the initial process phase with close temporal resolution. The validation of the method showed an error below 5 %. Differences in spore germination for various spore inocula ages and spore inoculum concentrations were monitored. The real-time applicability of the method suggests the implementation as a PAT tool in filamentous bioprocesses.

**Keywords** Filamentous fungi · Flow cytometry · Spore germination · Spore viability · Process analytical technology

### Introduction

Spore inoculum quality in filamentous bioprocesses is a critical parameter associated with viable spore concentration and spore germination (Nielsen and Krabben 1995). It influences pellet morphology and, consequently, process performance (Paul et al. 1993; Smith and Calam 1980; Tucker and Thomas 1994). An essential step before inoculation is the determination of the viable spore concentration in order to apply quality control and decrease batch-to-batch variability. The state-of-the-art method to investigate this variable is colony-forming unit (CFU) determination, which assesses the number of viable/germinating spores. This procedure is tedious, associated with significant inherent bias, and not applicable in real-time.

Previously, an at-line method based on a flow cytometer (FCM) and viability staining to investigate the concentration of viable spores has been developed. This method is based on the metabolic activity of viable spores and showed a correlation to CFU (Ehgartner et al. 2016). But, also spore germination is an important factor linked to spore quality. Germination is especially crucial in the CFU method, as only spores growing hyphae can form colonies. Therefore, monitoring of spore germination is not only necessary to investigate further spore

**Electronic supplementary material** The online version of this article (doi:10.1007/s00253-016-7787-y) contains supplementary material, which is available to authorized users.

✉ Christoph Herwig  
christoph.herwig@tuwien.ac.at

<sup>1</sup> CD Laboratory on Mechanistic and Physiological Methods for Improved Bioprocesses, Vienna University of Technology, Gumpendorferstrasse 1a/166, 1060 Vienna, Austria

<sup>2</sup> Institute of Chemical Engineering, Research Area Biochemical Engineering, Vienna University of Technology, Gumpendorferstrasse 1a/166, 1060 Vienna, Austria

quality attributes, but can also be used as a validation of the aforementioned method. Quality attributes connected to spore germination are not only the amount of germinating spores but also how long spores need for germination and whether all spores germinate at the same time or not. Spore swelling and spore germination have so far been monitored using microscopy (Demming et al. 2011; Oh 1996; Paul et al. 1993), which is hampered by complex medium background often observed in filamentous bioprocesses (Posch et al. 2012).

Germination was reported to be influenced by a variety of parameters such as spore age (Paul et al. 1993), medium composition (Demming et al. 2011; Fletcher and Morton 1970; Paul et al. 1993), spore concentration (Demming et al. 2011; Fletcher and Morton 1970), temperature (Demming et al. 2011), pH (Demming et al. 2011) and storage conditions of the spore inoculum (Gottlieb 1950).

Fluorescence stains indicating metabolic activity in the cell showed to reflect transitions to other physiological and morphological phases (Bradner and Nevalainen 2003; Dorsey et al. 1989). Metabolic activity during germination in filamentous fungi was reported to increase (Gottlieb 1950). Fluorescein diacetate (FDA) is converted to a fluorescent product (fluorescein) via esterases and hence is a stain marking metabolic activity in cells (Rotman and Papermaster 1966). Therefore, it could be applied not only to stain viable cells (Ehgartner et al. 2016) but also to indicate spore germination.

The study described here is based on advanced flow cytometry, providing multiple data points per channel per particle. This signal or so-called pulse shape is achieved for both scatter channels as well as green, orange and red fluorescence channels. Common flow cytometers provide only one value (integrated signal) each for forward scatter (FWS), sideward scatter (SWS) and fluorescence channels for each particle (Diaz et al. 2010; Hyka et al. 2013; Pereira and Ebecken 2011; Rieseberg et al. 2001). So far, this additional information provided by the pulse shape has been used in an aquatic environment (Pereira and Ebecken 2011; Thyssen et al. 2011) and for urine particles (Delanghe et al. 2000). Pulse shapes give access to additional morphologic information of the cell and therefore could be applied to detect spore germination.

The feature of image acquisition in the flow cytometer facilitates method development and method validation. Thereby, flow cytometric data is connected to a picture of the cell. This picture taken in the flow cell replaces a separate microscopic investigation and has the advantage of being usable in higher throughput (George et al. 2004; Pereira and Ebecken 2011).

The goal of this study is to develop a tool to at-line monitor spore germination of *Penicillium chrysogenum* in the bioreactor. Therefore, a combination of viability staining and advanced flow cytometry is used. The viability stain FDA should be applied to distinguish viable spores from other spore

sub-populations and complex media background. Furthermore, data from pulse shapes of fluorescence and light scatters is used to distinguish non-germinated and germinated spores. Thereby, a tool applicable at-line and which hence is adaptable as process analytical technology (PAT) should be provided.

## Material and Methods

### Strain

Spore suspensions of the P-14 *P. chrysogenum* candidate strain for penicillin production descending from the P-2 *P. chrysogenum* candidate strain (American Type Culture Collection with the access number ATCC 48271) (Lein 1986) were provided by Sandoz GmbH (Kundl, Austria) and used for all experiments.

### Bioreactor cultivations

Bioreactor cultivations were conducted in 10 and 20 l Techfors reactors (Infors, Bottmingen, Switzerland).

Fermentation temperature was kept at 25 °C via cooling/heating jacket. Aeration was controlled at 1 vvm in batch with mass flow controllers (Vögtlin, Aesch, Switzerland). Dissolved oxygen concentration was measured using a dissolved oxygen probe (Hamilton, Bonaduz, Switzerland) and maintained between 40 and 90 % by adjustment of the stirrer speed. The initial stirring speed was 320 rpm and the pressure was constantly held at 1 bar. pH was measured using a pH probe (Hamilton, Bonaduz, Switzerland).

The cultivations were carried out in batch mode on a complex bioreactor medium similar as described elsewhere (Posch et al. 2012). The pH was not controlled. The end of the batch was defined as an increase in pH of 0.5 by convention.

The culture was inoculated with  $2 \cdot 10^8$ – $2 \cdot 10^9$  spores/l cultivation medium. Spores of different ages (2–9 months) were used.

### Shake flask cultivations

Shake flask cultivations were conducted at 25 °C and 300 rpm in a Multitron Shaker (Infors, Bottmingen, Switzerland) on the same complex medium as used for bioreactor cultivations (but without antifoam). Five hundred-milliliter shake flasks were filled with 30 ml of sterile medium and were inoculated with  $2 \cdot 10^9$  spores/l cultivation medium.

**Sample preparation**

Samples from shake flasks or bioreactor were diluted 1:10 into phosphate-buffered saline (50 g/l of 2.65 g/l CaCl<sub>2</sub> solution, 0.2 g/l KCl, 0.2 g/l KH<sub>2</sub>PO<sub>4</sub>, 0.1 g/l MgCl \* 6 H<sub>2</sub>O, 8 g/l NaCl and 0.764 g/l Na<sub>2</sub>HPO<sub>4</sub> + 2 H<sub>2</sub>O) and stained with PI (Sigma Aldrich, St. Louis, Missouri/USA; 20 mM stock dissolved in DMSO, diluted to a final concentration of 20 μM) and FDA (Sigma Aldrich, St. Louis, Missouri, USA; stock solution of 5 g/l dissolved in acetone) was added to a final concentration of 50 mg/l. After an incubation of 10 min, the sample was further diluted (1:50 in the same buffer) for flow cytometric analysis.

**CFU determination**

For CFU determination, the shake flask samples were diluted in a sterile solution of 8.5 g/l sodium chloride and 1 ml/l Tween 80 and plated on agar plates. The medium of the latter resembled the one used for shake flask cultivations and included 25 g/l agar agar.

**Flow cytometry**

A CytoSense flow cytometer (CytoBuoy, Woerden, Netherlands) with two FWS, one SWS and three fluorescence channels (yellow, orange, red) was used for single-cell analysis. The implemented laser had a wavelength of 488 nm. The configuration of the filter set was 515–562 ± 5 nm for the green/yellow fluorescence channel (used for FDA) and 605–720 ± 5 nm for the red fluorescence channel (used for PI). The device was equipped with a PixeLINK PL-B741 1.3MP monochrome camera for in flow image acquisition. For data treatment, the software CytoClus (CytoBuoy, Woerden, Netherlands) and a custom-programmed Matlab 2009a script (MathWorks, Natick, Massachusetts, USA) were used.

**Results**

**Viable spore determination**

In order to distinguish FDA positive (metabolically active/viable) spores from other spore sub-populations such as dead spores (see Ehgartner et al. (2016) for more detailed information) and media background, gate setting was conducted. Gates/boards were set by measuring spores cultivated in filtrated medium, microwave treated spores and complex medium without spores in order to achieve a good distinction.

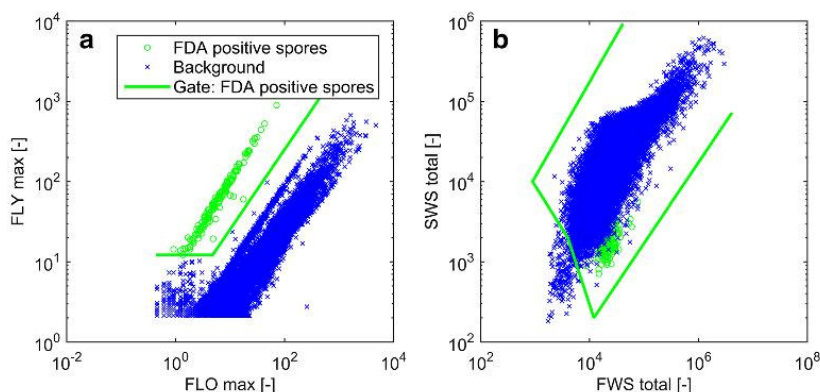
The discrimination of these FDA positive spores from other particles was based on maximum (max) fluorescence yellow (FLY) and fluorescence orange (FLO) as well as on FWS total and SWS total, as shown in Fig. 1. FLY and FLO were applied to distinguish green fluorescent from not or red fluorescent spores and media particles. FWS and SWS were used in addition to exclude any green fluorescent particles smaller than the spores. Only particles found in both gates (in-between the green boarders in Fig. 1a, b) were classified as FDA-positive spores, while particles found in one but not the other gate were not counted. The distinction of these spores from other particles enabled the quantification of this population.

Various spore inocula were measured with the FCM after 1 h of shake flask cultivation and the FDA-positive spore population was quantified. The same inocula (without previous cultivation) were plated on agar to result in a CFU count. The correlation of these showed to have a slope of almost 1 and an R<sup>2</sup> of 0.97 (see Fig. 2). This demonstrates that the FCM method determines the amount of spores which germinate on agar plates and hence are defined as viable.

**Distinguishing germinated from non-germinated spores**

The FCM applied here provides multiple data points per channel and particle, the so-called pulse shapes. These pulse

**Fig. 1** Gate setting to discriminate FDA-positive spores (green circles) from media background and other spore sub-populations (blue crosses). The classification was done via intensities in FLY and FLO max (a) as well as via FWS and SWS total (b)



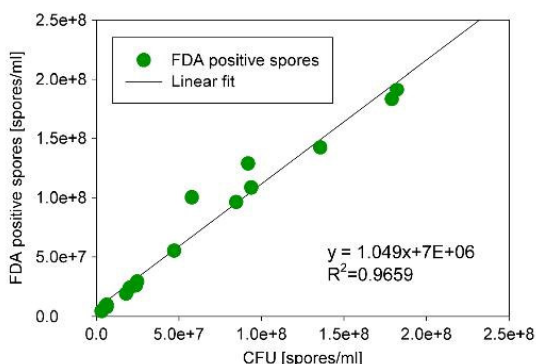


**Fig. 2** Correlation of FDA-positive spores and CFU counts. The slope of the linear fit was almost 1 with an  $R^2$  of 0.97

shapes differ for round (Fig. 3a) and germinated spores (Fig. 3b).

Furthermore, the FCM makes it possible to photograph particles in the flow cell and to connect these pictures to FCM data. This feature was applied to create a data set allowing a statistical-based distinction of germinated and non-germinated spores. Different states of germination were distinguished on pictures as shown in Fig. 4.

According to literature, a spore can be defined as germinated when the germ tube has the length of one-half of the biggest dimension of the spore (Paul et al. 1993). In the study conducted here, spores as shown in Fig. 4a were defined to be non-germinated. Figure 4a represents a germinating spore which is in a state between being non-germinated and germinated. However, spores like the aforementioned one were determined to belong to the group of germinated spores. Spores resembling the ones in Fig. 4c–e were categorized as germinated.

In the fast particle flow through the system, spores and hyphae are (almost) always aligned the same way in the flow cell. The flow direction in Fig. 4 was from right to left. Obviously, the spores are oriented into the direction of the flow.

A logistic regression was applied on the data set based on shake flask samples, following the goal to distinguish the non-

germinated spores as categorized before from the germinated ones, using data from FWS, SWS and fluorescence channels. The logistic regression revealed the following parameters to have a significant influence ( $p < 0.05$ ) on the distinction of non-germinated and germinated spores: FWS length (length of the FWS signal in  $\mu\text{m}$ ), FLY max (maximum of FLY signal), FLY inertia, FLY fill factor (indicates the solidity of the signal) and the coefficient of variation of the root mean squared error (CVRMSE) (also see Eq. 1 and Table 1). The latter parameter was calculated in Matlab (MathWorks, Natick, Massachusetts, USA). Therefore, a Gaussian curve was fitted to the FWS signal and the CVRMSE was applied as a quality factor of the fit. The other parameters were determined via CytoClus (CytoBuoy, Woerden, Netherlands). FLY inertia describes where the majority of the area beneath the curve is located in reference to the signal. Low inertia shows that a big part of the area below the signal curve is located near the centre of the signal curve. High inertia values indicate that a larger part of the signal area is near the edges of the signal.

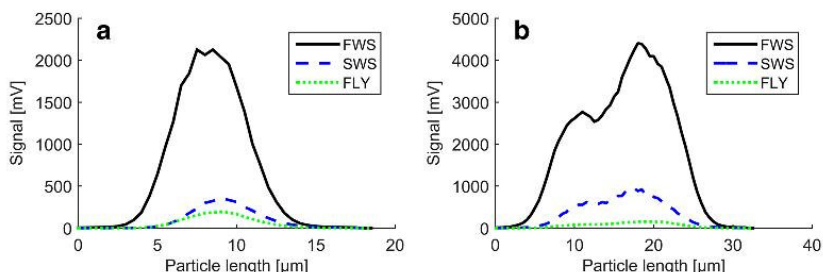
$$\ln \frac{p(\text{non-germinated spore})}{p(\text{germinated spore})} = a_0 + a_1 * \text{FWS length} + a_2 * \text{CVRMSE} + a_3 * \text{FLY max} + a_4 * \text{FLY inertia} + a_5 * \text{FLY fillfactor} \quad (1)$$

The coefficients in Eq. 1 are similar for different sensitivity levels (see Table 1), especially concerning the FWS. Different levels of sensitivities of FLY had to be used for measurements over process time in order to extract the highest amount of information possible from each sample. During the first 12–16 h, a higher sensitivity was needed than later, during spore germination, when metabolic activity was high and would hence have resulted in a saturated signal.

### Validation via image in flow

The method was applied on samples after 14, 20 and 24 h of bioreactor cultivation, which represented different stages in the germination process. After 14 h of cultivation, the spores were swollen, but not yet germinated. After 20 h of

**Fig. 3** FWS, SWS and FLY signals of a non-germinated (a) and a germinated spore (b)



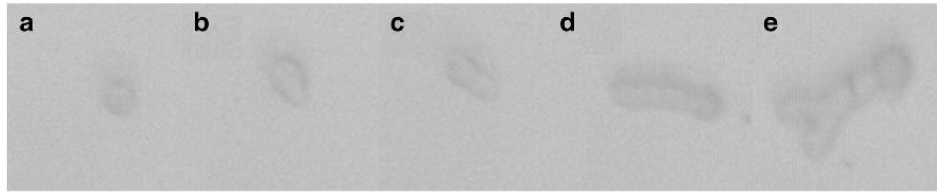


**Fig. 4** Spores and hyphae in the flow cell. **a** Non-germinated spore. **b** Germinating spore. **c** Germinated spore. **d** Unbranched hyphae. **e** Branched hyphae

cultivation, germination took place. After 24 h, the majority of spores was germinated and a high amount of unbranched hyphae and some branched hyphae were already found.

In order to validate the method, photographs from the flow cell were used to classify spores manually. By comparing the classification based on photographs with the classification via logistic regression, the method was evaluated. Table 2 shows the results of the evaluation for the measurement of FLY sensitivity level 65. The results were similar for the FLY sensitivity level 50 and are thus not shown.

Comparing the photos from the flow cell with the classification based on the logistic regression, weaknesses of the method were revealed:

- 3.2 % of the non-germinated spores were wrongly classified as germinated in cases when there were particles from the medium sticking on the spore or when a media particle was very close to the spore while passing the flow cell (see Fig. S1a in the supplementary material).
- Germinated spores and unbranched hyphae which flow through the cell upright were wrongly classified as non-germinated (see Fig. S1 in the supplementary material compared to the bottom photo in Fig. 3). This is caused by the fact that spores floating upright through the flow cell have a FWS signal similar to a Gaussian curve. On average 2.9 % of germinated spore were wrongly determined to be germinated due to different alignment.

As stated above, germinating spores are seen to be in a state between being non-germinated and germinated spores. For method development this sub-population was categorized as

**Table 1** Estimated coefficients for two sensitivity levels

	FLY sensitivity level of 50	FLY sensitivity level of 65
$a_0$	28.31	29.01
$a_1$	-0.337	-0.346
$a_2$	-0.184	-0.106
$a_3$	-0.006	-0.001
$a_4$	54.05	40.35
$a_5$	-59.54	-52.44

germinated spores. If the allocation of germinating spores to both classes—non-germinated and germinated—was accepted, the wrong negative counts in Table 2 would decrease significantly. The errors of the method for different sampling points during the cultivation were calculated without considering the classification of these spores being in-between non-germinated and germinated. These are shown in Table 3.

The error rate of 7.5 % in the 20-h sample when measured at a FLY sensitivity level of 65 underlines the importance to choose the right sensitivity level. During germination the metabolic activity in the spores is high. Therefore, the FLY signal is saturated leading to a wrong FLY max. Although FLY is often saturated when germination is finished, the classification into non-germinated vs. germinated spores has proven to be better. This is based on the increase of the hyphae length which further decreases the CVRMSE. In cases where the right sensitivity level had been chosen, the error of classification was below 5 %.

**Application of the method in bioreactor cultivations**

*Size distribution and distribution of green fluorescence over process time*

The developed method to classify spore germination was applied on the FDA-positive spores in bioreactor cultivations. Total spore size (measured via FWS) and green fluorescence increased over process time. At approximately 25- $\mu$ m spore

**Table 2** Contingency table for the evaluation of the spore germination method for samples measured at FLY sensitivity level 65

Cultivation time [h]	TP	FP	TN	FN	Total
14	0	1	134	0	135
20	114	2	37	20	173
24	124	1	6	4	135

Shown are the numbers of true positive (TP, germinated spores which were classified as germinated spores), false positive (FP, germinated spores not categorized as germinated), true negative (TN, non-germinated spores categorized as non-germinated) and false negative (FN, non-germinated spores categorized as germinated). Furthermore, the total amount of investigated spores is shown. Samples of three different cultivation times were evaluated

**Table 3** Error of the method to monitor spore germination

Cultivation time [h]	Error [%]	
	Sensitivity level 50	Sensitivity level 65
14	4.2	0.7
20	2.6	7.5
24	3.7	3.7

diameter, the spores germinated as the transition of round to germinated spores in Fig. 5 shows. Furthermore, the FLY (esterase activity) increased fast during and after spore germination.

In addition to the FWS curve, these changes in spore size and green fluorescence are the signals used for the distinction of non-germinated and germinated spores.

*At-line monitoring of spore germination*

Spore germination was monitored at-line for FDA positive spores in batch cultivations in the bioreactor. For these experiments spores of different ages and different spore inoculum concentrations ( $2 \times 10^9$  spores/l in batch 1,  $2 \times 10^8$  spores/l in batches 2–4) were used. The spore inoculum concentrations were determined beforehand with the method presented here using samples after 1 h of shake flask culture. At the beginning, no spores were germinated. After 15 h cultivation, germination started and within 10 h after the start of germination, the majority of the spores were germinated when younger spores (3 months, batches 1 and 4) were used. For older spore inocula (older than 8 months, batches 2 and 3), germination took longer and after 35 h of cultivation the percentage of germinated spores was lower than for younger spore inoculum after 20 h (see Fig. 6). The differences of spore germination

between different spore inoculum concentrations were minor (compare batch 1 and 4 in Fig. 6).

Not all FDA-positive spores germinated. For spore inocula older than 8 months, the percentage of germinating spores was 60 % and lower. This is worth noticing as the correlation of FDA-positive spores to the CFU was almost one (also including measurements of these spore inocula). Therefore, it seems that spores germinate on agar plates, but not in a liquid environment in the bioreactor, although the media composition was similar.

**Discussion**

**The necessity of at-line measuring spore germination**

The method developed here, enabling the at-line determination of spore inoculum quality, revealed that not all spores determined as viable by state-of-the-art methods (CFU or combination flow cytometry/viability staining) do really germinate. According to the definition of viable spores made by Nielsen and Krabben (1995), only spores which germinate are viable. Based on this definition, neither CFU nor the flow cytometry/viability staining method proved to be suitable for the determination of viable spores for bioreactor cultivations.

These results underline differences of spore germination in liquid cultures and on agar plates. Spores which seem to germinate on agar plates do not germinate in liquid environment. Although the spores show metabolic activity and even swell (data not shown), they do not germinate. The same observation has already been made in previous studies (Paul and Thomas 1998).

Altogether, if a certain concentration of germinating spores is to be achieved in the bioreactor, the measurement of spore

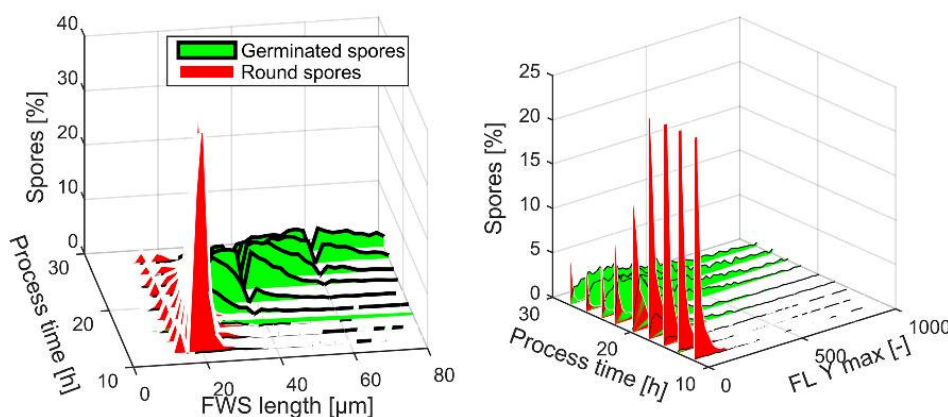


**Fig. 5** Size distribution (a) and distribution of FLY (b) of round and germinated spores in batch 1. The number of spores is normalized to show the amount of spores per sampling point in percent

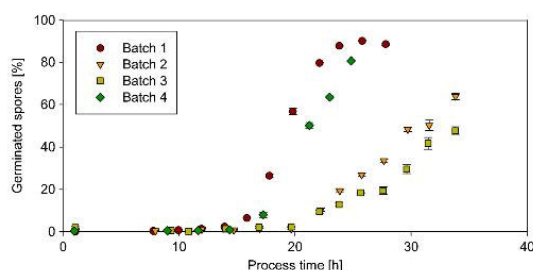


**Fig. 6** Spore germination over process time as percentage of total FDA-positive spore count. In batch 1 and 4, 90 % of the spores germinated. In the other two batches, the amount of germinated spores does not exceed 70 %

viability via CFU or flow cytometry is not sufficient. Therefore, two alternative procedures are suggested: first, a predetermination of the amount of spores needed for an inoculation can be carried out by shake flask cultivations. Spore germination can be evaluated in these flasks with the here presented method. Afterwards, the bioreactor could be exactly inoculated with the required volume of spore inoculum based on the spore germination investigation. A second possibility is to monitor spore germination in the bioreactor; this means that certain actions concerning parameters in the bioprocess can be set as a response directly to the at-line determined amount of germinating spores and the germination behaviour in order to improve the process performance.

#### Advantages of the method developed here in comparison to previous ones

Spore swelling and spore germination have so far been monitored using microscopy approaches (Demming et al. 2011; Oh 1996; Paul et al. 1993). But even if automated image analysis was used—Oh (1996) and Paul et al. (1993)—microscopy is more time-consuming than flow cytometry, especially if high numbers of spores are to be investigated in order to increase the robustness of the result. But, the big benefit of flow cytometry in comparison to microscopy is its applicability in complex medium environment. Via fluorescence and scatter measurements, flow cytometry enables the distinction of spores even in highly complex medium, as shown in the present study and in Ehgartner et al. (2016). In contrast to this, spores on microscopy slides are covered by medium particles and therefore not accessible by the method.

By monitoring spore germination, it is not only possible to investigate germination kinetics, but also to get information about the total spore viability. Thereby, the state-of-the-art method CFU cannot only be replaced by the at-line flow cytometry; moreover, the here presented approach highlights the differences between fungal growth in liquid environment and on agar.

The time-resolved measurement of germinating spore concentration is an addition to spore quality measurements presented in Ehgartner et al. (2016). The decision tree described in the latter can be complemented by a further step—the spore germination. This leads to a separation of the viable subpopulation in Ehgartner et al. (2016) further into a metabolically active but not germinating (hence, not viable) and a metabolically active and germinating (hence viable) subpopulation.

#### Applicability of the method in a process environment

The method presented here has been developed as an at-line tool, providing information in real-time. Therefore, it could be applied as a PAT tool (Rathore et al., 2010). Furthermore, flow cytometry is a method which is applicable online and which has been used in biotechnological processes (Hyka et al. 2013). In addition, the device used in this study (CytoBuoy, Woerden, Netherlands) is already applied in a fully automated way in aquatic environments (Malkassian et al. 2011). The online application of the tool developed here with enhanced automation would need some improvements. A big issue for invasive online tools such as flow cytometry is the sterile withdrawal of a representative sample at the bioreactor interface. Therefore, a flow injection system could be applied for sample taking and sample preparation, as it has already been described elsewhere (Broger et al. 2011; Zhao et al. 1999).

#### Method transfer to other media and new strains

The method was shown to be applicable to a penicillin-producing *P. chrysogenum* strain. If the method is to be applied on other strains/species or another medium environment, two steps need to be completed beforehand. First, the viability staining has to be investigated on spores and media particles. Media particles should not be stained with FDA, neither should dead spores (after microwave treatment, for example). Spores from cultivation should largely fluoresce with FDA. In a second step, different spore inocula ought to be measured to do the correlation to CFU. This is important in order to confirm the staining and measurement procedure—the FDA concentration and FDA incubation time could influence which particles are determined as FDA positive and which are not.

The evaluation of the method to discriminate germinated vs. non-germinated spores is not necessary for new strains and is totally independent of the medium. However, adjustments of measurement parameters (e.g., sensitivity) in the flow cytometer software lead to a re-evaluation of the method.

#### Benefits of the method developed here

To sum it up, the tool based on flow cytometry and viability staining is able to distinguish non-germinated from

germinated spores in complex media environment. Spore germination can be monitored with an error rate of less than 5 %.

Not all spores germinating on agar plates also germinate in the bioreactor. There seem to be differences between solid and liquid growth. Therefore, measurement of spore germination is crucial to determine the viable (= germinating) spore concentration in a bioreactor environment.

The implementation of this method as a PAT tool for at-line spore germination monitoring enables an intervention in early phases of the process. This offers a great opportunity in view of avoiding batch-to-batch variability. Furthermore, the monitoring of viable spores and spore germination on multiple processes and the linkage of these parameters to physiology and morphology in later phases enhances process knowledge.

**Acknowledgments** Open access funding provided by TU Wien (TUW), Vienna, Austria. We would like to thank Sandoz GmbH (Kundl, Austria) for kindly providing the strain used in this study.

#### Compliance with ethical standards

**Funding** This study was funded by Christian Doppler Gesellschaft (grant number 171).

**Conflict of interest** The authors declare that they have no conflict of interest.

**Ethical approval** This article does not contain any studies with human participants or animals performed by any of the authors.

**Open Access** This article is distributed under the terms of the Creative Commons Attribution 4.0 International License (<http://creativecommons.org/licenses/by/4.0/>), which permits unrestricted use, distribution, and reproduction in any medium, provided you give appropriate credit to the original author(s) and the source, provide a link to the Creative Commons license, and indicate if changes were made.

#### References

- Bradner JR, Nevalainen KM (2003) Metabolic activity in filamentous fungi can be analysed by flow cytometry. *J Microbiol Methods* 54: 193–201. doi:10.1016/S0167-7012(03)00043-5
- Broger T, Odermatt RP, Huber P, Sonnleitner B (2011) Real-time on-line flow cytometry for bioprocess monitoring. *J Biotechnol* 154:240–247. doi:10.1016/j.jbiotec.2011.05.003
- Delanghe JR, Kouri TT, Huber AR, Hannemann-Pohl K, Guderer WG, Lun A, Beier L (2000) The role of automated urine particle flow cytometry in clinical practice. *Clin Chim Acta* 301:1–18
- Demming S, Sommer B, Llobera A, Rasch D, Krull R, Buttgenbach S (2011) Disposable parallel poly (dimethylsiloxane) microbioreactor with integrated readout grid for germination screening of *Aspergillus ochraceus*. *Biomicrofluid* 5:14104. doi:10.1063/1.3553004
- Diaz M, Herrero M, Garcia LA, Quiros C (2010) Application of flow cytometry to industrial microbial bioprocesses. *Biochem Eng J* 48: 385–407
- Dorsey J, Yentsch CM, Mayo S, McKenna C (1989) Rapid analytical technique for the assessment of cell metabolic activity in marine microalgae. *Cytometry* 10:622–628. doi:10.1002/cyto.990100518
- Ehgartner D, Herwig C, Neutsch L (2016) At-line determination of spore inoculum quality in *Penicillium chrysogenum* bioprocesses. *Appl Microbiol Biotechnol* 100:5363–5373. doi:10.1007/s00253-016-7319-9
- Fletcher J, Morton G (1970) Physiology of germination of *Penicillium griseofulvum* conidia. *T Brit Mycol Soc* 54:65–81
- George TC, Basiji DA, Hall BE, Lynch DH, Orlyn WE, Perry DJ, Seo MJ, Zimmermann CA, Morrissey PJ (2004) Distinguishing modes of cell death using the ImageStream multispectral imaging flow cytometer. *Cytometry Part A* 59:237–245. doi:10.1002/cyto.a.20048
- Gottlieb D (1950) The physiology of spore germination in fungi. *Bot Rev* 16:229–257
- Hyka P, Lickova S, Pribyl P, Melzoch K, Kovar K (2013) Flow cytometry for the development of biotechnological processes with microalgae. *Biotechnol Adv* 31:2–16. doi:10.1016/j.biotechadv.2012.04.007
- Lein J (1986) The penicillin strain improvement program. In: Vanek Z, Hostalek Z (eds) Overproduction of microbial metabolites. Butterworths, Boston, p 105–139
- Malkassian A, Nerini D, van Dijk MA, Thyssen M, Mante C, Gregori G (2011) Functional analysis and classification of phytoplankton based on data from an automated flow cytometer. *Cytometry Part A* 79:263–275. doi:10.1002/cyto.a.21035
- Nielsen J, Krabben P (1995) Hyphal growth and fragmentation of *Penicillium chrysogenum* in submerged cultures. *Biotechnol Bioeng* 46:588–598. doi:10.1002/bit.260460612
- Oh K (1996) Morphological recognition of fungal spore germination by a computer-aided image analysis and its application to antifungal activity evaluation. *J Biotechnol* 45:71–79
- Paul GC, Thomas CR (1998) Characterisation of mycelial morphology using image analysis. *Adv Biochem Eng Biotechnol* 60:1–59
- Paul GC, Kent CA, Thomas CR (1993) Viability testing and characterization of germination of fungal spores by automatic image analysis. *Biotechnol Bioeng* 42:11–23. doi:10.1002/bit.260420103
- Pereira GC, Ebecken NFF (2011) Combining in situ flow cytometry and artificial neural networks for aquatic systems monitoring. *Expert Syst Appl* 38:9626–9632
- Posch AE, Spadiut O, Herwig C (2012) Switching industrial production processes from complex to defined media: method development and case study using the example of *Penicillium chrysogenum*. *Microb Cell Factories* 11:88. doi:10.1186/1475-2859-11-88
- Rathore AS, Bhambure R, Ghare V (2010) Process analytical technology (PAT) for biopharmaceutical products. *Anal Bioanal Chem* 398: 137–154. doi:10.1007/s00216-010-3781-x
- Rieseberg M, Kasper C, Reardon KF, Scheper T (2001) Flow cytometry in biotechnology. *Appl Microbiol Biotechnol* 56:350–360
- Rotman B, Papernmaster BW (1966) Membrane properties of living mammalian cells as studied by enzymatic hydrolysis of fluorogenic esters. *Proc Natl Acad Sci U S A* 55:134–141
- Smith GM, Calam CT (1980) Variations in inocula and their influence on the productivity of antibiotic fermentations. *Biotechnol Lett* 2:261–266
- Thyssen M, Ferreyra G, Moreau S, Schloss I, Denis M, Demers S (2011) The combined effect of ultraviolet B radiation and temperature increase on phytoplankton dynamics and cell cycle using pulse shape recording flow cytometry. *J Exp Mar Biol Ecol* 406:95–107
- Tucker KG, Thomas CR (1994) Inoculum effects on fungal morphology: shake flasks vs agitated bioreactors. *Biotechnol Tech* 8:153–156
- Zhao R, Natarajan A, Srienc F (1999) A flow injection flow cytometry system for on-line monitoring of bioreactors. *Biotechnol Bioeng* 62: 609–617

**Supplementary material**

**At-line determination of spore germination of *Penicillium chrysogenum* bioprocesses in complex media**

Daniela Ehgartner<sup>1,2</sup>, Jens Fricke<sup>1,2</sup>, Andreas Schröder<sup>1,2</sup> and Christoph Herwig<sup>1,2\*</sup>

\*to whom the correspondence should be addressed to

<sup>1</sup> CD Laboratory on Mechanistic and Physiological Methods for Improved Bioprocesses, TU Wien,  
Gumpendorferstrasse 1a/166, 1060 Vienna, Austria

<sup>2</sup> Research Area Biochemical Engineering, Institute of Chemical Engineering, TU Wien, Gumpendorferstrasse  
1a/166, 1060 Vienna, Austria

Corresponding author:

christoph.herwig@tuwien.ac.at

Tel (Office): +43 1 58801 166400

Fax: +43 1 58801 166980

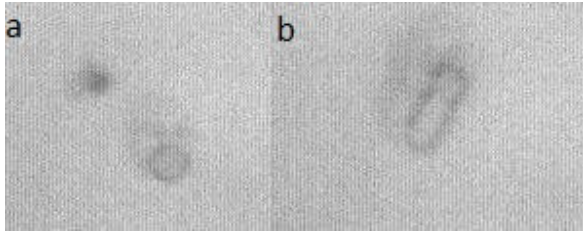
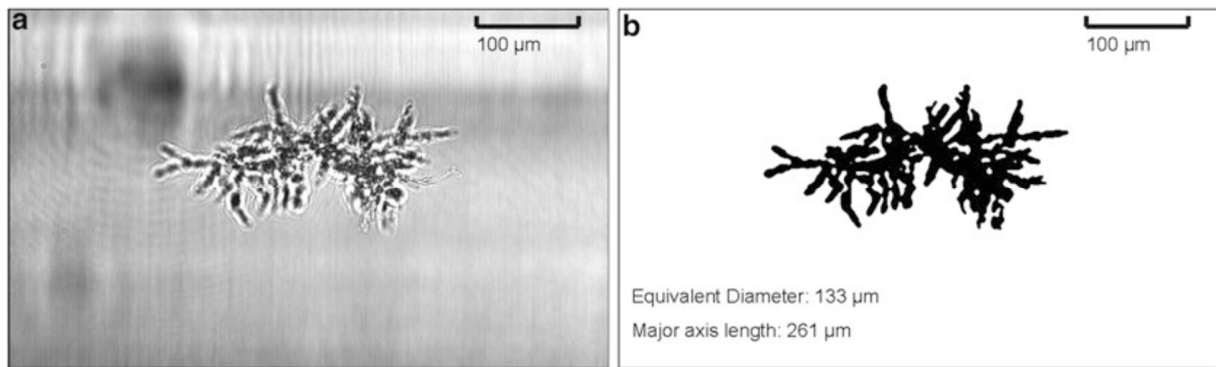


*Figure S1: Pictures of spores taken in the flow cell of the CytoSense. a) non-germinated spore and a medium particle, b) a germinated spore going upright through the cell*

## Imaging Flow Cytometry and High-Throughput Microscopy

Golabgir, A., Ehgartner, D., Neutsch, L., Posch, A. E., Sagmeister, P., & Herwig, C., Genetic Transformation Systems in Fungi, 2, 201 (2014)



# Imaging Flow Cytometry and High-Throughput Microscopy for Automated Macroscopic Morphological Analysis of Filamentous Fungi

17

Aydin Golabgir, Daniela Ehgartner,  
Lukas Neutsch, Andreas E. Posch,  
Peter Sagmeister, and Christoph Herwig

## 17.1 Introduction

Fungi exhibit cellular and macroscopic morphological variations in response to genetic as well as environmental influences. Morphological variations have been shown to be an indicator for assessing properties such as pathogenicity (Hnisz et al. 2011), efficiency of industrial bioprocesses (Posch et al. 2013), as well as ecological impacts (Pomati and Nizzetto 2013). Morphological characterization of fungi is highly dependent on the application. Whereas assessing pathogenicity might depend on the choice of color and cell size as indicators of underlying genetic variations, bioprocess applications have considered macro-

morphological attributes, such as affinity for pellet growth, rate of branching, and septation frequency as quality attributes for production processes (Krull et al. 2013; Posch et al. 2012; Krabben and Nielsen 1998). Choosing a collection of suitable methods for morphological characterization, consisting of image acquisition/processing and data analysis, depend on the variables to be measured. However, for all cases, the description of quantitative morphological features with sufficient statistical power is only possible by methods that allow for high-throughput analysis of multiple cells or cell populations in a given sample. Hence, to be of practical use, applied measurement methodologies should be robust, fast, and not subject to observer bias.

The presented acquisition methods, (1) imaging flow cytometry and (2) whole-slide microscopy are chosen based on the versatility of applications and statistical rigor respectively. Flow cytometry devices with imaging capability present a stand-alone, standardized technological platform for high-throughput sampling with diverse applicability. Combination of the flow cytometer signals, such as fluorescence intensity, with “in-flow” images, opens diverse research possibilities for assessment of the molecular and genetic basis for morphological variations. On the other hand, whole-slide microscopy in combination with automated image analysis has been shown capable of achieving statistically

A. Golabgir, D.I. M.Sc. (✉)  
Research Division Biochemical Engineering, Vienna  
University of Technology, Gumpendorferstraße  
1a/166-4, Vienna 1060, Austria  
e-mail: aydin.golabgir@tuwien.ac.at

D. Ehgartner, D.I. M.Sc. • A.E. Posch, Ph.D.  
C. Herwig, Ph.D.  
CD Laboratory for Mechanistic and Physiological  
Methods for Improved Bioprocesses, Vienna, Austria

L. Neutsch, Ph.D., M.Pharm.Sci.  
Department of Biochemical Engineering, Vienna  
University of Technology, Vienna, Austria

P. Sagmeister  
Vienna University of Technology, Graz, Styria,  
Austria

verified morphological characterization (Posch et al. 2012; Cox et al. 1998).

Despite the availability of several automatic image acquisition systems, required image processing and data analysis steps are often a limiting factor due to the absence of one-fit-all software packages. Here, in addition to presenting two automated image acquisition methods, we provide a step-by-step guide for implementation of simple Matlab scripts capable of performing common data analysis tasks such as computation of morphological variables as a first step towards implementation of more advanced data analysis algorithms such as regression, classification, and clustering. The ability to setup fast and reliable methods for automatic and high-throughput morphological analysis as well as being able to implement custom algorithms for efficient data analysis is not only a useful tool for mycological research, but will also improve our ability to design improved biotechnological processes.

## 17.2 Materials

Materials are grouped according to the choice of the image acquisition platform.

### 17.2.1 Microscopy

1. 1-mL-pipette-tips (cut tips to avoid size exclusion).
2. Lactophenol blue (Art. No.: 3097.1, Carl Roth, Germany).
3. Microscope slide (25×75 mm).
4. High Precision Microscope Cover Glasses (24×60 mm) (Art. No.: LH26.1, Carl Roth, Germany).
5. Brightfield microscope (Leitz, Germany) equipped with a 6.3 magnifying lense, 5 megapixel microscopy CCD color camera (DP25, Olympus, Germany), and a fully automated x-y-z stage (Märzhäuser, Austria).

6. Microscope control program analysis 5 (Olympus, Germany).
7. MATLAB 2013a including Image Processing Toolbox.

### 17.2.2 Imaging Flow Cytometry

1. Milli-Q water.
2. 1-mL-pipette-tips (cut tips to avoid size exclusion).
3. Flow cytometer, e.g., CytoSense (CytoBuoy, Netherland) equipped with a PixeLINK PL-B741 1.3MP monochrome camera.
4. Flow cytometer software, e.g., CytoClus (CytoBuoy, Netherlands).
5. MATLAB 2013a including Image Processing Toolbox (MATLAB, Image Processing Toolbox Release 2013a).

## 17.3 Methods

The workflow for morphological analysis consists of the choice of an image acquisition platform and implementation of subsequent image and data processing routines. Figure 17.1 provides an overview of the presented methodologies. All of the presented methods have been developed for the analysis of *Penicillium chrysogenum* grown in submerged cultures, but could be extended to other similar organisms.

### 17.3.1 Sample Preparation

The importance of sound protocols for sample workup and conditioning prior to the actual process of image acquisition and evaluation is often underrated. Since factors such as pH-value and osmolarity are known to affect morphology, it has to be assured that sample preparation does not interfere with results from morphological analysis. Staining steps may be included in order to focus the image-based analysis on selected

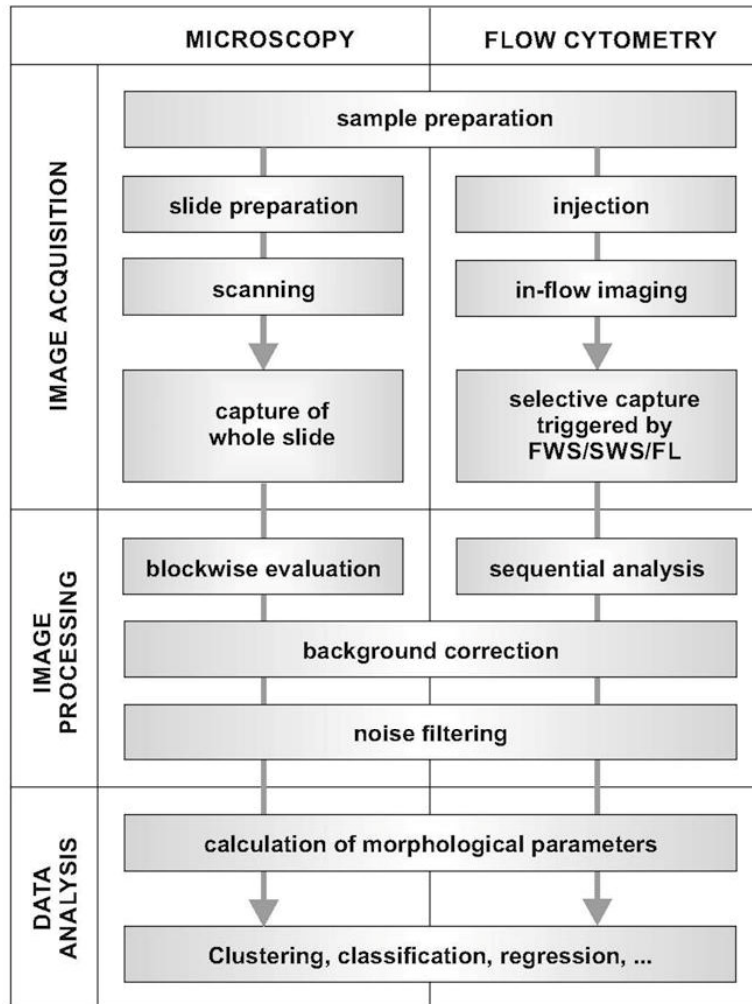


**Fig. 17.1** Overview of the steps involved in presented methods

elements in the sample, which can be distinguished by specific structural or functional parameters of the fungal cell. Individual sample preparation procedures for the presented image acquisition methods are presented in Sects. 17.3.2.1 and 17.3.2.2.

### 17.3.2 Image Acquisition

The choice of the most suitable method for image acquisition depends on the nature of the sample and the analysis criteria with regard to throughput, accuracy, and investigated morphological

features. Selection of a specific method will also be influenced by the available equipment in most laboratories.

The maximum number of images acquired per run, which influences the statistical robustness of a method, is one of the main differentiating factors of the two presented image acquisition systems. The flow cytometry system is capable of taking up to 150 images per run, each containing a single hyphal element, whereas scanning a microscope slide (at 63× magnification) can yield up to 900 images, each containing up to ten individual macromorphological fungal objects (such as pellets, mycelial clumps, and branched hyphae). Therefore, the microscopy-based system is at an advantage when it comes to recording a large number of images.

In both systems, discriminatory parameters (such as size and fluorescence intensity) may be utilized for confining the analysis to particles with given properties. However, in microscopy-based systems these parameters are not easily accessible, and the sorting process is carried out *post-hoc* (by analyzing the image and including or excluding certain structures). Flow cytometric analysis allows for in-situ control of image acquisition (by triggering acquisition based on the optical parameters of the particle in the flow cell). The signals required for selective acquisition are more readily available in flow cytometry systems. Sample handling and mounting on the device is another important factor. In microscopy systems, it usually involves spreading the sample on glass slides, which is more tedious and less standardized compared to fully automated systems of sample injection.

The maximum size of particles being analyzed has traditionally been a limiting factor for flow cytometric analyses of fungal samples. The system presented here has been specifically designed to allow for analysis of biomass particles up to a size range of 1.5 mm, which is still in line with the requirements of many applications. However, a potential shortcoming of imaging flow cytometry is that the maximum possible exposure time is determined by the relatively fast transit of the fungal biomass element through the flow cell.

This may interfere with analysis of certain image features or stains that require prolonged signal integration times.

### 17.3.2.1 Microscopy

1. Dilute the sample with to about 1 g/L biomass dry cell weight. For pipetting, use cut pipette tips to avoid size exclusion effects.
2. Add 100 µL/mL lactophenol blue solution to stain the sample.
3. Transfer 50 µL of the stained sample to a microscope slide. Ensure homogenous sample distribution.
4. Place a high precision cover slip on the slide using tweezers. Avoid agglomeration of biomass elements and inclusion of air bubbles, dust, or debris. The use of a high precision slip ensures that the images remain in focus throughout scanning of the entire slide, eliminating the need for manually adjusting focus at each step.
5. Transfer the microscope slide to the automated microscope stage.
6. Adjust acquisition parameters (i.e. contrast, brightness, exposure time) based on illumination settings and desired image features.
7. Scan the whole slide. For analysis of *P. chrysogenum*, at 63× magnification, typically 600–800 images are taken (adjacently arranged in a grid pattern without overlap as shown in Fig. 17.2).
8. Measure multiple slide replicates (in our case 3, amounting to approx. 2,000 images) of a sample to account for variations in sampling and sample preparation steps.

### 17.3.2.2 Imaging Flow Cytometry

1. Sample is diluted with MQ water to a final concentration of approximately  $10^4$  cells/mL and stained if required. 5–10 mL of diluted sample is needed for one measurement.
2. Sample measurement is performed by the flow cytometer via the standardized routine.
3. Depending on the particular selection criteria for taking pictures, the in-flow images are recorded.

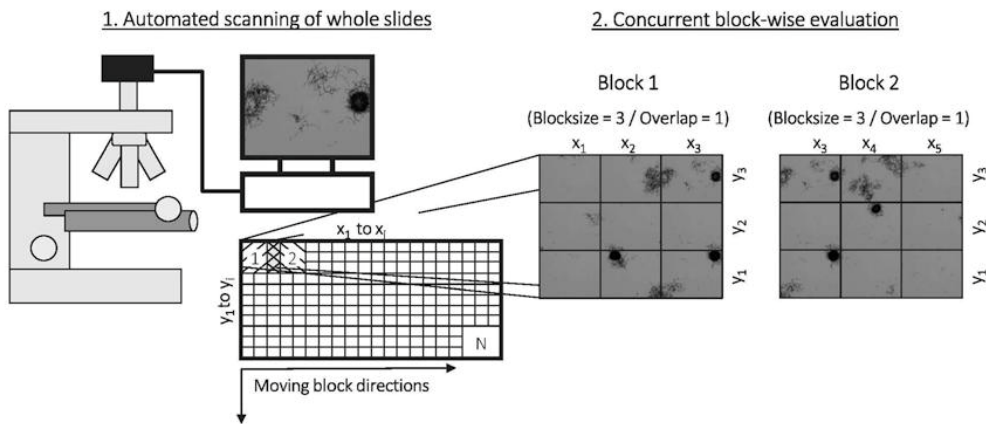


**Fig. 17.2** Implemented workflow for automated morphological analysis. Step 1 is controlled by the image recording software Analysis5; step 2 by the evaluation routine implemented in Matlab. (From Posch AE, Spadiut O,

Herwig C. A novel method for fast and statistically verified morphological characterization of filamentous fungi. *Fungal Genet Biol.* 2012 Jul;49(7):499–510 with permission.)

### 17.3.3 Image Processing and Data Analysis

Following the acquisition of a series of images, either via whole-slide microscopy or imaging flow cytometry, images are analyzed using custom-built Matlab scripts. In the following sections, the introduced programming functions (such as *imread* and *im2double*) either refer to inbuilt functions of MATLAB or are part of the MATLAB Image Processing Toolbox (MATLAB, Image Processing Toolbox Release 2013a).

#### 17.3.3.1 Image Processing for Whole-Slide Microscopy

In contrast to Imaging Flow Cytometry where only one hyphal biomass element is captured on an image, in whole-slide microscopy, each image often contains more than one biomass element. It is therefore required to either combine all images prior to evaluation or evaluate a set of multiple images sequentially because if only one image were to be evaluated at a time, the biomass elements spanning an image border would not be evaluated correctly. An iterative evaluation method of overlapping composite image blocks allows for the evaluation of all biomass elements

by using a combination of 4 or 9 microscope images at each iterative evaluation step.

1. Export/store all images of a slide in a folder
2. Implement the following Matlab functionalities in a script (m-file):
  - (a) Create an index of block numbers and be able to choose a set of  $n$  images (4 or 9) that are adjacent to each other. Implement a loop functionality that traverses through all images in a blockwise fashion as illustrated in Fig. 17.2.
  - (b) Open the set of 4 or 9 microscope images corresponding to a block using the *imread* function (MATLAB, Image Processing Toolbox Release 2013a) and combine them into one image .
  - (c) Convert the images from RGB format to grayscale using the *rgb2gray* function (MATLAB, Image Processing Toolbox Release 2013a). Further convert the image values to double precision using the *im2double* function (MATLAB, Image Processing Toolbox Release 2013a).
  - (d) Convert the images to binary (black/white) using the *im2bw* function (MATLAB, Image Processing Toolbox Release 2013a). Adjust the threshold value based on particular light conditions.

- (e) Apply mean and median filters to enhance image quality.
  - (f) Convert to binary (black/white) using the *im2bw* function. Use a threshold value according to the camera settings of the microscope.
  - (g) Identify connected objects using the *bwconncomp* function (MATLAB, Image Processing Toolbox Release 2013a) and append to list of objects (excluding border-touching elements and eliminating duplicates stemming from overlapping composite image blocks)
  - (h) Go back to step b and evaluate the next block (repeat until all images have been analyzed)
  - (i) Save the list of objects as a MAT file for subsequent data analysis steps.
3. Find the length of a pixel (magnification) in the camera software. This will depend on the resolution of the installed camera. Square this value to get the area [ $\mu\text{m}^2$ ] corresponding to each pixel.

### 17.3.3.2 Image Processing for Imaging Flow Cytometry

Image acquisition via imaging flow cytometry eliminates the need for blockwise evaluation because each image captures only one hyphal biomass element. In rare cases where the biomass elements is not captured wholly and touches the image border, the image can be discarded automatically.

1. Export images from the Cytosense software (using the *export all images* function) to a common folder
2. Perform following activities in a Matlab script (m-file). Programming functions (such as *rg2gray* and *im2double*) either refer to inbuilt functions of MATLAB or are part of the MATLAB Image Processing Toolbox (MATLAB, Image Processing Toolbox Release 2013a).
  - (a) Open an image and a background image.
  - (b) Convert both images from RGB format to grayscale using *rgb2gray* function. Also convert the image data format to double precision using the *im2double* function.
  - (c) Subtract the background image from the actual image being analyzed.
  - (d) Convert to binary (black/white) using the *im2bw* function. Use a threshold value according to the camera settings of the flow cytometer. For our settings values between 0.04 and 0.1 work best.
  - (e) Apply mean and median filters to enhance the image quality and remove noise.
  - (f) Convert to binary (black/white) again. Use a threshold value according to the camera settings of the flow cytometer. For our settings values between 0.4 and 0.6 work best.
  - (g) Detect all connected objects using the *bwconncomp* function. Ideally, if the right pre-processing parameters are chosen, each image should result in one connected object only. If additional small elements are found, i.e. due to noise, the largest element should be chosen automatically using the *bwconncomp* function to output the area of the connected objects.
  - (h) Append the largest connected object to a list for later processing and iterate steps a–g until all images of a flow cytometer run have been analyzed.
  - (i) Save the list of objects as a MAT file for subsequent data analysis steps.
3. Compute the length and area of each pixel from the scale bar on one of the output images. The resolution (number of pixels) of each exported image should be the same for each analyzed sample.
  - (a) Count the number of pixels in the scale bar of an image by cropping the image, loading it in Matlab, and then using the *length* function. For instance: Length of scale bar=670 pixels=450  $\mu\text{m}$ .
  - (b) Length of a pixel=450/670=0.67  $\mu\text{m}/\text{pixel}$ .
  - (c) Area of a pixel=0.67 $\times$ 0.67=0.45  $\mu\text{m}^2/\text{pixel}$ .

### 17.3.3.3 Data Analysis and Calculation of Morphological Variables

The output of either method (microscopy or imaging flow cytometry) will be the same type of Matlab structure, namely a collection of binary

images of individual hyphal elements. Subsequent data analysis steps will be the same for both image acquisition methods. Here, we describe the procedure for deriving a set of commonly-used morphological variables using easy-to-implement Matlab routines. For statistical verification of calculated morphological data, the reader is referred to Posch et al. (2012).

### Area

Area of the 2d slice through the hyphal element is proportional to the size of the hyphal element. This property can be calculated according to the following procedure.

1. Use the *regionprops* function to get a list of all region properties.  
`properties=regionprops(input_bw, 'all');`
2. In the resulting structure, access the “Area” matrix using “`props.Area`.”
3. Multiply the pixel number by the “area of each pixel [ $\mu\text{m}^2/\text{pixel}$ ]” (calculated in previous steps) to get the area of the hyphal element in units of  $\mu\text{m}^2$ .
4. The properties structure contains a collection of variables such as circularity and roughness which can be used for a variety of tasks, such as classification of hyphal elements.

### Equivalent Diameter and Major Axis Length

The “equivalent diameter” parameter is a scalar that specifies the diameter of a circle with the same area as the region. Similarly, the “major axis length” specifies the length of the major axis of the ellipse that has the same normalized second central moment as the region. Both parameters provide an appropriate measure of the size of the biomass elements and are calculated by the *regionprops* function, which returns these values in units of pixels. Multiplication by pixel length (calculated in previous steps) returns the *EquivDiameter* and *MajorAxisLength* in units of  $\mu\text{m}$ .

### Classification of Hyphal Elements

Each fungal object can be classified into distinct morphological classes, such as pellets, large and small clumps, branched and unbranched hyphae.

The decision for such classification is based on a combination of morphological parameter and simple if/else rules. Combination of classification and area can be used to derive the area fraction of each class for a sample, such as area fraction of pellets or large clumps (Fig. 17.3).

### Hyphal Growth Unit

The hyphal growth unit (HGU), defined as the average length of a hyphae supporting a growing tip, is used for studying the growth kinetics and morphology of filamentous organisms. It can be given by the equation:

$$\text{HGU} = \frac{L_t}{N_t}$$

where  $L_t$  is total mycelial length, and  $N_t$  is the total number of tips. The procedure for calculating the total mycelial length and the total number of tips is as follows:

1. Starting from the binary image of the previous steps, apply the *bwmorph* function with the “skel” method. The operation “skel” removes pixels on the boundaries of objects but does not allow objects to break apart. The pixels remaining make up the image skeleton. Use “inf” as the n (input) parameter, which causes the skeleton to have a width of 1 pixel.  
`T1=bwmorph(input_bw,'skel',inf);`
2. Apply the *bwmorph* function with the “shrink” method in order to eliminate tips which are smaller than a specified length. Use the minimum tip size [pixels] as the n (input) parameter.  
`T2=bwmorph(T1,'shrink',2/pxl_length);`
3. The total hyphal length is calculated by considering the length of a rectangle having the same area and perimeter as the hyphal object (Cox et al. 1998).

$$\text{Total length} = \frac{\text{Perimeter} + \sqrt{\text{Perimeter}^2 - 16 \times \text{Area}}}{4}$$

4. Apply the *bwmorph* function with the “end-point” method in order to identify all of the endpoints.  
`T3=bwmorph(T2,'endpoints');`

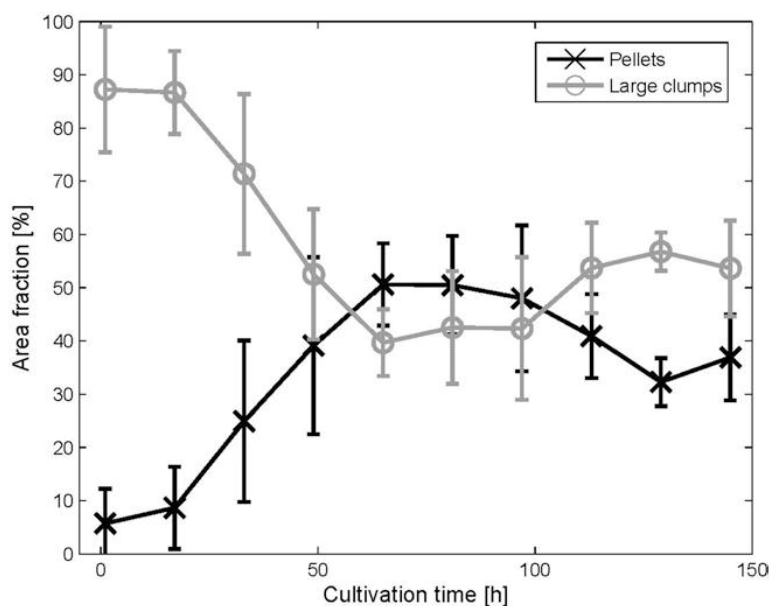


**Fig. 17.3** Time course of area fraction of pellets and large clumps over a *P. chrysogenum* fed-batch cultivation using the whole-slide microscopy method

5. Apply the `bwconncomp` function to find all connected objects in the resulting image. The `NumObjects` property of the resulting structure is equivalent to the number of tips.
6. Dividing total length by number of tips results in the hyphal growth unit parameter.

## 17.4 Illustrative Examples

### 17.4.1 Imaging Flow Cytometry

The advantage of the imaging flow cytometry method lies in its ability to combine classical morphological analysis with flow cytometer detector signals. Equipped with appropriate staining methods, it would be possible to differentiate hyphal elements on a functional level (i.e. pathogenicity, live/dead), and these subpopulations can then be analyzed with respect to macroscopic morphological differences. In comparison to whole-slide microscopy, an advantage of this method lies in the fact that overlapping and touching elements are eliminated since the

flow cytometer adjusts the flow such that every image contains only one biomass element.

As an example for calculation of common size parameters, Fig. 17.4 depicts a hyphal element and the corresponding calculated values. Figure 17.5 shows an example of skeletonization used for calculation of total hyphal length, number of tips, and HGU. Figure 17.6 shows an image of a pellet and the corresponding detector signals of the flow cytometer which can be used as a criteria for capturing images at specific signal levels. Lack of detailed focus for larger particles is a clear drawback of the in-flow image acquisition method as seen by the example of Fig. 17.6. Further optimization of the method may result in images with improved quality.

### 17.4.2 Whole-Slide Microscopy

Application of the described whole-slide microscopy method has been previously shown to significantly enhance characterization of bioprocesses (Posch et al. 2013). As an example, classification

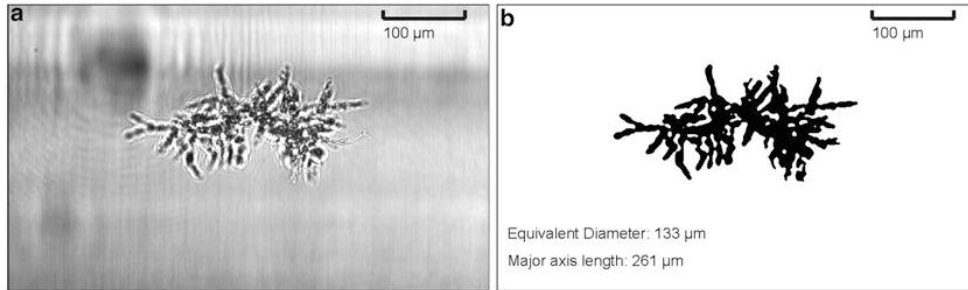


**Fig. 17.4** (a) Image of a branched hyphae captured by the in-flow camera. (b) Calculation of the equivalent diameter and major axis length of a biomass element

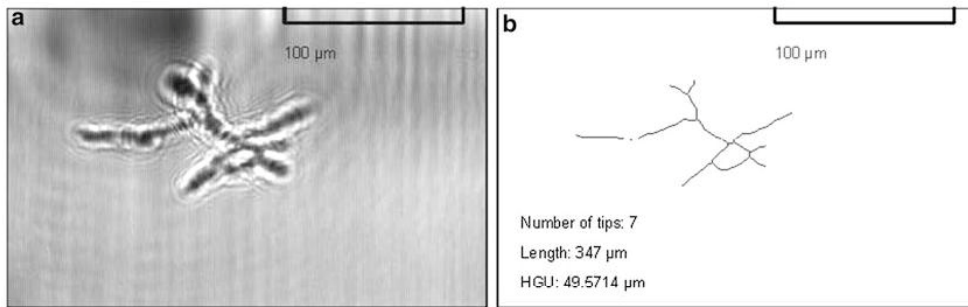


**Fig. 17.5** (a) Image of a branched hyphae captured by the in-flow camera. (b) Calculation of the number of tips, total length, and hyphal growth unit from an image taken in the flow cell of the flow cytometer is performed via skeletonization of the image

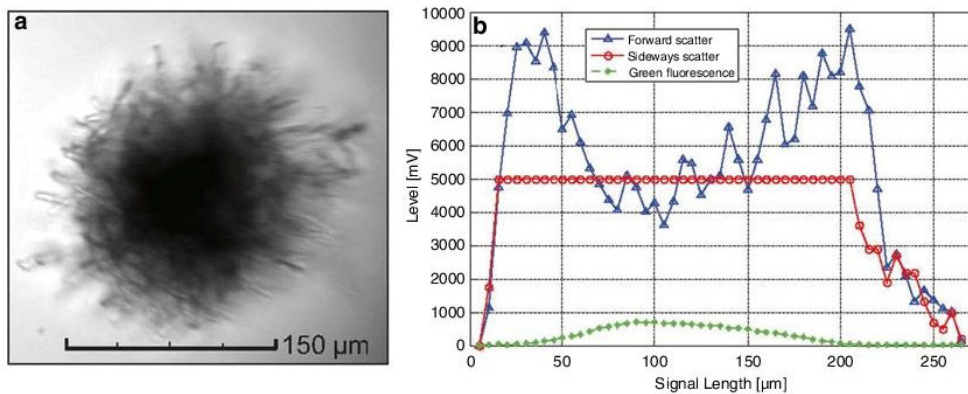


**Fig. 17.6** (a) Image of a pellet captured by the in-flow camera. (b) detector signals of the flow cytometer which can be used as a criteria for capturing images at specific signal levels. The sideways scatter detector has become saturated due to the limitations of the device. The size of the pellet can be easily calculated using the forward scatter signal

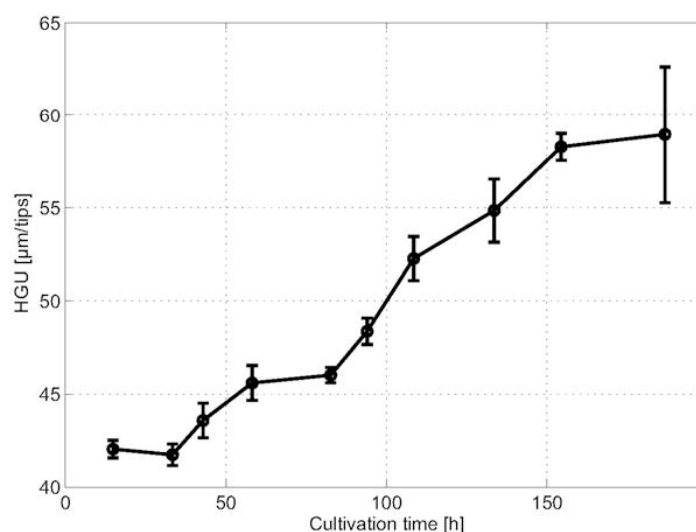


**Fig. 17.7** Time course of hyphal growth unit (HGU) over a *P. chrysogenum* fed-batch cultivation using the whole-slide microscopy method

of biomass into distinct morphological classes according to a rule-based method can provide the time course of morphological variations over a typical industrial cultivation process of *P. chrysogenum* (Fig. 17.3). The dynamics of pellet growth and subsequent breakage provides insights for optimization of rheological properties of the culture. The time course of the hyphal growth unit over process time (Fig. 17.7) can serve for assessing the effects of process conditions, such as agitation speed, on the branching behavior of the organisms.

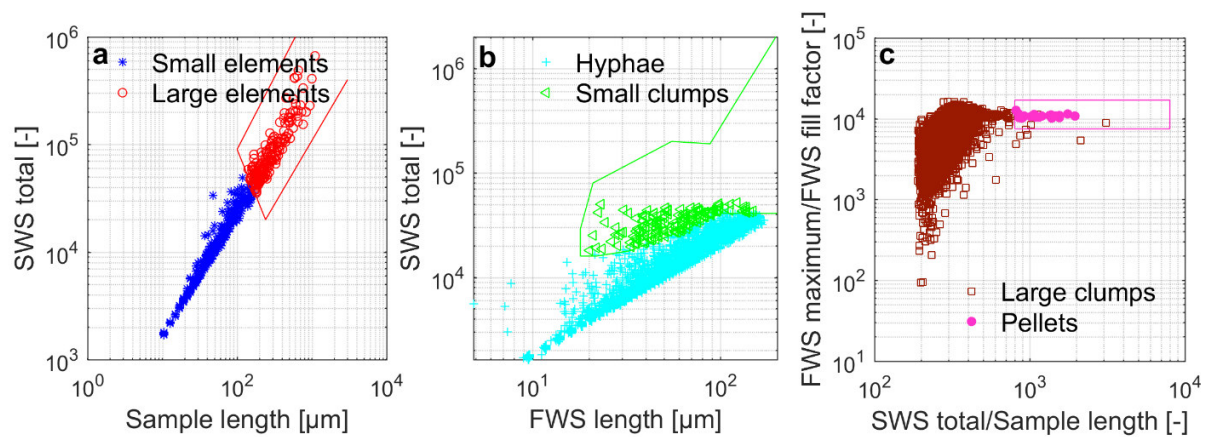
**Acknowledgements** The authors would like to thank Sandoz GmbH for providing the strains and guidance. Financial support was provided by the Austrian research funding association (FFG) under the scope of the COMET program within the research network “Process Analytical Chemistry (PAC)” (contract # 825340).

## References

- Cox P, Paul G, Thomas C (1998) Image analysis of the morphology of filamentous micro-organisms. *Microbiology* 144(Pt 4):817–827
- Hnisz D, Tscherner M, Kuchler K (2011) Morphological and molecular genetic analysis of epigenetic switching of the human fungal pathogen *Candida albicans*. *Methods Mol Biol* 734:303–315
- Krabben P, Nielsen J. (1998). Modeling the mycelium morphology of *Penicillium* species in submerged cultures. In: Schügerl K, ed. *Relation between morphology and process performances* [Internet]. Springer: Berlin. [cited 2013 Apr 25]. p. 125–52. Available from: <http://link.springer.com/chapter/10.1007/BFb0102281>
- Krull R, Wucherpfennig T, Esfandabadi ME, Walisko R, Melzer G, Hempel DC et al (2013) Characterization and control of fungal morphology for improved production performance in biotechnology. *J Biotechnol* 163(2):112–123
- MATLAB and Image Processing Toolbox Release. (2013a). Natick: The MathWorks, Inc.
- Pomati F, Nizzetto L (2013) Assessing triclosan-induced ecological and trans-generational effects in natural phytoplankton communities: a trait-based field method. *Ecotoxicology* 22(5):779–794
- Posch AE, Spadiut O, Herwig C (2012) A novel method for fast and statistically verified morphological characterization of filamentous fungi. *Fungal Genet Biol* 49(7):499–510
- Posch AE, Herwig C, Spadiut O (2013) Science-based bioprocess design for filamentous fungi. *Trends Biotechnol* 31(1):37–44

# Morphological analysis of filamentous fungi using flow cytometry – the fast alternative to microscopy and image analysis

Ehgartner, D., Herwig, C., & Fricke, J., Applied Microbiology and Biotechnology, submitted



**Morphological analysis of filamentous fungi using flow cytometry - the fast alternative to microscopy and image analysis**

Daniela Ehgartner<sup>1,2</sup>, Christoph Herwig<sup>1,2</sup> and Jens Fricke<sup>\*,1,2</sup>

\*to whom the correspondence should be addressed to

<sup>1</sup> CD Laboratory on Mechanistic and Physiological Methods for Improved Bioprocesses, TU Wien, Gumpendorferstrasse 1a/166, 1060 Vienna, Austria

<sup>2</sup> Research Area Biochemical Engineering, Institute for Chemical, Environmental and Biological Engineering, TU Wien, Gumpendorferstrasse 1a/166, 1060 Vienna, Austria

\*Corresponding author:

jens.fricke@tuwien.ac.at; Tel (Office): +43 1 58801 166462

Gumpendorferstrasse 1a / 166-4

1060 Wien, Austria

**Abstract:**

An important parameter in filamentous bioreactor cultivations is the morphology of the fungi, due to its interlink to productivity and its dependency to process conditions. Filamentous fungi show a large variety of morphological forms in submerged cultures. These range from dispersed hyphae, to interwoven mycelial aggregates, to denser hyphal aggregates, the so-called pellets. Depending on the objective function of the bioprocess, different characteristics of morphology are favorable and need to be quantified accurately.

The most common method to quantitatively characterize morphology is image analysis based on microscopy. This method is work intensive and time consuming. Therefore, we developed a faster, at-line applicable alternative method based on flow cytometry. Within this contribution this novel method is compared to microscopy for a penicillin production process. Both methods yielded in comparable distinction of morphological sub-populations and described their morphology in more detail. In addition to the appropriate quantification of size parameters and the description of the hyphal region around pellets, the flow cytometry method even revealed a novel compactness parameter for fungal pellets which is not accessible via light microscopy.

Hence, the here presented flow cytometry method for morphological analysis is a fast and reliable alternative to common tools with some new insights in the pellet morphology, enabling at-line use in production environments.

**Keywords:**

Filamentous fungi, flow cytometry, morphology, pellets, microscopy, image analysis, hyphae

## **Introduction**

An important parameter in filamentous bioreactor cultivations is the morphology of the fungi, because morphology and productivity are highly interlinked and depend on process conditions. Filamentous fungi exhibit a large variety of morphological forms in submerged culture. These forms range from dispersed hyphae, to interwoven mycelial aggregates, to denser hyphal aggregates, the so-called pellets. Depending on the aimed product, different characteristics of morphology are favorable (Papagianni 2004). Dispersed growth was described to achieve better production performance of glucoamylase (Gibbs et al. 2000), while pellets were related to citric acid production (Papagianni 2004). However, it is not just that productivity is directly linked to morphology, but also the process is affected. Several studies were conducted investigating the connection of morphology and viscosity. The latter is linked to mass transfer and energy input (Chain et al. 1966; Petersen et al. 2008; Riley et al. 2000). As a general trend, it can be stated that filamentous growth with high amounts of hyphae causes increased viscosity (Quintanilla et al. 2015). Furthermore, high fraction of pellets result in better mass and heat transfer, and lower power input levels needed for mixing (Znidarsic and Pavko 2001). Various factors build a complex system of interactions. Operation conditions influence growth, product formation and morphology. In addition, filamentous growth directly influences morphology, which, consequently, further changes viscosity and which in turn has an impact on operation conditions (Quintanilla et al. 2015).

In the recent decades, the investigation of fungal morphology in submerged bioreactor cultures is a central issue. Microscopy in combination with image analysis is the most common method (Cox et al. 1998; Paul and Thomas 1998; Posch et al. 2012; Vanhoutte et al. 1995). Automated image recording and automated analysis of images allows a high-throughput, statistically verified morphological analysis (Posch et al. 2012). Furthermore, online methods for image analysis exist like quantification of morphology in flowthrough cells. These last mentioned online analyses focused only on hyphal morphology. The flow cell with a high of 40  $\mu\text{m}$  limits the tools to dispersed growing cultures (Christiansen et al. 1999; Spohr et al. 1998).

Most common morphological classifications distinguish between freely dispersed mycelia and aggregates. Freely dispersed mycelia include hyphae, which are long and can have branches (Cox et al. 1998). Simple clumps, also called small clumps or entanglements, are larger freely dispersed mycelia where the main hypha is not identifiable. These are often referred as “artificially overlapping hyphae” (Cox et al. 1998; Paul and Thomas 1998; Posch et al. 2012). A further dispersed morphological class are clumps, also called large clumps (Cox et al. 1998; Paul and Thomas 1998; Posch et al. 2012). These

consist of aggregated or clumped hyphae (Cox et al. 1998). Large clumps are distinguished from so-called pellets by the missing of a dense core. Latter is a central dark region in the center of the aggregate, which is typical for pellets. The core is surrounded by a brighter outer mycelial region, the “hairy” annular region. Pellets have the size of several hundred micrometer to more than one millimeter (Cox et al. 1998; Paul and Thomas 1998). Cox et al. (1998) pointed out, that pellets are three-dimensional, which possibly cannot be sufficiently covered by image analysis based on microscopy. As a more appropriate investigation a chamber on the microscope stage to preserve the shape is proposed. Methods making pictures on microscope slides assume pellets to be nearly spherical (Cox et al. 1998). Various morphological parameters are evaluated concerning length/size/diameter of hyphae and hyphal aggregates. Morphological evaluation of pellets focusses apart from size evaluation, especially on the description of the annular area and the annular area compared to the core (Paul and Thomas 1998).

Although flow cytometry has often been applied for the morphological description of microorganisms as bacteria (Ehgartner et al. 2015; Langemann et al. 2016), investigations of filamentous organisms apart from the spore stadium (Ehgartner et al. 2016a; Ehgartner et al. 2016b) are scarce. Main reason for that is the size limitation of common flow cytometers. Hyphal aggregates risk to clog the tubing (Dubelaar and Gerritzen 2000). Only large-particle flow cytometers ought to cope with pellets of several hundred micrometers diameter. So far, investigations of filamentous fungi in pellet stadium focused on size, density and fluorescence measurement but did not go more into detail concerning morphology (de Bekker et al. 2011; Delgado-Ramos et al. 2014). In addition, an application of image analysis for morphological investigation of pictures taken in the flow cell was recently published (Golabgir et al. 2015).

We aim to develop an at-line applicable high throughput morphology analysis method for filamentous fungi as a faster and easier applicable method to image analysis via microscopy. The method ought to be applicable for disperse morphology and pellet cultures. The detail of morphological classification and description should be comparable to image analysis via microscopy in terms of the range of measurement error. In this work, we present how morphological data was extracted, compare the results to the standard image analysis method developed by Posch et al. (2012) and show the application of morphological analysis in two fed-batch bioreactor cultivations.

## **Materials and methods**

### **Strain**

Spore suspensions of the P-14 *P. chrysogenum* candidate strain for penicillin production descending from the P-2 *P. chrysogenum* candidate strain (American Type Culture Collection with the access number ATCC 48271) (Lein 1986) were kindly provided by Sandoz GmbH (Kundl, Austria) and used for all experiments.

### **Bioreactor cultivations**

Cultivations were performed in two Techfors S bioreactors (Infors HT, Bottmingen, Switzerland) with 10 l and 20 l maximal working volume respectively. The batch was cultivated with an initial volume of 6.5 l in the first mentioned bioreactor and inoculated with  $2 \cdot 10^8$  spores/l. During batch phase pH was not controlled. The end of the batch was defined as an increase in pH of 0.5 by convention. After the batch, the broth was diluted with fed-batch medium (15% broth, 85% medium) and two fed-batches were started in parallel with an initial volume of 6.5 l and 13 l respectively. Batch and fed-batch media were similar as described elsewhere (Posch and Herwig 2014).

During fed-batch phase, pH was kept constant at  $6.5 \pm 0.1$  by addition of 20% (w/v) KOH or 15% (v/v)  $H_2SO_4$ , respectively. pH was measured using a pH probe (Hamilton, Bonaduz, Switzerland). After additional 12 h nitrogen and phenoxyacetate feed were started. Ammonium and phenoxyacetate were fed at constant rates. In the first 48 h of fed-batch, 500 g/l glucose solution was fed at a constant rate of 1.01 ml/(l·h). Afterwards, the feed was continued at the same level (fed-batch (FB) 1) or an exponential ramp was started (FB2). Three additional fed-batches were carried out for method development varying in spore inoculum concentration ( $2 \cdot 10^9$  spores/l),  $pO_2$  (<10% vs. <40%) and feeding strategy (constant feeding rate of constant rate of 1.01 ml/(l·h) vs. constant feeding rate plus glucose pulse).

The stirrer was equipped with three six bladed Rushton turbine impellers, of which two were submersed and one was installed above the maximum liquid level for foam destruction. Fermentation temperature was kept at 25 °C via a cooling/heating jacket. Aeration was controlled at 1 vvm in batch and initial fed-batch with mass flow controllers (Vögtlin, Aesch, Switzerland). Dissolved oxygen concentration was measured using a dissolved oxygen probe (Hamilton, Bonaduz, Switzerland) and controlled between 40% and 90% during batch and between 40% and 60% during fed-batch, via adjustment of stirrer speed. The initial conditions were 325 rpm stirring speed in batch and 500 rpm in fed-batch.  $CO_2$  and  $O_2$  concentration in the off gas were analyzed with an off-gas analyzer (M. Müller AG, Egg, Switzerland).

---

### Light microscopy and image analysis

Light microscopy imaging with subsequent automated image analysis was carried out based on the method developed by Posch et al. (2012).

Cultivation samples were diluted, so that the final biomass dry weight was around 1 g/l. 50 µl of Loeffler's methylene blue per ml sample were added. Following, 50 µl of the stained sample were pipetted onto a standard glass slide (25 x 75 mm) and then covered with an extra-large cover slide (24 x 60 mm). The slide was then automatically scanned using a Leitz wide field microscope (Leitz, Stuttgart, Germany) with 63-fold magnification and an automated x-y-z stage (Märzhäuser, Wetzlar, Germany). Images were recorded with a five megapixel microscopy CCD color camera (DP25, Olympus, Tokio, Japan) and the image recording software analysis5 (Olympus, Tokio, Japan). 450 images (1354.2 x 1015.65 µm) were recorded per slide, scanning two slides per sample.

Images were then automatically evaluated. Hyphal elements were thereby classified into unbranched hyphae, branched hyphae, small clumps, large clumps and pellets. For all of these morphological classes, different size parameters were calculated. In addition, roughness and fullness (see Equation 1 and Equation 2) were determined for pellets. Further information including a list of evaluable morphological parameters, calculations and statistical background can be found elsewhere (Golabgir et al. 2015; Posch et al. 2012).

$$\text{roughness} = \frac{\text{perimeter}^2}{4 \cdot \text{Pi} \cdot \text{area}}$$

*Equation 1: Calculation of roughness due to Paul and Thomas (1998)*

$$\text{fullness} = \frac{\text{area}}{\text{convex area}}$$

*Equation 2: Calculation of fullness due to Paul and Thomas (1998)*

### Flow cytometry

Samples from fed-batch were diluted 1:10 into phosphate buffered saline (50 g/l of 2.65 g/l CaCl<sub>2</sub> solution, 0.2 g/l KCl, 0.2 g/l KH<sub>2</sub>PO<sub>4</sub>, 0.1 g/l MgCl · 6 H<sub>2</sub>O, 8 g/l NaCl and 0.764 g/l Na<sub>2</sub>HPO<sub>4</sub> + 2 H<sub>2</sub>O) and stained with propidium iodide (Sigma Aldrich, St. Louis, Missouri/USA; 20 mM stock dissolved in DMSO, diluted to a final concentration of 20 µM). After incubating 10 min, the sample was further stained with

fluorescein diacetate (Sigma Aldrich, St. Louis, Missouri, USA; stock solution of 5 g/l dissolved in acetone) to a final concentration of 5 mg/l. After incubation of 1 min, the sample was further diluted (1:100 in the same buffer) for flow cytometric analysis.

A CytoSense flow-cytometer (CytoBuoy, Woerden, Netherlands) with two forward scatter (FWS), one sideward scatter (SWS) and three fluorescence channels (yellow, orange, red) was used for single cell analysis. The implemented laser had a wavelength of 488 nm. The configuration of the filter set was 515-562 ± 5 nm for the green/yellow fluorescence channel (used for fluorescein diacetate) and 605-720 ± 5 nm for the red fluorescence channel (used for propidium iodide). The device was equipped with a PixelINK PL-B741 1.3MP monochrome camera for in flow image acquisition. For data treatment, the software CytoClus (CytoBuoy, Woerden, Netherlands) and a custom-programmed Matlab 2016b script (MathWorks, Nattick, Massachusetts, USA) were used.

The CytoSense flow-cytometer provides multiple data points per channel per particle. This signal or so-called pulse shape is achieved for both scatter channels as well as green, orange and red fluorescence channels (Dubelaar and Gerritzen 2000). For exemplary pulse shapes see Ehgartner et al. (2016a). These pulse shapes are the basis for multiple curve parameters. Except for length parameters in  $\mu\text{m}$ , all parameters are in arbitrary units. The most relevant for the here presented study are the following:

- Maximum: Maximum of signal curve
- Total: Area beneath the curve
- Length: Length of the signal
- Sample length: Length of signal above trigger level
- Fill factor: Similarity of the curve to a block (0-1; the more block-shaped, the higher)

Furthermore, the image-in-flow feature enables picture taking of particles in the flow cell. These pictures are connected to measurement data of the respective particle, facilitating method development by the visual evaluation of the measured particle.

## **Results**

### **Differentiation of morphological classes via clustering**

To differentiate morphological classes like the ones described in the introduction section, visual and statistical clustering was applied based on curve properties of SWS and FWS signal. The investigation was based on FWS and SWS which represent size, shape and surface properties of measured elements (Dubelaar and Gerritzen 2000).

For the distinction of fungal elements from media background, only elements with a threshold of total green fluorescence higher than 30 representing fluorescein diacetate staining were evaluated. In a first step, scatter plots were created and gates were set to represent observed clusters. The image-in-flow feature supported the identification of the morphological classes, as it could be identified whether this class represented single hyphae or rather loose aggregates or pellets with a dense core.

*Table 1: Cluster analyses and morphological classes distinguished*

<b>Cluster analysis</b>	<b>Nr. Of clusters</b>	<b>Clusters equivalent to visual clustering</b>
k-means	4	1 cluster represented all hyphal aggregates
k-means	3	Pellets, large clumps
Hierarchical average Euclidean	2	Small elements vs. large elements

For more exact setting of the gate boundaries defined by this visual clustering, cluster analyses were calculated in Matlab (MathWorks, Nattick, Massachusetts, USA). Only analyses resulting in up to five clusters were then further investigated. Some clusters found by cluster analysis were totally different than the clusters found via visual clustering. Differences between these clusters could not be enabled watching the pictures of the flow cell. But single clusters were equivalent to the clusters found by visual clustering. These were helpful for setting exact boundaries of the gates for morphological differentiation (see Table 1).

### Definition of morphological classes

The thereby extracted differentiation of morphological classes is shown in Figure 1. Summarizing the scatter plots in Figure 1, the following values are needed to distinguish the four sub-classes hyphae, small clumps, large clumps and pellets:

- Small vs. large elements: sample length vs. SWS total (Figure 1a)
  - Further differentiation of small elements → Hyphae vs. small clumps: FWS length vs. SWS total (Figure 1b)
  - Further differentiation of large elements → Large clumps vs. pellets: SWS total/sample length vs. FWS maximal/FWS fill factor ((Figure 1c)

A further distinction of pellets from large clumps apart from the properties depicted in Figure 1c is that pellets are defined to have a dense core. This is reflected in a saturation in the FWS signal (FWS maximum =  $10^4$ ).

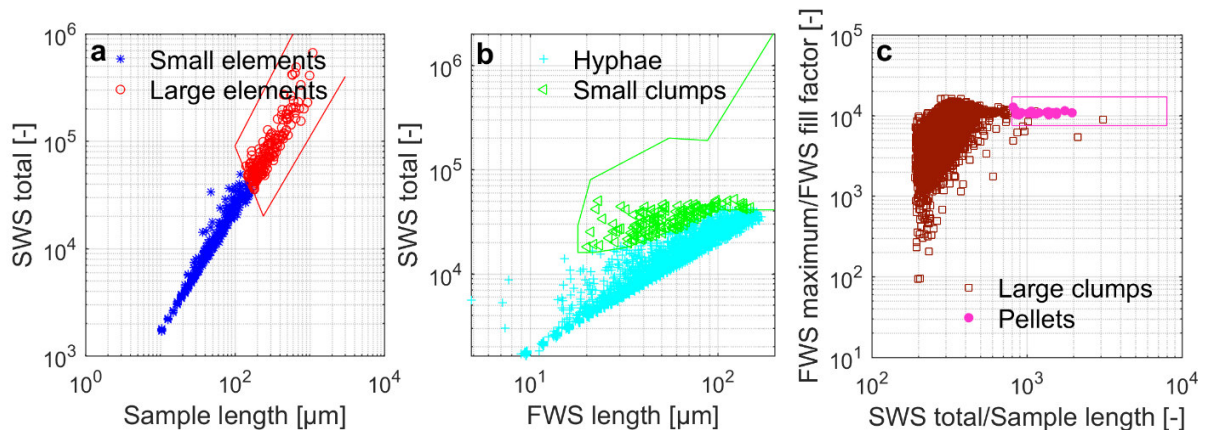


Figure 1: Distinction of morphological classes. A) Small elements including single hyphae and small clumps are represented as blue stars while large elements consisting of large clumps and pellets are in the red gate shown as red circles. These two populations are distinguished by sample length and SWS total. B) Further investigation of small elements: Distinguishing hyphae (turquoise crosses) and small clumps (green triangles). Latter must be placed in the green gate. Else, the small element was defined to be a hypha. C) Further investigation of large elements: One distinction criteria for pellets from large clumps was by SWS total/sample length and FWS maximum/FWS fill factor. A large element found in the pink square-like gate which in addition has a saturated FWS was defined to be a pellet (see pink dots). Large elements not meeting one or both criteria are large clumps which are represented by dark red squares

## **Comparing flow cytometry and microscopy method**

### Definition of morphological classes

In Table 2 the definitions of the morphological classes as described above are compared to the morphological classes of image analysis developed by Posch et al. (2012).

While the distinction of hyphae and small clumps as well as of small and large elements is clearly based on size and shape, the definition of pellets except from the saturated FWS seems more complex. Both, FWS maximal/FWS fill factor and SWS total/sample length, give a more-dimensional representation of the measured element. FWS maximal/FWS fill factor combines size (maximum of signal curve) with three-dimensional shape properties given by the fill factor. Similar is the case for SWS total/sample length. Here, the ratio of three-dimensional size (area beneath the curve being influenced by the length of the element but also by height and surface) to the one-dimensional size (length of element) is presented.

Table 2: Definition of morphological classes for the flow cytometry method vs. image analysis

	Microscopy	Flow cytometry
<b>Hyphae</b>	<ul style="list-style-type: none"> <li>• Area bigger than 100 <math>\mu\text{m}^2</math>:  <ul style="list-style-type: none"> <li>→ When a hyphal diameter of 3 <math>\mu\text{m}</math> is assumed, this means that the minimal length of hyphae is 33.3 <math>\mu\text{m}</math>.</li> </ul> </li> <li>• Area smaller than 3500 <math>\mu\text{m}^2</math></li> <li>• Skeletonized pictures do not form a loop (Paul and Thomas 1998)</li> </ul>	<ul style="list-style-type: none"> <li>• Sample length between 10 <math>\mu\text{m}</math> and 150 <math>\mu\text{m}</math></li> <li>• SWS total smaller than <math>4 \cdot 10^4</math>*</li> <li>• FWS length below 190 <math>\mu\text{m}</math>*</li> </ul>
<b>Small clumps</b>	<ul style="list-style-type: none"> <li>• Area in-between 1000 <math>\mu\text{m}^2</math> and 3500 <math>\mu\text{m}^2</math></li> <li>• Skeletonized pictures forms a loop (Paul and Thomas 1998).</li> </ul>	<ul style="list-style-type: none"> <li>• Sample length between 10 <math>\mu\text{m}</math> and 150 <math>\mu\text{m}</math></li> <li>• SWS total in-between <math>1.8 \cdot 10^4</math> and <math>9 \cdot 10^4</math>*</li> <li>• FWS length higher than 18 <math>\mu\text{m}</math>*</li> </ul>
<b>Large clumps</b>	<ul style="list-style-type: none"> <li>• Area bigger than 3500 <math>\mu\text{m}^2</math></li> <li>• Hyphal aggregate not classified as pellet</li> </ul>	<ul style="list-style-type: none"> <li>• SWS total higher than <math>2 \cdot 10^4</math> and sample length bigger than 100 <math>\mu\text{m}</math></li> <li>• Is not a pellet</li> </ul>
<b>Pellet</b>	<ul style="list-style-type: none"> <li>• Area bigger than 7500 <math>\mu\text{m}^2</math></li> <li>• Has a core</li> <li>• Core area bigger than 7000 <math>\mu\text{m}^2</math></li> </ul>	<ul style="list-style-type: none"> <li>• SWS total higher than <math>4 \cdot 10^4</math> and sample length bigger than 120 <math>\mu\text{m}</math></li> <li>• A core exists (saturated FWS)</li> <li>• Ratio of FWS maximal:FWS fill factor bigger than <math>7.5 \cdot 10^3</math></li> <li>• SWS total:sample length bigger than <math>8 \cdot 10^2</math></li> </ul>

\* For exact ratios see Figure 1

Element sizes and total size distribution

Figure 2 shows average size and size distribution over process time determined by both methods (microscopy and flow cytometry) for small clumps (a), large clumps (b) and pellets (c). Although the sizes are overlapping, clumps tend to be smaller in flow cytometry, while pellets are in average slightly larger. These differences are caused by variations in the definition of morphological classes between the two methods. However, the average size of the morphological classes is for both methods in the same dimension. This is an important finding as the methodology for morphological description via flow cytometry differs from microscopy, but still, the definition of the morphological sub-classes ought to be equivalent. Hence, the flow cytometry method does not aim to invent new morphological sub-classes but stresses much more to yield well-known classification into hyphae, clumps and pellets and its statistically consistent quantification.

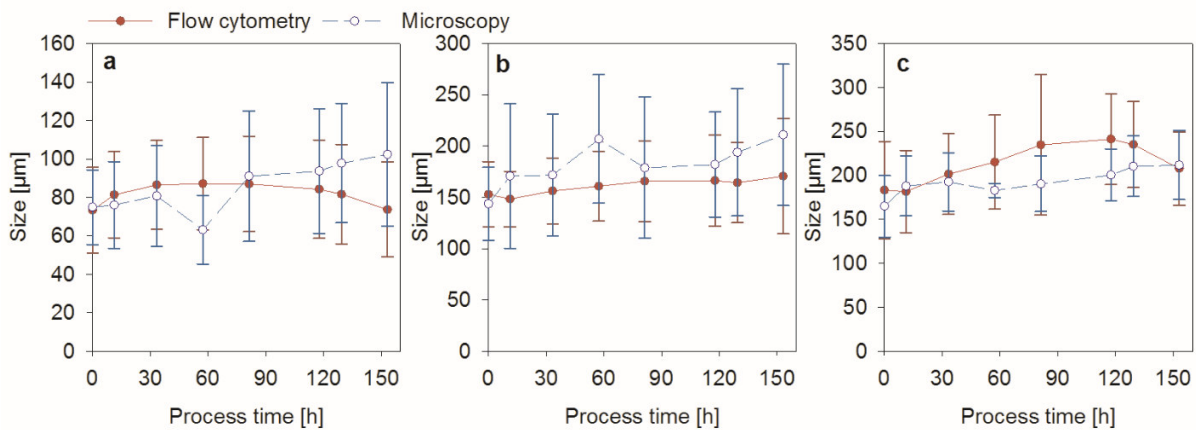


Figure 2: Average size of small clumps (a), large clumps (b) and pellets (c) over process time of FB1 determined by flow cytometry and the microscopy method. The error bars show the size distribution for each class

Figure 3 shows that size distributions of hyphal aggregates and large elements resulting from both methods are in the same range. Microscopy reveals in average slightly bigger aggregates and large elements than flow cytometry. The size distributions are presented in relative values related to the total number of hyphal aggregates (Figure 3a) respective large elements (Figure 3a) measured with each of the two methods.

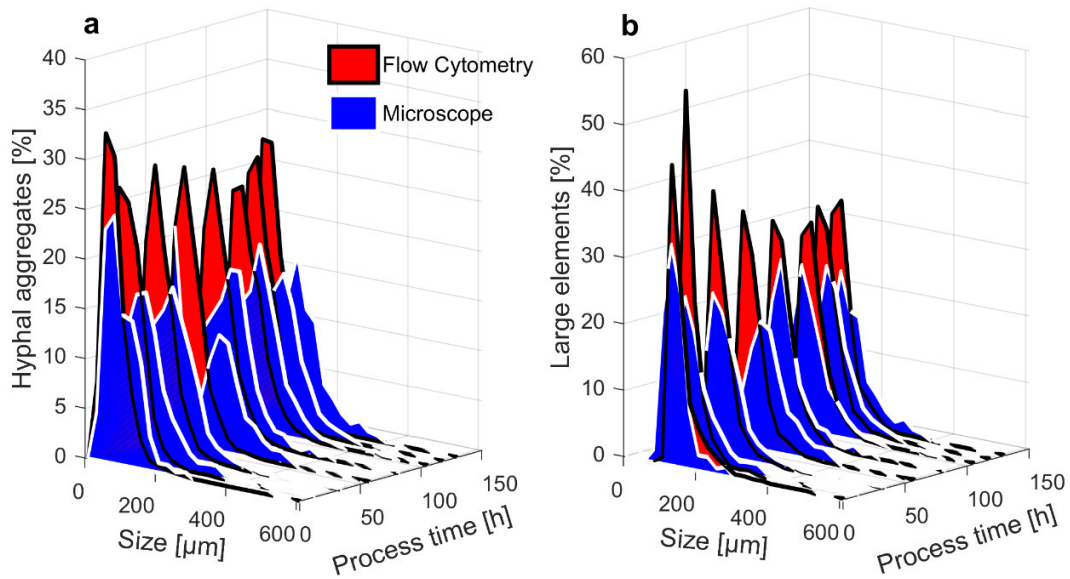


Figure 3: Size distribution over process time determined via flow cytometry and the microscopy method for FB1. a) hyphal aggregates, b) large elements (large clumps and pellets)

### Pellet morphology

Signal properties can be used to describe single morphological classes more in detail, as for example pellets. Fullness and roughness are parameters resulting from light microscopy comparing pellet core and the less dense hyphal area in the outer layer. For more details of calculation see Equation 1 and Equation 2. The parameter “relative annular diameter” (RAD) (see Equation 3) was set up for the flow cytometry method, to reveal a parameter with similar information about pellet morphology. The value of RAD decreases when the layer of hyphae at the outside of the pellet is smaller (see Figure 4a-c, Figure S1 in the supplementary material). Plotting RAD over process time together with pellet fullness and roughness (see Figure 4f) shows the similarity of the information.

$$RAD = \frac{\text{Annular diameter}}{\text{Particle length}}$$

Equation 3: Relative annular diameter (RAD). The annular diameter is the length of the annular area (outside of pellet core – see Figure 4a-c). Particle length is the length of the FWS signal as shown in Figure 4a-c

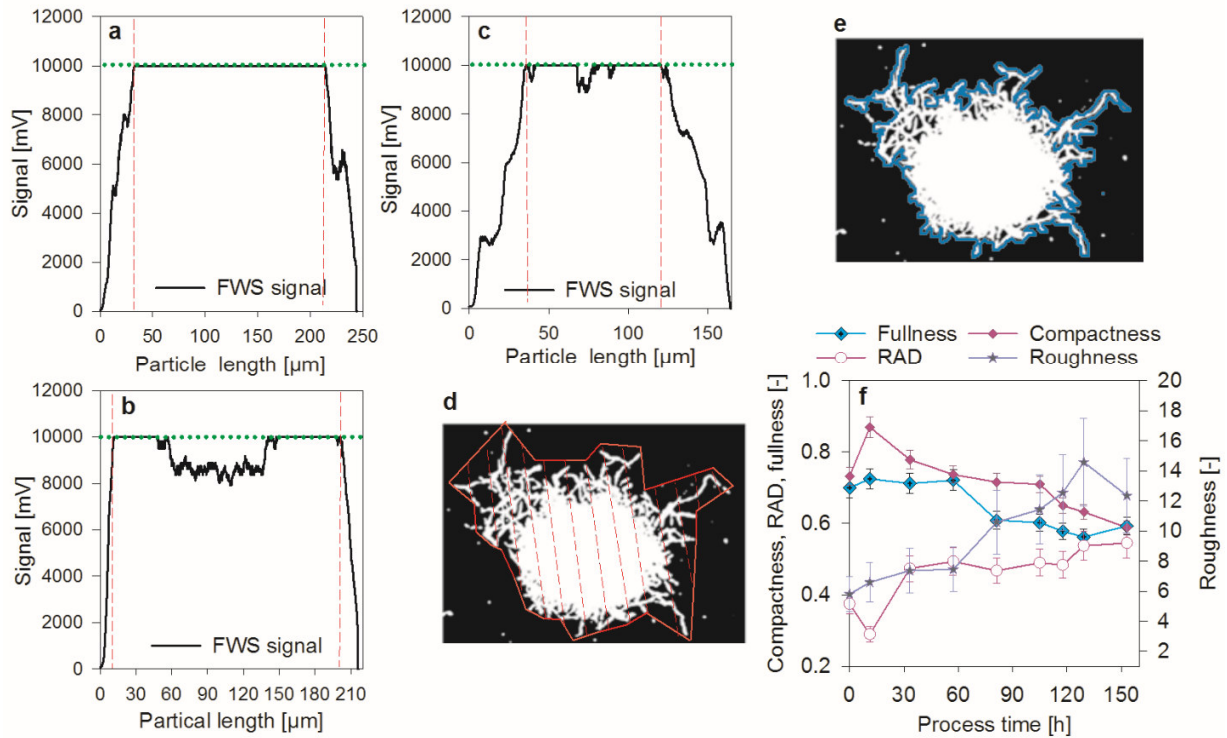


Figure 4: Fullness and roughness from the microscopy method and corresponding parameters deriving from the FWS signal of the flow cytometer. a-c) The FWS signals of three pellets are shown. The inner pellet core is indicated by two vertical lines. The horizontal line shows the saturation of the FWS signal. (a) Pellet with low relative annular diameter (0.26) and high compactness (1.0). b) Pellet with very low relative annular diameter (0.12) and low core compactness (0.49). c) Pellet with high relative annular diameter (0.46) and average core compactness (0.77) d-e) Pellet pictures from microscopy after conversion to binary image. The convex area for fullness calculation (d) and the perimeter for roughness calculation (e) are shown. The area for calculation of these two parameters is the sum of all white pixels of the pellet. f) Comparison of RAD determined via flow cytometry and pellet fullness and roughness measured with microscopy for FB2. In addition, core compactness is shown. Pictures of the pellets shown in Figure 4a-c can be found in Figure S1 in the supplementary material

By considering the definitions of morphological classes for the flow cytometry and the image analysis, differences in the time courses of the pellet specific parameters are self-evident. While the roughness is based on changes of the real perimeter respective to the perimeter of a circle of the same area, RAD calculation is based on the ratio of the diameter of the annular region and the diameter of the whole pellet. The annular diameter is the length of FWS from the begin of the signal until the first saturation of the signal is reached, and this from both sides of the pulse shape. However, a FWS signal below saturation does not necessarily represent loose hyphal structure, but may as well represent degraded core regions as shown in Figure 4b. The FWS signal in the center of this pellet is not saturated. This region of the pellet would be supposed to be the “weak point” of the pellet, the region where it may break at high shear forces. After breakage of such a pellet, this region would be counted as annular area, as it is between the start of the FWS signal and its first saturation. Thus, such a broken pellet has a high RAD, while the roughness determined by microscopy would be proportionally low. Latter is the case

because this vacuolized/lysed region seems black/dark on the picture as a normally dense core does. Hence, it is not visible under the microscope (see Figure S1b in the supplementary material).

As the RAD does not distinguish between young rough pellets and broken degraded ones, the compactness can be used as additional parameter for the discrimination of those. A pellet with high RAD and low compactness is more likely to be a degraded one than a young rough pellet, were the pellet core is still intact. Furthermore, RAD and compactness over passage of time give insight why a RAD value is high.

A weak point, which both methods for annular region description – roughness determination via microscopy and RAD via flow cytometry – have in common, is that these values represent a 2-dimensional measurement of a 3-dimensional phenomenon. In large pellets, the core may seem bigger than it really is, as hyphae from the annular region are pressed together and hence seem dark when put on the microscopy slide. Similar it may occur in flow cytometry. In larger pellets the light needs to pass through more hyphae in the annular region to reach the detector because of the higher pellet diameter. Therefore, the FWS signal may easier be saturated than in pellets with lower diameter.

Another parameter based on the pulse shape of FWS, is the pellet core compactness (short “compactness”). As Figure 4a-c and Equation 4 show, this parameter represents the density of the pellet core. Older hyphae are described to contain high numbers of vacuoles, which makes them weak and more possible to break (Paul et al. 1998). The here presented compactness value decreases with the age of the pellets (Equation 4f), possibly due to vacuolization and lysis.

$$\text{Compactness} = \frac{\text{Saturated FWS signal in pellet core}}{\text{Core diameter}}$$

*Equation 4: Compactness of the pellet core. This parameter is calculated as the relative length of saturated FWS signal in the pellet core*

### Measurement error and robustness

As stated in the introduction section, we aim to present an at-line applicable high throughput method for morphological analysis which is faster, but comparable to state-of-the-art image analysis via microscopy. To be a reasonable alternative, the robustness and validity of the method is of utter importance.

By taking 900 pictures per sample with the image analysis method, approximately a volume of 0.5 µl to 2.5 µl is analyzed. In detail, two microscopy slides with 50 µl of 1:10 to 1:50 diluted broth per slide are

investigated. The dilution depends on the biomass concentration, as the samples ought to be diluted to a final biomass concentration beneath 1 g/l to avoid overlapping of hyphal elements. Compared to the volume of 0.5 µl to 2.5 µl investigated via microscopy, approximately 5 µl of sample are investigated with the flow cytometry method. This is 2- to 10-fold more investigated sample. In flow cytometry, each sample is measured at least four times in a 1:1000 dilution. The in average measured volume of diluted sample per single measurement is 1200 µl.

*Table 3: Measurement errors for the most common morphological parameters of microscopy and flow cytometry. The average measurement errors are given in % and in absolute units*

	Microscopy		Flow Cytometry	
	%	Absolute	%	Absolute
<b>Diameter/SWS sample length small clumps</b>	5	4 µm	1	1 µm
<b>Diameter/SWS sample length large clumps</b>	4	7 µm	1	2 µm
<b>Diameter/SWS sample length pellets</b>	6	11 µm	4	9 µm
<b>Roughness/Fullness pellets</b>	20/4	1.6/0.03	-	-
<b>Compactness pellets</b>	-	-	3	0.02
<b>Relative annular diameter pellets</b>	-	-	8	0.03
<b>Conc./ml hyphae</b>	-	-	7	58*10 <sup>4</sup> hyphae/ml
<b>Conc./ml small clumps</b>	-	-	4	61000 small clumps/ml
<b>Conc./ml large clumps</b>	-	-	10	39000 large clumps/ml
<b>Conc./ml pellets</b>	-	-	24	7500 pellets/ml

The average errors of the two methods are shown in Table 3. Errors were evaluated using three samples, taken at different process times. The samples varied in various parameters as DCW (10-25 g/l), pellet fraction (13-23%), SWS length of pellets (182-237 µm). For microscopy, six slides were measured per sample to evaluate the error. In flow cytometry, a 4-fold measurement was applied for error calculation.

Only few parameters can be compared, as the microscopy method does not allow the evaluation of absolute concentrations. Image analysis based on microscopy is no method resulting in concentration measurements. All data received are relative values compared to the measured population. A big part of the microscope slide is scanned, but nevertheless there are regions not measured. In addition, excess

fluid at the border of microscope slides is discarded. Hence, an exact calculation of the measured concentration of hyphal aggregates is not possible.

Concerning the determination of the size of pellets, the error is comparable (6% vs. 4%). The error for diameter investigation of clumps is lower for the flow cytometry method (1%) compared to microscopy (4-5%). Errors of the microscopy method could be decreased by evaluating higher amounts of pictures (e.g. 4000 instead of 900) which was done when originally published (Posch et al. 2012). But taking four times more pictures than it was done for this study, would increase the workload for morphological investigation by far and is thus not applicable for using it as real-time method.

Concerning the description of pellet morphology, the most robust determination was the evaluation of fullness (4%). The pendant of the flow cytometry method – RAD – showed an average error of 8%. The high variation (20%) for roughness determination can be explained by the high dependency of perimeter calculation on the conversion of the original picture to a binary one. Dependent on the evenness of Köhler illumination and the contrast during microscopy, the quality of the microscopic pictures, especially of the hyphae, varies. For the conversion to a binary image a threshold level has to be set. The difficulty thereby is to adjust the threshold in that way, that all hyphae are fully recognized as part of the hyphal aggregate, but that shadows are not recognized as such. Hence, it is a factor of variation, especially when the pictures are taken on different days and hence, slightly different adjustments of the microscope.

The average errors of parameters not accessible via image analysis but measurable with the flow cytometry method are compactness and the concentration of hyphae and hyphal aggregates as shown in Figure 4. For compactness, the average error was 3%, which is by far lower as for example the error on RAD (8%). Concerning the concentration of the morphological classes, the error increases with the decrease of prevalence of representations of each class. For illustration, in the sample at  $t = 80$  h of FB1  $3 \cdot 10^4$  pellets/ml were measured. 20 times more large clumps were found. Numbers for hyphae and small clumps were above  $10^6$  per milliliter sample. Hence, the number of pellets in the 1:1000 diluted sample for flow cytometry is extremely low – especially when compared to hyphae and small clumps.

**Application of flow cytometry method: Morphological description of two fed-batches**

Morphological classes

In the following, two fed-batches are analyzed with the here presented flow cytometry method. The fed-batches derived from one batch and differed in their feeding profiles. While FB1 had a constant feed throughout the whole process, FB2 was fed with an exponential profile starting after 48 h.

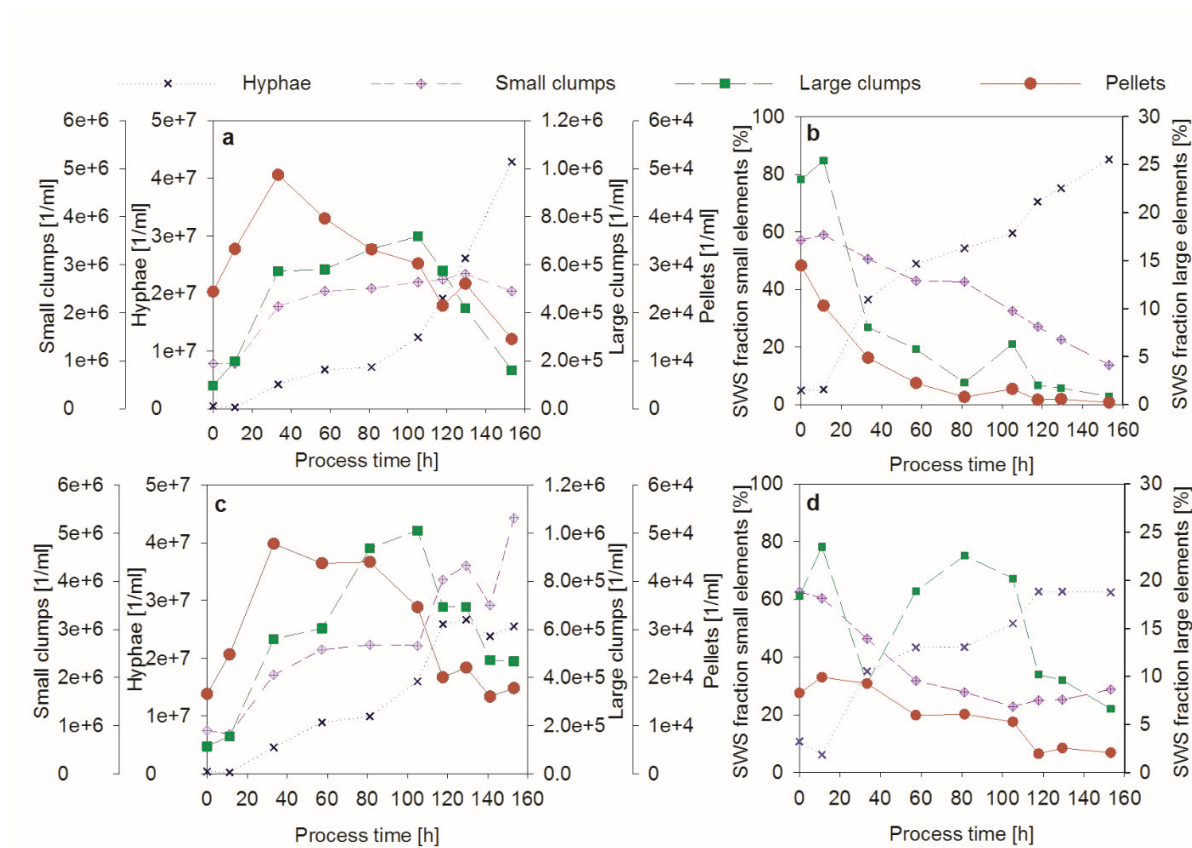


Figure 5: Distribution of the hyphal elements in the different morphological classes for FB1 (a, b) and FB2 (c, d). a, c) represent absolute concentrations of hyphae and hyphal aggregates in the different morphological classes. b, d) represent SWS fractions of morphological classes

The concentration of elements divided into morphological classes is shown in Figure 5a/c. An alternative representation of the morphological classes is the SWS fraction (see Equation 5/ Figure 5b/d).

$$\text{SWS fraction} = \frac{\sum \text{SWS total}_{\text{Elements class } x}}{\sum \text{SWS total}_{\text{AllElements}}} * 100$$

Equation 5: SWS fraction

The SWS fraction explains the ratio between the SWS total values of an elemental class to the total value. With this fraction the distribution of fungal biomass in morphological classes could be better shown than with the specific concentration of elements. This is explainable by the enormous differences in volume of one single hyphae compared to one single pellet. Therefore the SWS fraction ought to be more feasible to represent the distribution of biomass volume in the morphological classes. However, for direct comparison of fed-batches, the concentration of elements could be of advantage as a direct measurement is available.

An alternative to SWS fraction could be FWS fraction, as FWS is better known to represent size. However, FWS is saturated when pellets are measured. Thus, the number of pellets would be underestimated.

Comparing concentration of hyphae and hyphal aggregates for FB1 and FB2, as shown in Figure 5a and Figure 5c, results in the following insights: In the first 40 h nearly identical trends for the fed-batches were observable. Only the concentration of pellets in FB1 was slightly higher. Concentrations in all morphological sub-classes were raising for the first 40 h of fed-batch. As both fed-batches were inoculated from the same batch and had the same feeding profile during the first 48 h, the same trends and concentrations of morphological sub-classes were expected. Slight differences especially concerning the pellet concentration may result from sedimentation effects during the transfer of batch culture to the fed-batch medium.

After 48 h the feed in FB2 began to raise exponentially, while the feed in FB1 was constant. This difference in feeding profile is reflected in morphological differences. The pellet concentration in FB1 decreased sharply while the concentrations of clumps raised slowly. Further, the concentration of hyphae increased almost exponentially to reach a maximum at the end of cultivation. In FB2 the pellet concentration was constant until  $t=80$  h. In addition, the concentration of large clumps increased until  $t=105$  h and afterwards the concentration of small clumps followed the same trend. The concentration of hyphae increased throughout the fed-batch. Still, the final concentration was only approximately the half of the more than  $4 \cdot 10^7$  hyphae/ml in FB1.

The SWS fraction, shown in Figure 5b/d, described a partially different situation. In FB1, there is a tendency to more large elements. There were not only more pellets, but also the SWS fraction of large clumps was higher. As the concentrations of large clumps showed to be the same in Figure 5a/c, this could be explained by the size of the single elements. In FB1 with the constant low feed rate, aggregates

diminish in favor of free dispersed growth. Contrary, FB2 shows an increase in larger aggregates, especially until 80 h of process time. The largest contrast due to different feeding profiles was observed for large clumps. While the concentration constantly decreased in FB1, it strongly raised in FB2. At  $t=80$  h, the SWS fraction of large clumps in FB1 was 2% compared to 23% in FB2.

### Size distribution

Figure 6 compares the size distributions of FB1 and FB2. Concerning hyphal aggregates and large elements, the size distribution did not differ significantly between the two cultivations. As a trend, the size distribution of hyphal aggregates became wider to reach a maximum at approximately 100 h. Further on, the wideness of the distribution decreased. The trend for large elements was different. Size distribution became wider over the whole process time.

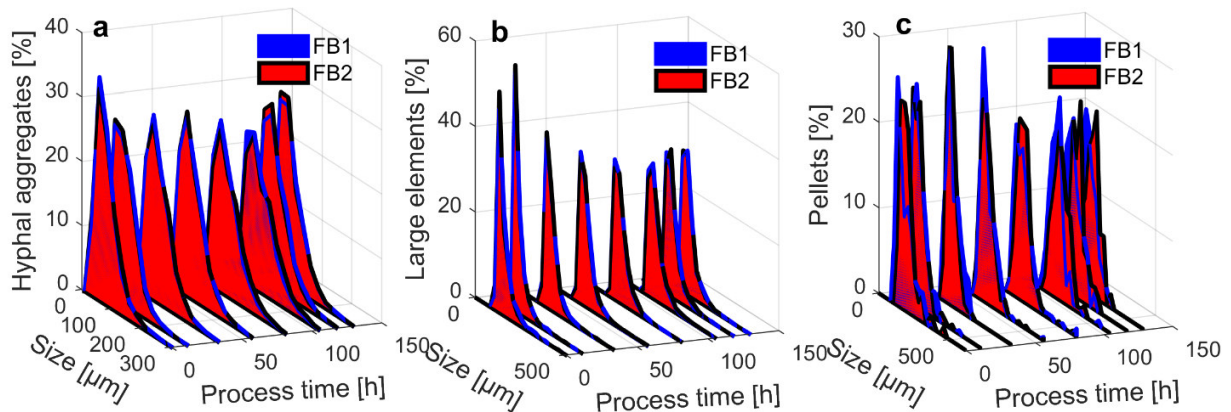


Figure 6: Comparing size distribution over process time for FB1 and FB2. Shown is the distribution of aggregates including small clumps, large clumps and pellets (a), large elements including large clumps and pellets (b) and pellets only (c)

### Pellet morphology

As already described above, RAD was introduced to describe the relative roughness/hairiness and the percentage annular area of the pellet. Figure 7 compares RAD for FB1 and FB2 over process time. Apart from the last sample, the time courses of RAD were comparable in both cultivations. The value decreased in the first 12 h of fed-batch, probably due to pellet formation and the growth to denser hyphal aggregate. After re-increasing until 40 h of fed-batch, it stayed constant for 80 h. In the last 30 h of fed-batch it decreased in both cultivations, but to a higher extend in FB1.

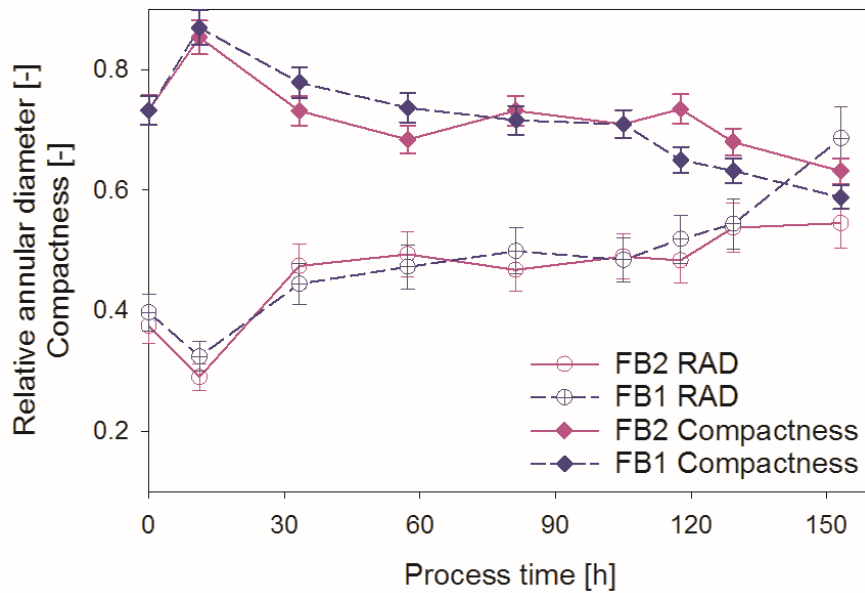


Figure 7: Relative annular diameter and compactness of pellets in FB1 and FB2

Figure 7 compares the compactness for FB1 and FB2 over process time. In sum, the trend of compactness was opposed to the one of RAD. In FB1 the value decreased with ongoing process time. Opposed to that, it was constant in FB2 between 60 h and 120 h. Then, it further decreased at the end of cultivation. In the last hours of fed-batch, the compactness of FB2 was slightly lower than in FB1. This difference could probably be due to higher substrate limitation in the lower feeding regime of FB1.

The high increase of RAD at the end of FB1 could be connected to the decrease of pellet compactness and ongoing pellet breakage. This goes in line with the sharp decrease of pellet and large clump concentration at the end of FB1 as shown in Figure 5.

## Discussion

### **Comparability of the methods**

Within this contribution, a novel method for morphological analysis based on flow cytometry was presented. It aimed to be a faster alternative to image analysis via microscopy, and was thus compared to the image analysis method described by Posch et al. (2012). In general, the question should be answered: Are these two methods comparable? The morphological principle based on the flow

cytometry method as well as image analysis is the same. Both methodologies differentiate several classes of morphology depending on their size and grade of aggregation. Historically, this was the basis for several morphological analysis methods (Cox et al. 1998; Paul and Thomas 1998; Posch et al. 2012; Quintanilla et al. 2015). Both methods are applicable for filamentous cultures with a mixture of dispersed and pellet growth, but could also be applied for pure pellet cultures. The morphological parameters gained from the here presented method focus on size parameters for all morphological classes and the more detailed description of pellet morphology. Apart from the pellet compactness, which is not accessible as such by microscopy, all parameters fitted well between the two methods or showed the same trends in time courses. The occurrence of partially larger elements in size distribution for the image analysis method can be explained by differences in measurement principle. Hyphal aggregates ought to overlap on microscopy slides. Due to the branched morphology, hyphae and aggregates tend to intercalate, which makes differentiation on microscopic slides difficult. The sheath flow in the flow cytometer hampers overlapping of separate hyphae/hyphal aggregates.

Not comparable is the information about hyphae and hyphal aggregate concentrations. Image analysis per se is not a fully quantitative method, but results in relative distributions within the measured population. Hence, no absolute concentrations can be evaluated. Of course, rough estimations about absolute concentrations can be done, but these ought to be quite error prone. Quantitative data about the distribution of biomass within the morphological subclasses in image analysis are gained by the so-called area fractions. This parameter results from summing the area of all hyphal elements and relating the summed area of each sub-class to the total area (for more details see (Golabgir et al. 2015)). Thereby, the relative area of the sub-classes can be compared. But this method is not directly comparable to a concentration measurement, as a pellet takes more area in relation to hyphae. A similar approach to area fraction is the here presented SWS fraction. But the principle behind the two methods – area vs. scatter signal curve – is too different to try comparisons.

Another issue of comparability is the method of elimination of background as for example media particles. In image analysis this is done via shape and fullness measurements (Paul and Thomas 1998). For the here presented flow cytometry method, a viability staining with fluorescein diacetate was conducted. All particles with green fluorescence were concluded to be hyphae and hyphal aggregates. Investigation of fluorescein diacetate staining with fluorescence microscopy had revealed that medium particles from our culture were not stained by this marker (Ehgartner et al. 2016b). Only some small hyphae were red fluorescent without showing green fluorescence. Although pellets showed to include

dead biomass in the core, sufficient green fluorescence was present to be above the threshold and hence being classified as viable hyphal element. Consequently, a comparability of the flow cytometry method with image analysis should not be hampered by the methodology of background separation.

### **Advantages and disadvantages of flow cytometry method**

The here developed flow cytometry method for morphological analysis is able to describe pellet morphology and in addition it produces information about size of other morphological subclasses. So far, these other morphological subclasses were not further described by the here developed method. Hence, detailed description of freely dispersed cultures concerning branching grade, hyphal growth unit and vacuolization grade as it was shown via image analysis methods is not (yet) possible (Cox et al. 1998; Paul and Thomas 1998; Posch et al. 2012; Vanhoutte et al. 1995). Description of hyphal tips as it is done via hyphal growth unit is possibly easier via microscopy, as hyphae are well represented on a two-dimensional space as a microscope slide. Approaching hyphal morphology via light scattering might be more abstract, but could be possible. The easy applicability of fluorescence dyes in flow cytometry promises to be a big advantage compared to image analysis. Via fluorescence staining, information about vacuolization and the evaluation of other physiological states as it was shown by Vanhoutte et al. (1995) is accessible. Evaluation of physiological states via fluorescence microscopy is possible, but automation of this microscopy method and development of an automated image analysis is even more difficult and time consuming than image analysis of light microscopy. In contrast, in flow cytometry fluorescence staining is easily combinable with morphological analysis. Although the fluorescence was not further investigated, a viability staining combination was applied in this study. So far, it was only used to distinguish hyphal elements from background. An example would be the staining and herewith the localization of vacuoles via flow cytometry in hyphae or substrate diffusion in pellets. A similar approach was presented for the red fluorescence of chlorophyll in phytoplankton (Dubelaar et al. 2004).

Further advantages of the flow cytometer method are – as already mentioned – the measurement of hyphal elements in a liquid flow. Thereby, the overlap of hyphal elements is avoided.

The method is faster, even at-line applicable, and much higher throughput than in microscopy is possible. In the way, the method was conducted for this study, at-line application is even crucial. The reason for this is the application of viability staining for the distinction of hyphal elements from background. Hence, offline measurements at a later stage are limited.

The higher throughput makes an investigation of more sample volume possible, giving higher robustness to the method. This is shown by the comparison of average measurement error between image analysis and the flow cytometry method. Latter tended to have a lower error. Another advantage in respect to lower measurement errors is the influence of the operator. Preparation of microscopic slides (regular distribution of hyphal element on the slide), adjusting of illumination and contrast as well as threshold setting for binarization of images, is a matter of routine and partially operator dependent. These manual manipulations of the cultivation sample decrease the robustness of the microscopy method. Contrary to that, sample preparation for flow cytometry only consists of dilution steps and fluorescence staining. Data treatment is conducted with beforehand provided software files in CytoClus (CytoBuoy, Woerden, Netherlands) and Matlab scripts (MathWorks, Nattick, Massachusetts, USA), and thereby totally independent of the user.

Finally, the already addressed quantitative information gained from the flow cytometry method is evaluated as a great advantage and can be used as an at-line tool in production environments.

#### **Applicability of the method**

The here presented flow cytometry method generates the same outputs regarding fungi morphology as image analysis methods do so far. As described in the introduction section, morphology is a central point in filamentous biocultures. It is linked to broth viscosity which influence substrate transport and power input (Paul et al. 1994; Petersen et al. 2008). Furthermore, productivity is linked to morphology, which could be important for industrial production as well as process development (Papagianni 2004). On the other hand, process conditions influence morphology (Quintanilla et al. 2015). This chain of effect is an important reason to monitor morphological parameters during process development and scale up. Apart from pharmaceutical bioprocesses, various fields of science are associated with filamentous fungi as for example environmental research on soil, water, air and food (Prigione and Filipello Marchisio 2004).

To sum it up, the here developed flow cytometry method for morphological analysis is a fast and at-line applicable alternative to common morphology tools as image analysis. The application for a penicillin production process was presented, but applications in other bioprocesses and even other fields of investigation seem possible. The method distinguishes four morphological sub-populations and describes their morphology in more detail. Within this application, the focus was especially on pellets.

### **Acknowledgements:**

We thank the Austrian Federal Ministry of Science, Research and Economy in course of the Christian Doppler Laboratory for Mechanistic and Physiological Methods for Improved Bioprocesses for financial support. Strains for the experiments were gratefully provided by Sandoz GmbH (Kundl, Austria).

### **Compliance with Ethical Standards**

**Funding:** This study was funded by Austrian Federal Ministry of Science, Research and Economy in course of the Christian Doppler Laboratory for Mechanistic and Physiological Methods for Improved Bioprocesses (grand number 171).

**Conflict of Interest:** The authors declare that they have no conflict of interest.

**Ethical approval:** This article does not contain any studies with human participants or animals performed by any of the authors.

### **References**

- Chain EB, Gualandi G, Morisi G (1966) Aeration Studies. IV. Aeration Conditions in 3000-Liter Submerged Fermentations with Various Microorganisms. *Biotechnol Bioeng* 8:595-619  
doi:10.1002/bit.260080411
- Christiansen T, Spohr AB, Nielsen J (1999) On-line study of growth kinetics of single hyphae of *Aspergillus oryzae* in a flow-through cell. *Biotechnol Bioeng* 63:147-153
- Cox PW, Paul GC, Thomas CR (1998) Image analysis of the morphology of filamentous micro-organisms. *Microbiol* 144 ( Pt 4):817-827 doi:10.1099/00221287-144-4-817
- de Bekker C, van Veluw GJ, Vinck A, Wiebenga LA, Wosten HA (2011) Heterogeneity of *Aspergillus niger* microcolonies in liquid shaken cultures. *Appl Environment Microbiol* 77:1263-1267  
doi:10.1128/AEM.02134-10
- Delgado-Ramos L, Marcos AT, Ramos-Guelfo MS, Sanchez-Barrionuevo L, Smet F, Chavez S, Canovas D (2014) Flow cytometry of microencapsulated colonies for genetics analysis of filamentous fungi. *G3: Genes Genomes Gen* 4:2271-2278 doi:10.1534/g3.114.014357
- Dubelaar GB, Geerders PJ, Jonker RR (2004) High frequency monitoring reveals phytoplankton dynamics. *J Environment Monit : JEM* 6:946-952 doi:10.1039/b409350j
- Dubelaar GBJ, Gerritzen PL (2000) CytoBuoy: a step forward towards using flow cytometry in operational oceanography. *Scientia Marina* 64:255-265 doi:10.3989/scimar.2000.64n2255
- Ehgartner D, Fricke J, Schroder A, Herwig C (2016a) At-line determining spore germination of *Penicillium chrysogenum* bioprocesses in complex media. *Appl Microbiol Biotechnol* 100:8923-8930  
doi:10.1007/s00253-016-7787-y

- Ehgartner D, Herwig C, Neutsch L (2016b) At-line determination of spore inoculum quality in *Penicillium chrysogenum* bioprocesses. *Appl Microbiol Biotechnol* 100:5363-5373 doi:10.1007/s00253-016-7319-9
- Ehgartner D, Sagmeister P, Herwig C, Wechselberger P (2015) A novel real-time method to estimate volumetric mass biodensity based on the combination of dielectric spectroscopy and soft-sensors. *J Chem Technol Biotechnol* 90:262-272
- Gibbs PA, Seviour RJ, Schmid F (2000) Growth of filamentous fungi in submerged culture: problems and possible solutions. *Crit Rev Biotechnol* 20:17-48 doi:10.1080/07388550091144177
- Golabgir A, Ehgartner D, Neutsch L, Posch AE, Sagmeister P, Herwig C (2015) Imaging Flow Cytometry and High-Throughput Microscopy for Automated Macroscopic Morphological Analysis of Filamentous Fungi. In: van den Berg MA, Maruthachalam K (eds) *Genetic Transformation Systems in Fungi*, vol 2. *Fungal Biology*. Springer International Publishing, pp 201-210. doi:10.1007/978-3-319-10503-1\_17
- Langemann T, Mayr UB, Meitz A, Lubitz W, Herwig C (2016) Multi-parameter flow cytometry as a process analytical technology (PAT) approach for the assessment of bacterial ghost production. *Appl Microbiol Biotechnol* 100:409-418 doi:10.1007/s00253-015-7089-9
- Lein J (1986) The Panlabs penicillin strain improvement program. *Biotechnol Ser*
- Papagianni M (2004) Fungal morphology and metabolite production in submerged mycelial processes. *Biotechnol Adv* 22:189-259
- Paul GC, Kent CA, Thomas CR (1994) Hyphal vacuolation and fragmentation in *penicillium chrysogenum*. *Biotechnol Bioeng* 44:655-660 doi:10.1002/bit.260440513
- Paul GC, Syddall MT, Thomas CR (1998) A structured model for penicillin production on mixed substrates. *Biochem Eng J* 2:11 doi:10.1016/S1369-703X(98)00012-6
- Paul GC, Thomas CR (1998) Characterisation of mycelial morphology using image analysis. *Adv Biochem Eng/Biotechnol* 60:1-59 doi: 10.1007/BFb0102278
- Petersen N, Stocks S, Gernaey KV (2008) Multivariate models for prediction of rheological characteristics of filamentous fermentation broth from the size distribution. *Biotechnol Bioeng* 100:61-71 doi:10.1002/bit.21732
- Posch AE, Herwig C (2014) Physiological description of multivariate interdependencies between process parameters, morphology and physiology during fed-batch penicillin production. *Biotechnol Progr* 30:689-699 doi: 10.1002/Btpr.1901
- Posch AE, Spadiut O, Herwig C (2012) A novel method for fast and statistically verified morphological characterization of filamentous fungi. *Fungal Genet Biol* : FG & B 49:499-510 doi:10.1016/j.fgb.2012.05.003
- Prigione V, Filipello Marchisio V (2004) Methods to maximise the staining of fungal propagules with fluorescent dyes. *J Microbiol Methods* 59:371-379 doi:10.1016/j.mimet.2004.07.016
- Quintanilla D, Hagemann T, Hansen K, Gernaey KV (2015) Fungal Morphology in Industrial Enzyme Production--Modelling and Monitoring. *Adv Biochem Eng/Biotechnol* 149:29-54 doi:10.1007/10\_2015\_309
- Riley GL, Tucker KG, Paul GC, Thomas CR (2000) Effect of biomass concentration and mycelial morphology on fermentation broth rheology. *Biotechnol Bioeng* 68:160-172 doi: 10.1002/(SICI)1097-0290(20000420)68:2<160::AID-BIT5>3.0.CO;2-P
- Spohr A, Dam-Mikkelsen C, Carlsen M, Nielsen J, Villadsen J (1998) On-line study of fungal morphology during submerged growth in a small flow-through cell. *Biotechnol Bioeng* 58:541-553 doi: 10.1002/(SICI)1097-0290(19980605)58:5<541::AID-BIT11>3.0.CO;2-E
- Vanhoutte B, Pons MN, Thomas CR, Louvel L, Vivier H (1995) Characterization of *Penicillium chrysogenum* physiology in submerged cultures by color and monochrome image analysis. *Biotechnol Bioeng* 48:1-11 doi:10.1002/bit.260480103

Znidarsic P, Pavko A (2001) The morphology of filamentous fungi in submerged cultivations as a bioprocess parameter. *Food Technol Biotech* 39:237-252

**Supplementary material**

**Morphological analysis of filamentous fungi using flow cytometry - the fast alternative to microscopy  
and image analysis**

Daniela Ehgartner<sup>1,2</sup>, Christoph Herwig<sup>1,2</sup> and Jens Fricke<sup>\*,1,2</sup>

\*to whom the correspondence should be addressed to

<sup>1</sup> CD Laboratory on Mechanistic and Physiological Methods for Improved Bioprocesses, TU Wien, Vienna, Austria

<sup>2</sup> Research Area Biochemical Engineering, Institute for Chemical, Environmental and Biological Engineering, TU Wien, Vienna, Austria

Corresponding author:

jens.fricke@tuwien.ac.at

Tel (Office): +43 1 58801 166462

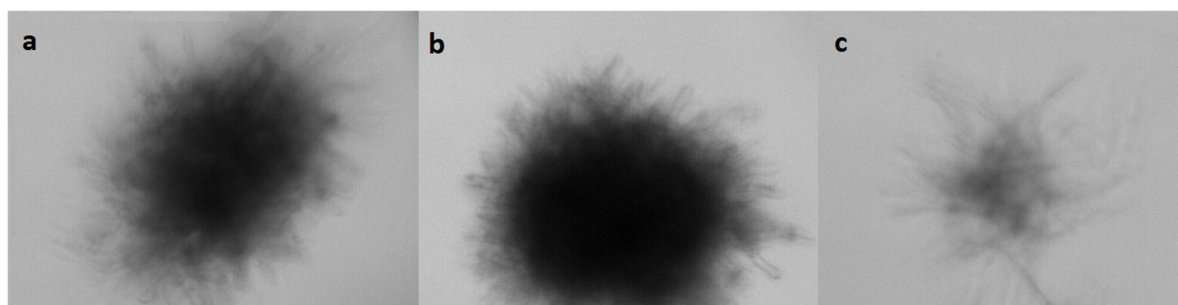
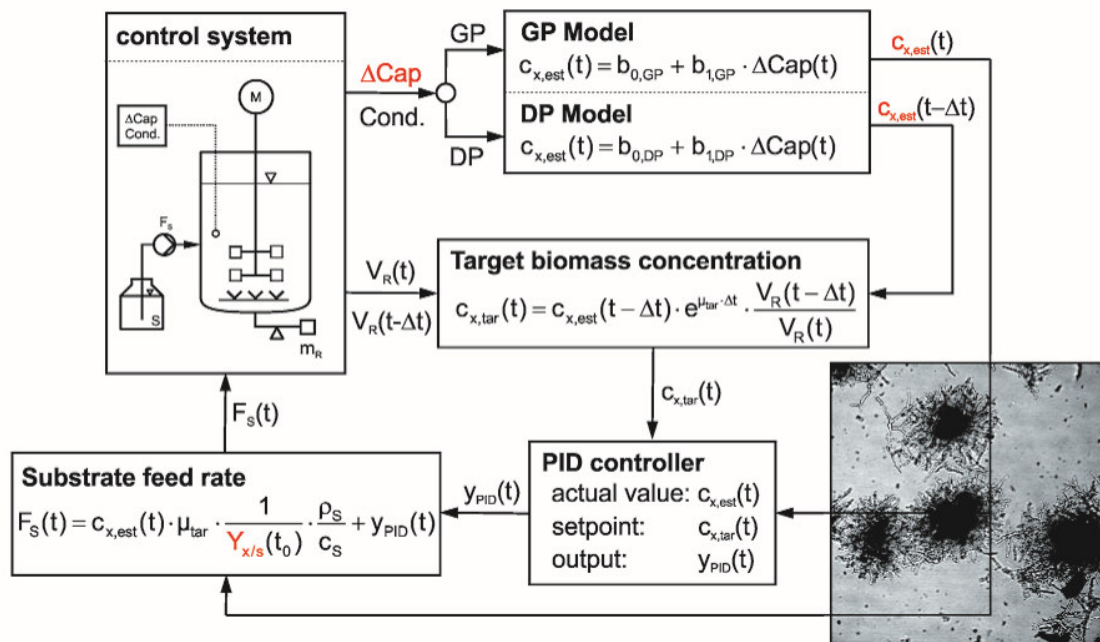


*Figure S1: Pictures of pellets taken in the flow cell of the flow cytometer. The FWS signals of these pellets are presented in Figure 4a-c in the same order*

## Controlling the specific growth rate via biomass trend regulation in filamentous fungi bioprocesses

Ehgartner, D., Hartmann, T., Heinzl, S., Frank, M., Veiter, L., Kager, J., Herwig, C., & Fricke, J., Chemical Engineering Science, submitted



**Controlling the specific growth rate via biomass trend regulation in filamentous fungi bioprocesses**

Daniela Ehgartner<sup>1,2</sup>, Thomas Hartmann<sup>1,2</sup>, Sarah Heinzl<sup>1,2</sup>, Manuela Frank<sup>1,2</sup>, Lukas Veiter<sup>1,2</sup>, Julian Kager<sup>2</sup>, Christoph Herwig<sup>1,2</sup> and Jens Fricke<sup>\*,1,2</sup>

\*to whom the correspondence should be addressed

<sup>1</sup> CD Laboratory on Mechanistic and Physiological Methods for Improved Bioprocesses, TU Wien, Gumpendorferstrasse 1a/166, 1060 Vienna, Austria

<sup>2</sup> Research Area Biochemical Engineering, Institute for Chemical, Environmental and Biological Engineering, TU Wien, Gumpendorferstrasse 1a/166, 1060 Vienna, Austria

\*Corresponding author:

jens.fricke@tuwien.ac.at; Tel (Office): +43 1 58801 166462

Gumpendorferstrasse 1a / 166-4

1060 Wien, Austria

## **Abstract**

Increasing pressure on product quality and quantity pushes solutions of process control to be a central issue in pharmaceutical bioprocesses. Especially online biomass estimation, and further control of the specific growth rate are of central importance because they describe the catalyst of the reaction. For penicillin producing bioprocesses with filamentous microorganisms, this was underlined by recent findings describing the influence of the specific growth rate on the specific production rate. Hence, the specific growth rate needs to be controlled on a certain level to achieve high productivity.

In this study, we developed a control strategy for the specific growth rate based on online estimation of viable biomass via dielectric spectroscopy. The method was verified using an at-line staining method for viability measurement. The online viable biomass estimation is applicable in the growth and decline phase, coping with physiological and morphological changes of filamentous fungi. Furthermore, the control strategy adapts to changing biomass yields, which is a big issue in the bioprocess for penicillin production applied in this study.

Two application runs were conducted, yielding in proper online viable biomass estimation and control of the specific growth rate at a constant level of  $0.012 \text{ h}^{-1}$ . We achieved biomass predictions with an average error of 1.5 g/l over the whole fed-batch process. In the decline phase, the control of specific growth rates was not possible due to physiological constraints. However, in the growth phase, a total specific growth rate of  $0.013 \text{ h}^{-1}$  was achieved, which met the pre-defined acceptance criterion for this method.

The method is thus ready for viable biomass estimation in the growth and in the decline phase of the penicillin production process. Furthermore, the method is applicable to control the specific growth rate during the growth phase.

## Keywords:

penicillin, dielectric spectroscopy, bioprocess control, viability, online biomass estimation, filamentous fungi

Abbreviations

*Symbols*

c	concentration	[g/l]
$\Delta\text{Cap}$	delta Capacitance	[pF/cm]
F	feed rate	[g/h]
$\mu$	specific growth rate	[h <sup>-1</sup> ]
$\rho$	density	[g/l]
r	rate	[g/h]
t	time	[h]
$V_R$	reactor volume	[l]
$Y_{\text{PID}}$	output of PID controller	[g/h]
$Y_{x/s}$	biomass yield	[g/g]

*Indices*

tar	set-point; target value
est	predicted value based on the model
s	substrate
total	total biomass measured <i>via</i> DCW or wet weight
viable	viable biomass measurements (vs. total biomass)
x	biomass

## 1. Introduction

Process control is of utmost importance in pharmaceutical bioprocesses to maximize productivity and to ensure product quality. The importance of the latter was underlined by the Quality by Design (QbD) initiative (FDA 2006). One parameter which is often the focus is biomass growth. Various methods of biomass estimation for different processes and organisms have been applied (Mou and Cooney 1983b; Riesenbergl et al. 1991; Sagmeister et al. 2013; Jenzsch et al. 2006). Studies presenting the influence of the specific growth rate,  $\mu$ , on penicillin production (Douma et al. 2010; Pirt and Righelato 1967; van Gulik et al. 2000) underline the importance of  $\mu$ -control strategies in filamentous fungi bioprocesses.

The basis for the control of  $\mu$  is the availability of real-time biomass measurements. Hereby, two different principles can be distinguished: hard type sensors and soft sensors. The former are *in-situ* measurements of the biomass concentration, while soft sensors estimate the biomass based on mathematical models (Olsson and Nielsen 1997). Commonly, soft sensors require high process knowledge and historical data for the development of mathematical models. Soft sensors were reportedly applied for biomass concentration and biomass growth estimation of filamentous organisms (Golabgir and Herwig 2016; Massimo et al. 1992; Thompson and Kramer 1994; Mou and Cooney 1983b). The online biomass estimation based on carbon balancing was already applied for the  $\mu$ -control of penicillin processes (Mou and Cooney 1983a, b). *In situ* biomass measurements applied for filamentous organisms were fluorescence probes (Haack et al. 2007) and dielectric spectroscopy (Fehrenbach et al. 1992; Mishima et al. 1991; Neves et al. 2000; Sarra et al. 1996). Fluorescence probes were found to be not applicable for penicillin-producing cultures in complex media, as changes in the medium composition influence fluorescence. Furthermore, penicillin is a fluorescent product which interferes with the measurement of fluorescence (Nielsen et al. 1994).

The principle for biomass measurement via dielectric spectroscopy is based on the function of cells as capacitors. The measured signal is a function of the volume fraction of the cells. Only cells with an intact membrane potential are recorded with dielectric spectroscopy. Hence, the method is insensitive to dead cells and only measures viable biomass (Dabros et al. 2009). This fact is of high importance for filamentous organisms who grow pellets, as the inner parts of these hyphal aggregates tend to die due to substrate and oxygen limitation, leading to considerable amounts of dead biomass (Bizukojc and Ledakowicz 2010; Hille et al. 2005; Manteca et al. 2008). In contrast to this dead biomass, only viable biomass is responsible for biomass growth and productivity (Bizukojc and Ledakowicz 2010; Paul et al. 1998).

Most contributions, in which dielectric spectroscopy was applied on filamentous fungi for the estimation of biomass concentration, differentiate between a growth phase and a decline phase (at the end of cultivation). For the growth phase, biomass prediction via dielectric spectroscopy is reported to be highly applicable. However, biomass prediction in the decline phase still shows results that are very error-prone (Neves et al. 2000; Rønneest et al. 2011; Sarra et al. 1996).

Within this contribution, an online  $\mu$ -control strategy in a penicillin production process based on viable biomass measurement via dielectric spectroscopy is established. So far, biomass estimation in the decline phase was reported to not work properly. We aim to predict the viable biomass concentration in the growth and the decline phase to further apply  $\mu$ -control in both phases. The goal is to predict viable biomass in a similar error range as at-line and offline reference methods (6-12%).

The control of the specific growth rate in filamentous cultures presents a special challenge as growth rate levels are rather low compared to other organisms as *E. coli*. These low specific growth rates make the control and the evaluation of the control strategy difficult as they have a lower signal-to-noise-ratio (Wechselberger et al. 2013). Furthermore, changing biomass yields during the penicillin production process appeared to be a main issue in  $\mu$ -control. The developed control strategy aims to be applicable in the growth phase as well as in the decline phase and enables an automatic adaption to changing biomass yields. To avoid error propagation in the calculation of the specific growth rate, the control strategy focuses on biomass trends rather than the specific growth itself.

## **2. Materials & Methods**

### **2.1. Strains and inoculum**

One strain of *Penicillium chrysogenum* (code BCB1\_V2) was regenerated from an ancestor strain BCB1 and kindly donated by Sandoz GmbH (Kundl, Austria).

### **2.2. Bioreactor cultivation**

Cultivations were performed in either of two Techfors S bioreactors (Infors HT, Bottmingen, Switzerland) with a maximum working volume of 10 l and 20 l respectively. The initial batch and fed-batch volumes were 6.5 l for the 10-l-bioreactor and 13 l for the bigger one. The stirrer was equipped with three six-bladed Rushton turbine impellers, of which two were submersed and one was installed above the maximum liquid level for foam destruction.

The fermentation temperature was kept at 25°C via a double jacket. Aeration was controlled at 1 vvm in batch and initial fed-batch with mass flow controllers (Vögtlin, Aesch, Switzerland). The concentration of dissolved oxygen was measured using a probe of dissolved oxygen (Hamilton, Bonaduz, Switzerland). If not stated otherwise, the  $pO_2$  was controlled via an adjustment of the stirrer speed at a level higher than 40%. The pH was measured using a pH probe (Hamilton, Bonaduz, Switzerland).  $CO_2$  and  $O_2$  concentrations were analysed with an off-gas analyser (M. Müller AG, Egg, Switzerland).

Dielectric spectroscopy was applied in dual frequency mode using a Biomass Monitor 220 (Aber Instruments, Aberystwyth, UK). Every minute the delta capacitance ( $\Delta Cap$ ) was recorded for the following frequencies: 100/15650 kHz. For further application, the signal was smoothed using a Savitzky-Golay-filter (first order, window of 60 data points).

The batch was carried out on a complex bioreactor medium similar to the one described in Posch et al. (2013). The culture was inoculated with a spore inoculum concentration of  $2 \cdot 10^8$  spores/l. During this phase, the pH was not controlled. The end of the batch was indicated by an increase in pH by 0.5.

After the batch, a fed-batch was performed on a defined medium (similar to Posch et al. (2013)). For this purpose, 10% of the batch broth were added to 90% of the initial fed-batch volume. The initial fed-batch volumes were 6.5 l and 13 l respectively. During the first 48 h, glucose was fed at a constant rate (1.01 ml/(l\*h) of a 500 g/l glucose solution). During this phase, the pH was kept constant at  $6.5 \pm 0.1$  by addition of 20% (w/v) KOH or 15% (v/v)  $H_2SO_4$ , respectively.

### *2.2.1. Fed-batch parameters*

To achieve different viable biomass concentrations and trends, 13 fed-batches were run by varying the following parameters: spore inoculum concentration ( $2 \cdot 10^8$  spores/l and  $2 \cdot 10^9$  spores/l), feed profile starting after 48 h (constant, linearly increasing, exponentially increasing), feed rates at the start of the feeding profile (1.0 ml/(l\*h), 3.0 ml/(l\*h) of a 500 g/l glucose solution) and  $pO_2$  (>40% vs. <10%). These runs were used for the development of the online biomass estimation strategy.

Additionally, two fed-batches were conducted to show the application of  $\mu$ -control - fed-batch 1 and 2 (FB1&2). Apart from some minor changes described in the following, these two cultivations were conducted as stated in 2.2. An initial constant feed of 1.01 ml/(l\*h) of 500 g/l glucose solution was applied for only 24 h, then  $\mu$ -control was started. The first biomass sample of these two fed-batches was used to analyse the viable biomass concentration at-line. This was necessary to calculate the offset of  $\Delta Cap$ , and thus to be able to apply the model for biomass prediction described in 3.3. All other steps of

biomass estimation and  $\mu$ -control were conducted online. During the first 24 h, both fed-batches were controlled at a  $pO_2$  level higher than 40%. After 24 h, the  $pO_2$  of FB1 was decreased to 4% by mixing the air flow with nitrogen.

### *2.2.2. Calculations*

Calculations of yields, rates and specific rates like the specific growth rate were carried out as stated elsewhere (Sagmeister et al. 2012). This study focuses on the measurement of viable biomass. Thus, the viable biomass was used as a basis for all calculations.

## 2.3. Analytics

### 2.3.1. At-line viability measurement

To investigate the viability via propidium iodide (PI) staining, 200  $\mu$ l of the sample were diluted 1:5 with phosphate buffered saline (PBS, see Ehgartner et al. (2016)). In addition, 1 ml of the sample was diluted 1:5 with PBS and microwave-treated by leaving it in a M510 microwave oven (Philips, Amsterdam, Netherlands) for 30 s at 940 W. One millilitre of the microwave-treated sample was used for further investigation. In a next step, duplicates of all samples (including microwave-treated and untreated samples) were centrifuged for 15 min at 500 rpm. 800  $\mu$ l of the supernatant were removed and 800  $\mu$ l of PBS buffer were added. The pellet was resuspended and the washing step repeated. 100  $\mu$ l of the resuspended sample was pipetted into a microtiter well and 1  $\mu$ l of 200  $\mu$ M PI solution (Sigma Aldrich, St. Louis, Missouri/USA) was added. The PI was prepared by diluting a 20 mM PI stock solution in DMSO, 1:100 in PBS. After an incubation time of 20 min at room temperature in darkness, the measurement was performed in a Tecan well-plate reader (Tecan, Männedorf, Switzerland; ex./em. 535/600 nm). Six aliquots of each sample were measured simultaneously using 96 well plates.

### 2.3.2. Total biomass concentration

Two methods for the determination of the total biomass concentration were applied. For the at-line determination of viable biomass, the wet weight was measured. Due to a lower degree of measurement error (4% vs. 10%), the total biomass concentration for offline use was determined through the dry cell weight (DCW). One exception was the decline phase in FB2, where wet weight data was also used for offline investigations. This was due to an increased and highly fluctuating DCW measurement caused by the crystallisation of salts from the highly conductive broth in this phase.

Measurements were carried out in quadruplicates by transferring 5 ml of fermentation broth into weighed glass eprouvettes and centrifuging them at 4800 rpm for 5 min at 4°C. The supernatant was

removed and stored at  $-20^{\circ}\text{C}$  for further analysis. The pellets were then resuspended in 5 ml of deionized water and the eprouvettes were centrifuged again at the conditions mentioned above. The supernatant was discarded. For wet weight determination, the eprouvettes were weighed and the biomass concentration was calculated using a predefined regression to the DCW. After the wet weight determination, the eprouvettes were dried at  $105^{\circ}\text{C}$  for at least 72 h and weighed again, resulting in the DCW.

### 2.3.3. Confocal microscopy

Microscopic images of pellets were taken using a confocal fluorescence microscope (TE2000-E, Nikon, Tokio, Japan). Hence, 100  $\mu\text{l}$  of the bioreactor sample were diluted with 900  $\mu\text{l}$  of PBS buffer and then centrifuged for 2 min at 500 rpm at room temperature. 800  $\mu\text{l}$  of the supernatant were discarded and replaced with 800  $\mu\text{l}$  of PBS buffer. Afterwards, 10  $\mu\text{l}$  of the 200  $\mu\text{M}$  PI reagent (prepared as described in 2.3.1) were added and the sample was incubated for at least 10 min in the dark. Furthermore, 20  $\mu\text{l}$  of the sample were applied on a cover slide and 50 mg/l FDA reagent (Sigma Aldrich, St. Louis, Missouri/USA; from 5 g/l stock solution by diluting 1:100 with PBS) were added. The measurements were conducted using two different lasers and filters: ex./em. 543/580 nm for PI and ex./em. 488/507 nm for FDA.

### 2.3.4. Light microscopy

A morphological analysis via scanning of microscopic images was conducted as described in Posch et al. (2012). To do so, 900 images per sample were recorded with a Leitz wide field microscope (Leitz, Stuttgart, Germany). It was equipped with a five megapixel microscopy CCD colour camera (DP25, Olympus, Tokio, Japan) and a fully automated x-y-z stage (Märzhäuser, Wetzlar, Germany). The software used for the image recording was analysis5 (Olympus, Tokio, Japan).

### 2.3.5. Sugar and metabolites

Gluconic acid, glucose and mannitol were quantified through ion chromatography. The analysis was carried out using a Dionox column (Thermo Fisher Scientific, Waltham, Massachusetts, US) at a column temperature of  $30^{\circ}\text{C}$ . For detection, a Dionex PAD detector in quadrupole potential mode (Thermo Fisher Scientific, Waltham, Massachusetts, US) was used. A gradient profile was applied combining three different solvents (MQ water, 0.1 N NaOH and 1 N NaOH).

### 3. Results

#### 3.1. Monitoring of the viable biomass concentration

The application for the online determination of the viable biomass concentration was based on at-line viability measurements. This was a combination of total biomass determination via wet weight (or DCW for offline purposes) and viability determination. For this purpose, the viability stain PI, microwave treatment and the Tecan well-plate reader (Tecan, Männedorf, Switzerland) were used. As described in section 2.3.1, one aliquot of the sample was microwave-treated, another one was used in its native state. Both were stained with PI and the ratio of red fluorescence described the viability of the culture (see Equation 1). In addition to quantitative viability measurements, confocal fluorescence microscopy in combination with the viability stains FDA and PI was conducted to support the quantitative methodology. Confocal fluorescence microscopy pictures taken during the process reveal the decrease of viability as shown in Figure A.1 in the appendix.

Equation 2 shows how the viable biomass concentration ( $c_{x,viable}$ ) was calculated using viability measurements. If not stated otherwise, biomass concentration refers to the viable biomass as determined by Equation 2.

$$\text{Viability} = 1 - \frac{\text{Red Fluorescence native sample}}{\text{Red Fluorescence microwaved sample}}$$

*Equation 1: Viability of biomass*

$$c_{x,viable} = c_{x,total} * \text{Viability}$$

*Equation 2: Viable biomass concentration at-line. The viable biomass concentration ( $c_{x,viable}$ ) is calculated from the total biomass concentration ( $c_{x,total}$ ) and the viability. The total biomass concentration was either determined via wet weight (at-line application) or DCW (offline application).*

Cultivations with the goal to achieve different viable biomass concentrations and trends were conducted, where the viability was measured at-line. The total biomass concentration, viable biomass concentration and viability are shown exemplarily for two cultivations in Figure 1. In both cultivations, a significant decrease in the viability after around 100 h could be observed. The cultivation shown in Figure 1b depicts a strong decline of viability to a final value of 30%.

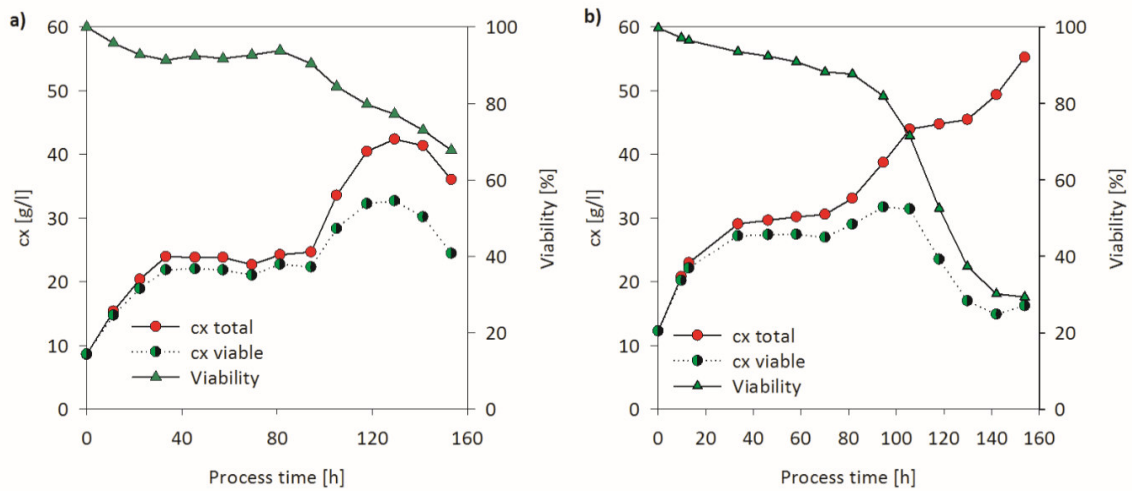


Figure 1: Time courses of the viability, viable and total biomass concentration for two fed-batch cultivations. The cultivations differed in their feeding profile. While the fed-batch in a) had an exponential feeding profile ( $0.02 \text{ h}^{-1}$ ) starting with  $1.0 \text{ ml}/(\text{l} \cdot \text{h})$  of a  $500 \text{ g/l}$  glucose solution, the fed-batch in b) was conducted with a feed starting with  $3.0 \text{ ml}/(\text{l} \cdot \text{h})$  of a  $500 \text{ g/l}$  glucose solution, which then constantly increased to a final rate of  $9.0 \text{ ml}/(\text{l} \cdot \text{h})$ .

### 3.2. Distinction between the process phases: growth phase vs. decline phase

In order to make a distinction between the different process phases, the aforementioned cultivations were examined. In most of the performed cultivations two different phases were observable: the growth phase and the decline phase. As it is shown exemplarily for one cultivation in Figure 2, two correlations between  $\Delta\text{Cap}$  and viable biomass could be distinguished.

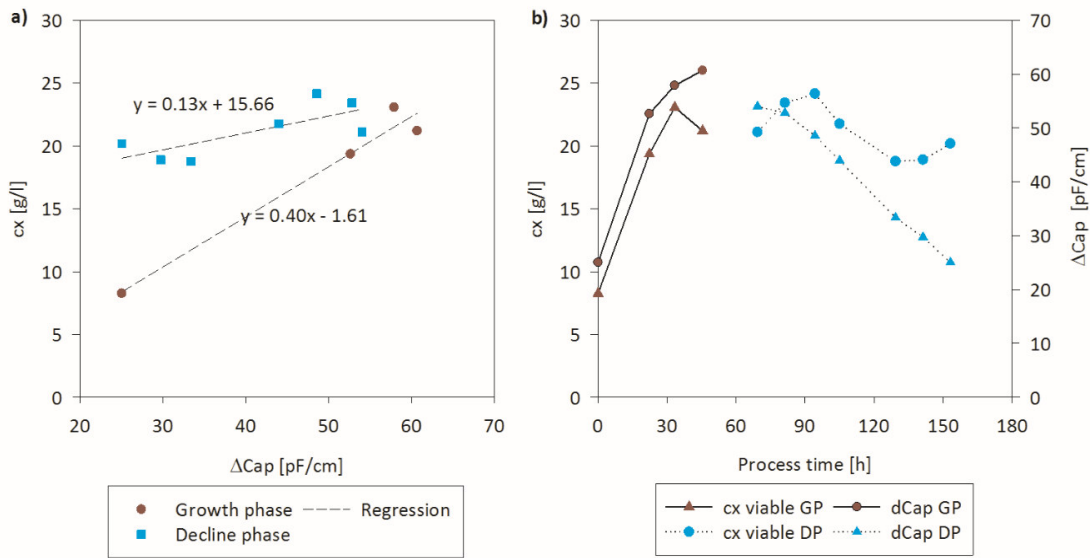


Figure 2:  $\Delta\text{Cap}$  and  $c_{x,viable}$  in the two phases. A) Correlation of  $\Delta\text{Cap}$  and  $c_{x,viable}$  for growth and decline phase. B) Time courses of  $\Delta\text{Cap}$  and  $c_{x,viable}$  for growth phase (GP) and decline phase (DP).

The change from one phase (growth phase) to the second phase (decline phase) was indicated by the decrease of the  $\Delta\text{Cap}$  signal. This indication for the switch from the first to the second phase cannot be applied when  $\mu$  is controlled on a constant level, because the biomass ought to increase with the intended specific growth rate. Thus, another indicator for the change of phases needed to be found.

Several permittivity probe parameters were investigated as indicators for the start of the decline phase. Certain trends were observed for typical capacitance measurement parameters like  $F_c$  and Cole Cole Alpha (Dabros et al. 2009). However, these trends were not specific for the observed phase change. Opposed to this, an increase of conductivity was found to be distinctive for the start of the decline phase. The conditions that must be met for the increase of the conductivity signal to indicate the start of the decline phase are shown in Figure 3.

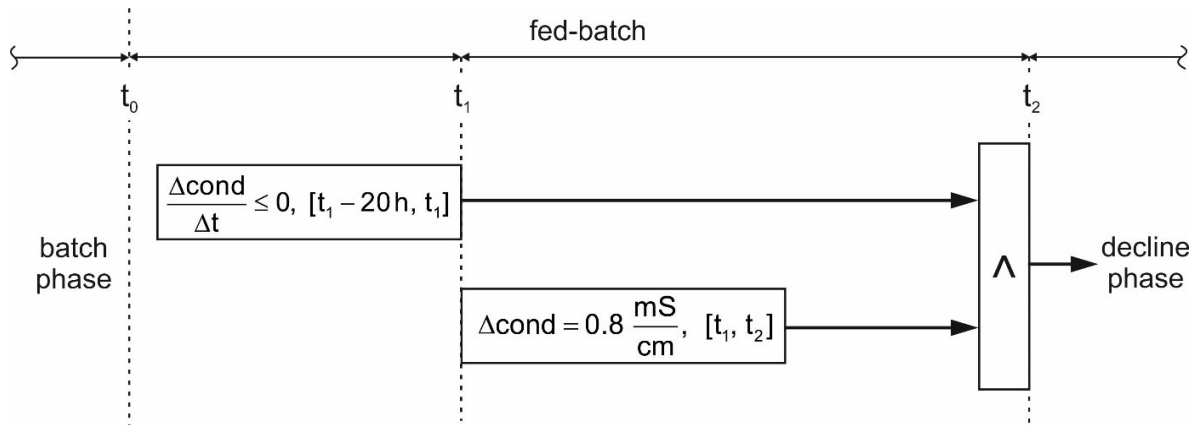


Figure 3: Decision scheme for the indication of the decline phase onset via conductivity (cond.) signal. The following points in the fed-batch are crucial:  $t_0$ : start of fed-batch,  $t_1$ : start increase of conductivity,  $t_2$ : start decline phase. The conditions are 1.) a constant or decreasing conductivity for a defined period of time before the signal starts increasing [ $t_1 - 20$  h,  $t_1$ ] and 2.) an increase of the conductivity ( $0.8 \text{ mS/cm}$ ).

Exemplary trends of conductivity and the defined indication of phase change for two cultivations are shown in Figure 4. The increase of conductivity at the start of the fed-batch in Figure 4a was caused by the addition of higher amounts of acid and base for the control at a constant pH and was hence no indicator for the start of the decline phase. This occurrence underlines the importance of condition 1 as described in Figure 3, which must be met before condition 2 can be of significance. On the other hand, the decline phase of the fed-batch presented in Figure 4b and Figure 4c was successfully detected via conductivity measurement.

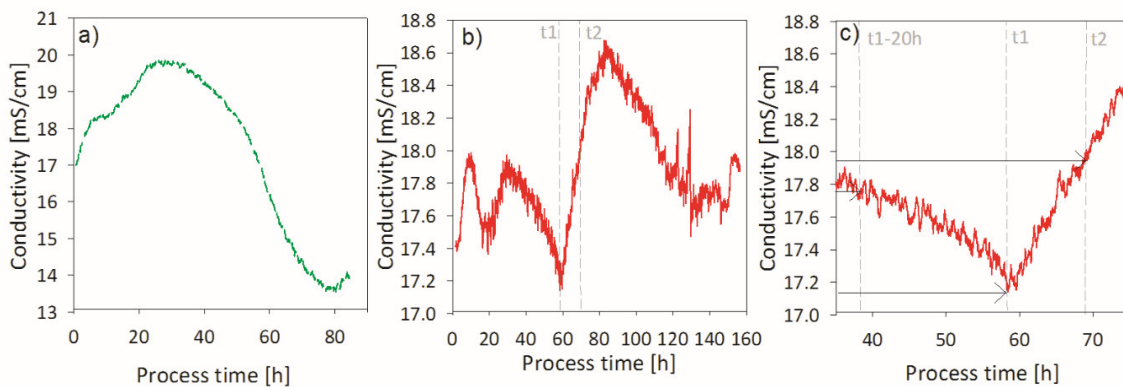


Figure 4: Conductivity of two fed-batch cultivations. a) The conductivity signal in the first 30 h of the fed-batch shown here, increases. Still, there is no decline phase as condition 1 is not met (20 h before the beginning of the increase in conductivity, the value of the signal needs to be higher than at the start of the increase. This is not possible as the increase starts directly with the beginning of the fed-batch.). In b-c) another fed-batch is shown. While in b) the conductivity throughout the whole fed-batch is

shown, c) presents the phases  $t_1-20$  h to  $t_2$  in more detail. At the start of the increase in conductivity at  $t_1 = 58.4$  h, condition 1 as presented in Figure 3 was accomplished: the value of the conductivity signal at  $t_1-20$  h was higher than it was at  $t_1$ . Furthermore, the signal rose 0.8 mS/cm between  $t_1 = 58.4$  h and  $t_2 = 68.6$  h. Hence condition 2 was accomplished as well, indicating the start of the decline phase.

The increase of the conductivity signal indicates a lysis of cells or the release of a metabolite into the surrounding medium at the onset of the decline phase. Furthermore, cell size and morphology were reported to influence the  $\Delta\text{Cap}$ -biomass-correlation (Ehgartner et al. 2015). Hence, there ought to be a morphological change resulting in the difference of correlation of viable biomass and  $\Delta\text{Cap}$  between these two phases. Thus, morphological parameters like the average size of morphological aggregates, the differentiation of morphological aggregates in fractions (e.g. pellets, smaller elements) and the parameters describing the pellet itself (e.g. fullness, roughness) were examined (data not shown). The morphological parameters are described elsewhere (Golabgir et al. 2015; Posch et al. 2012). However, no significant correlation between morphology and the phase change could be observed.

In summary, two different phases (growth and decline phase) were clearly distinguished based on the correlation  $\Delta\text{Cap}$  and  $c_{x,\text{viable}}$ . The onset of the decline phase as a second phase in the process was detectable via an increase in the conductivity signal.

### 3.3. Model for online viable biomass estimation

The model for viable biomass estimation by using the capacitance signal is shown in Figure 5. Data to establish the model was taken from the 13 fed-batch cultivations as described in 2.2. The model contains a correlation between the growth phase (a) and the decline phase (b).

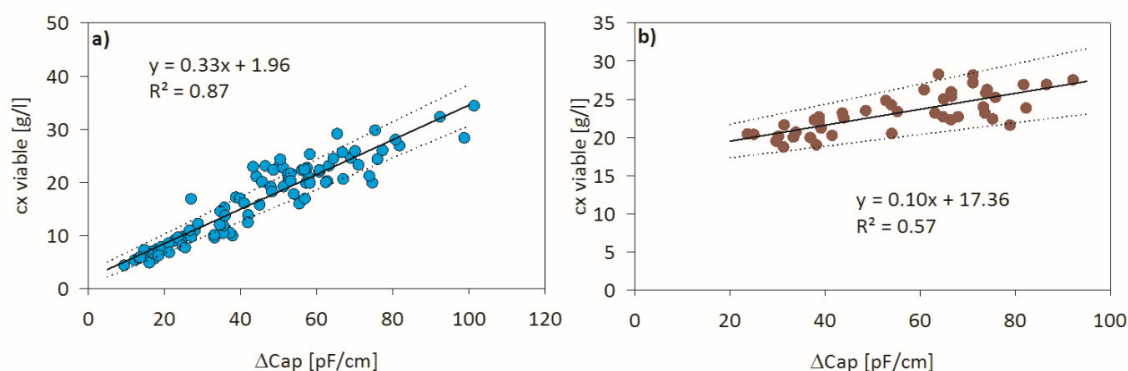


Figure 5: Correlation including a 95% confidence interval for  $\Delta\text{Cap}$  and  $c_{x,\text{viable}}$  for the growth phase (a) and the decline phase (b).

Based on these correlations, the viable biomass can be estimated ( $c_{x,est}$ ) with Equation 3 (growth phase, GP) and Equation 4 (decline phase, DP) respectively.

$$c_{x,est} = b_{0,GP} + b_{1,GP} * \Delta Cap$$

*Equation 3: Calculation of the estimated viable biomass concentration ( $c_{x,est}$ ) during the growth phase. It is based on the offset ( $b_{0,GP}$ ) from the correlation of  $c_{x,viable}$  and  $\Delta Cap$  during the growth phase and its slope ( $b_{1,GP}$ ).*

$$c_{x,est} = b_{0,DP} + b_{1,DP} * \Delta Cap$$

*Equation 4: Calculation of the estimated viable biomass concentration ( $c_{x,est}$ ) during the decline phase. It is based on the offset ( $b_{0,GP}$ ) from the correlation of  $c_{x,viable}$  and  $\Delta Cap$  during the decline phase and its slope ( $b_{1,GP}$ ).*

The determined parameters for the linear correlation between  $c_{x,viable}$  and  $\Delta Cap$  are shown in Table 1.

*Table 1: Parameters for the linear correlation between  $c_{x,viable}$  and  $\Delta Cap$*

	growth phase, GP	decline phase, DP
$b_0$	1.96	17.36
$b_1$	0.33	0.10

The application of the growth phase model (Figure A.2a in the supplementary material) shows a slight overestimation of  $c_{x,viable}$ , as the correlation trend line does not cross the zero point (intercept of 0.8-3.3 g/l).

The plot in Figure A.2b in the appendix, showing the residuals, underlines what can already be seen in Figure 5: For lower biomass concentrations, the predictions made based on the model are more accurate than for higher biomass concentrations. Apart from this, no trend of the residuals is obvious.

### 3.4. Process control strategy

The applied control strategy is described in Figure 6. The process control system (Lucillus PIMS, Securecell AG, Schlieren, Switzerland) records the process signals and sends these to Matlab (MathWorks, Natick, Massachusetts, US). Therefor the equations shown in Equation 3 and Equation 4 with the parameters from Table 1 are used. Apart from the current  $c_{x,est}$ , the viable biomass concentration target ( $c_{x,tar}$ ) is determined. These values are sent back to the process control system,

where the current  $c_{x,est}$  and  $c_{x,tar}$  are fed into a PID controller. The output of the controller acts on the feed rate  $F_S$  to adjust for changes in the substrate yield.

The feed flow calculation contains a constant value for the initial biomass yield ( $Y_{x/s}(t_0)$ ). This value changes according to the cultivation. It is evaluated in advance, using an on former data based regression model predicting  $Y_{x/s}$  dependent on the process time and  $\mu$ .

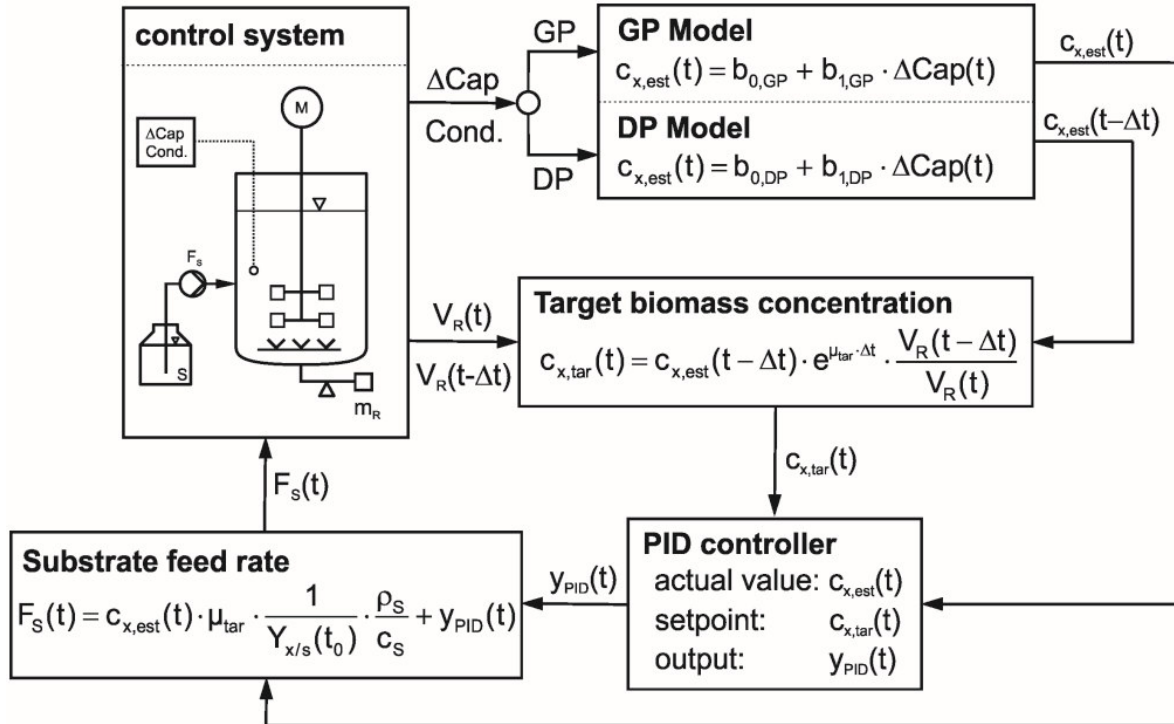


Figure 6: An overview of the process control strategy. The applied process control system records process data and transfers them to Matlab. The current process phase is determined via the conductivity signal (Cond.). Then the viable biomass concentration ( $c_{x,est}$ ) based on the measured  $\Delta Cap$  signal is estimated. To do so, Equations 3 and 4 with the parameters from Table 1 are used. In addition to the current  $c_{x,est}$  the viable biomass concentration target ( $c_{x,tar}$ ) is determined. For  $c_{x,tar}$  the specific growth rate target ( $\mu_{tar}$ ),  $\Delta t$  and the reactor volume ( $V_R$ ) are required. The process data is sent back to the process control system, where the current viable biomass  $c_{x,est}$  and the viable biomass target  $c_{x,tar}$  are fed into a PID controller. The output of the controller ( $y_{PID}$ ) is added to the feed flow ( $F_S$ ) to adjust for changes in the substrate yield ( $Y_{x/s}(t_0)$ ). In addition, the glucose concentration in the feed ( $c_S$ ) and the density of the feed ( $\rho_S$ ) are crucial for the calculation of the substrate feed rate.  $\Delta t$  is the set control interval, e.g. 1 h.

### 3.5. Application of the method

The application of the control strategy is exemplarily shown in Figure 7 and Figure 8 for FB1 and FB2, respectively. The specific growth rate  $\mu$  in FB2 was controlled exactly as sketched in Figure 6. In the case of FB1, the control was conducted in a slightly different way. The inputs for the PID controller were not

$c_{x,est}$  and  $c_{x,tar}$ , but  $\mu_{tar}$ , and the current  $\mu$  was calculated from  $c_{x,est}$ . In comparison to the slightly altered control strategy for FB1, the control strategy presented in Figure 6, has the advantage that the influence of the error of  $c_{x,est}$  is not multiplied by calculating  $\mu$ .

FB1 contained only a growth phase, lacking a decline phase, as the conductivity signal in Figure 7 depicts. Although there is an increase in the conductivity signal before the start of  $\mu$ -control, it does not indicate the beginning of the decline phase as the first condition, which compares the signal at  $t_1-20$  h and  $t_1$ , is not fulfilled. This first condition would only be met at about 60 h, but consecutively no increase of the conductivity was observed, thus lacking the achievement of condition 2.

The prediction of the biomass concentration in the first 40 h of this cultivation worked well. After 40 h,  $c_{x,viable}$  was constantly underestimated and the offset increased with time. While the deviation was 2 g/l after 45 h, it increased to more than 3 g/l at the end of fed-batch at 94 h. The average error of prediction was 2.1 g/l.

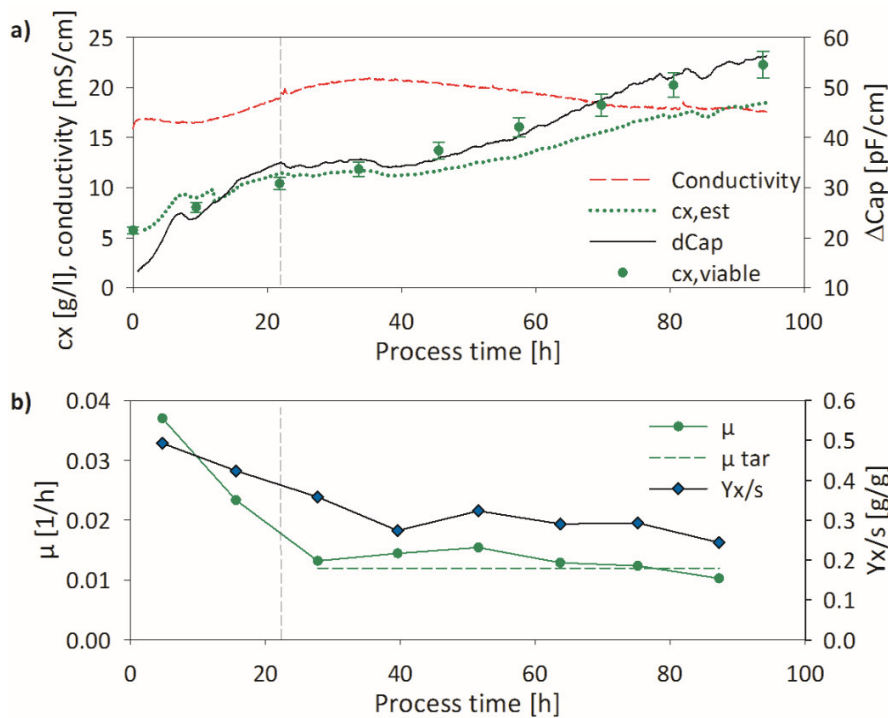


Figure 7: FB1. a) Online signals and offline determined  $c_{x,viable}$  b)  $\mu_{tar}$  as well as  $\mu$  based on at-line and offline measurements. In addition, the biomass yield is presented. The start of  $\mu$ -control is indicated by the vertical line at  $t = 22$  h.

At  $t = 22$  h the  $\mu$ -control was started. While  $\mu$  reached values of about  $0.037 \text{ h}^{-1}$  in the first 12 h, it decreased to an average of  $0.013 \pm 0.002 \text{ h}^{-1}$  at the onset of  $\mu$ -control. The  $\mu$  target of  $0.012 \text{ h}^{-1}$  was

missed by  $0.002 \text{ h}^{-1}$  on average. The total specific growth rate during  $\mu$ -control (calculated between the first and last biomass sample of this period) was  $0.013 \text{ h}^{-1}$ .

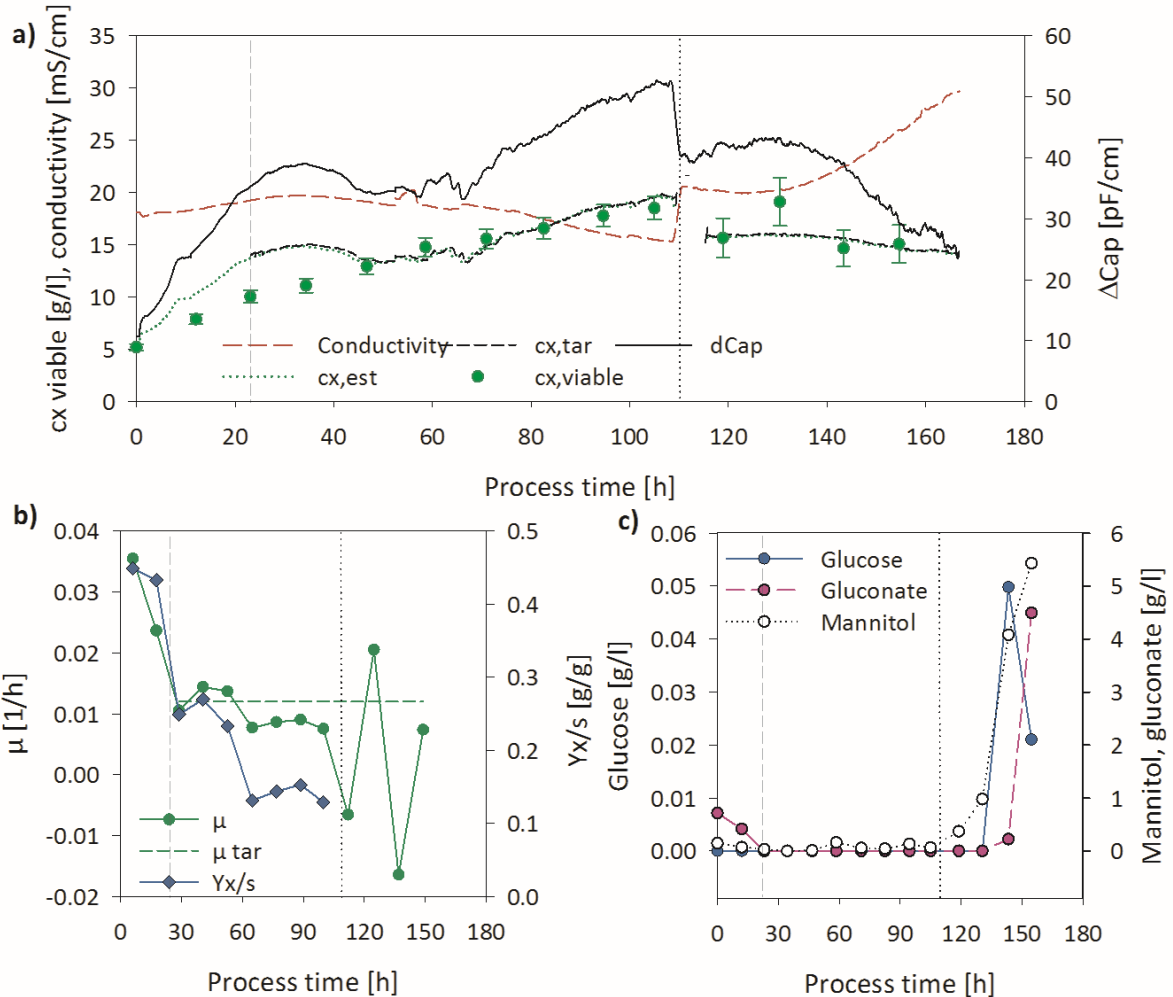


Figure 8: FB 2. a) online signals and measured  $c_{x,viable}$ . Between  $t=109 \text{ h}$  and  $t=115 \text{ h}$  the connection between the process control system and Matlab was cut. Hence, neither  $c_{x,est}$  nor  $c_{x,tar}$  are shown for this period. b)  $\mu$ -control:  $\mu_{tar}$  as well as  $\mu$  based on at-line and offline measurements are shown. The former is only shown for the period of  $\mu$ -control.  $Y_{x/s}$  in this figure represents glucose as the only substrate and ignores the initial consumption of gluconate. c) Sugars and metabolites measured in the medium. The vertical lines at  $t=23 \text{ h}$  indicate the start of  $\mu$ -control, the ones at  $t=111 \text{ h}$  depict the onset of the decline phase.

FB2 consisted of a growth and a decline phase (see Figure 8). The decline phase – indicated by an increase of the conductivity signal – started at  $t=111 \text{ h}$ . The values of the viable biomass prediction are in good match to the measured viable biomass concentrations for both phases. The average error of prediction was  $1.5 \text{ g/l}$  during the growth phase,  $1.2 \text{ g/l}$  during the decline phase and  $1.4 \text{ g/l}$  for the whole fed-batch phase. During the growth phase, the measured specific growth rate deviated  $0.003 \text{ h}^{-1}$  on

average from the  $\mu$  target of  $0.012 \text{ h}^{-1}$ . The average specific growth rate during the growth phase was  $0.010 \pm 0.003 \text{ h}^{-1}$ . The total specific growth rate during  $\mu$ -control (calculated between the first and the last biomass sample of the control period in the growth phase) was  $0.010 \text{ h}^{-1}$ .

Although viable biomass prediction worked well in the decline phase, it was not possible to maintain a constant  $\mu$  level of  $0.012 \text{ h}^{-1}$ . Glucose accumulated after 130 h, resulting in gluconate build up, and from the start of the decline phase, the mannitol concentration increased considerably in the medium (see Figure 8c). The accumulation of glucose and metabolites depicts that more glucose is fed than consumed. Hence, the maximum specific growth rate decreased significantly during the decline phase, falling below  $0.012 \text{ h}^{-1}$ . Therefore, it was not possible to control the obtained  $\mu$  during this phase. As already shown for FB1, the biomass yield from glucose also varied in FB2, with a tendency to decrease over process time. This is demonstrated in Figure 8. During  $\mu$ -control, the maximal yield  $Y_{x/s}$  was  $0.27 \text{ g/g}$  and the minimal one was  $0.13 \text{ g/g}$ .

## 4. Discussion

### 4.1. Challenges

#### 4.1.1. Morphological and biological changes

The biomass- $\Delta\text{Cap}$ -correlation is the basis for a viable biomass prediction, distinguishing two process phases with different  $\Delta\text{Cap}$ -biomass-correlations – the growth and the decline phase. As the application runs FB1 and FB2 show, there are slight changes in  $\Delta\text{Cap}$ -biomass-correlation during the initial phase of fed-batch. Thus, the viable biomass is either overestimated in this initial phase or underestimated later in the growth phase. To find explanations for this occurrence, morphological parameters were investigated and compared to the biodensity, representing the  $\Delta\text{Cap}$ -biomass-correlation, which is described in more detail elsewhere (Ehgartner et al. 2015). In the early growth phase, first pellets are detectable and cells start to produce penicillin. Different trends in cell fractions and other morphological phases were observed (see Figure A.3 in the appendix for morphological data of FB1). Yet, no clear relationship between one of these parameters and the changes in the  $\Delta\text{Cap}$ -biomass-correlation could be detected. The morphological changes may be too complex to be easily deducible.

Possibly, a third phase – an initial growth phase – ought to be necessary to increase accuracy in viable biomass prediction. However, this would make the prediction and control strategy more complex. In

particular, an unambiguous indicator and clearly recognizable criteria for the change between these two phases would be needed.

Nevertheless, viable biomass prediction worked well with an average deviation of 1.4 g/l for more than 160 h in FB2 and an average deviation of 2.1 g/l (12%) error in FB1. Even for *E. coli* processes, where a lot of work has been done in the area of biomass prediction, errors rates of 11-13% occur for single methods (Reichelt et al. 2016). The at-line method for viable biomass measurement applied here has an error rate of 12%.

#### 4.1.2. Control strategy

The achieved specific growth rates tended to exceed the specific growth rate target of  $0.012 \text{ h}^{-1}$  at the start of  $\mu$ -control and to remain below it at the end. This trend can be explained by the continuously decreasing biomass yield. The control strategy adapts to changing biomass yields, but the feed-back regulation could still be improved. Depending on the level of the growth rate target and the current biomass concentration, the control interval was set between 1 h and 4 h. Especially for low specific growth rates, the control interval is crucial. In fact, an interval of several hours is necessary to achieve significantly different biomass concentrations due to the high error rate of biomass estimation. To avoid an even higher impact of the error rate of the estimated biomass, the biomass concentration target  $c_{x,\text{tar}}$  was invented as set-point for the PID controller in the final control strategy. Initially – as applied in FB1 – the set-point in the PID controller was  $\mu_{\text{tar}}$ , which was compared to the current  $\mu_{\text{est}}$ . This approach using  $\mu_{\text{tar}}$  is significantly more affected by the error of biomass estimation than the approach using the biomass concentration target (Wechselberger et al. 2013).

When larger control intervals are applied, the system becomes more inert. For instance, if the biomass growth in the last few hours was too low, a higher feed rate would be required at a certain point. This would be necessary to achieve the overall specific growth rate target of this control interval, as  $\mu$  had been too low before. Although the average specific growth rate ought to be close to the  $\mu_{\text{tar}}$ , the specific growth rate in-between would fluctuate highly, thus not meeting the aim of obtaining a constant  $\mu$ .

On average, the specific growth rate in FB1 slightly exceeded  $\mu_{\text{tar}}$ , while the measured  $\mu$  in FB2 was  $0.002 \text{ h}^{-1}$  beneath the set-point in total. The measured  $\mu$  better matched the  $\mu_{\text{tar}}$  in FB1. This was due to the overestimation of  $c_{x,\text{viable}}$  during the final growth phase, which balanced the trend of a decreasing  $\mu$ . The relatively low offline-determined  $\mu$  is *inter alia* caused by neglecting dying biomass. This effect of neglecting dying biomass by using  $c_{x,\text{viable}}$  for all calculations may be relevant when  $\mu$  is calculated in a 12-

h interval - contrary to the interval of approximately 1 h utilized for online calculation of the  $\mu$  set-point. A considerable amount of biomass dies in this time span.

$$\mu = \frac{\Gamma_{x,\text{viable}}}{c_{x,\text{viable}} * V_R}$$

*Equation 5: Actual calculation of  $\mu$ .  $r_{x,\text{viable}}$  [g/h] is the biomass production rate calculated from viable biomass ( $c_{x,\text{viable}}$ ).  $V_R$  represents the reactor volume [l].*

$$\mu = \frac{\Gamma_{x,\text{total}}}{c_{x,\text{viable}} * V_R}$$

*Equation 6: Alternative calculation of  $\mu$ .  $r_{x,\text{total}}$  [g/h] is the biomass production rate calculated from total biomass ( $c_{x,\text{total}}$ ) measured via DCW or wet weight.  $V_R$  represents the reactor volume [l].*

By calculating biomass rates for  $\mu$  determination based on  $c_{x,\text{viable}}$ , dead cells are not taken into account (see Equation 5). An alternative calculation of  $\mu$  considering dying biomass is shown in Equation 6. However, the offline calculation of  $\mu$  using Equation 6 is not equivalent to the applied online control strategy, which is fully based on  $c_{x,\text{viable}}$ . Using dielectric spectroscopy, the evaluation of  $c_{x,\text{total}}$  is not possible. Applying Equation 6 for calculating  $\mu$  in the growth phase of FB2 results in an overall  $\mu$  of 0.014  $\text{h}^{-1}$ . Hence,  $\mu_{\text{tar}}$  was exceeded by 0.002  $\text{h}^{-1}$  while it was lower by 0.002  $\text{h}^{-1}$  when using only viable biomass concentrations (Equation 5) for  $\mu$  calculation.

#### 4.1.3. Error propagation

The deviation of the offline-determined  $\mu$  from the  $\mu_{\text{tar}}$  is minimal, compared to the observed errors on the calculated specific growth rate. Using the combination of DCW and viability measurements as an offline method for viable biomass calculation results in an average error rate of 6% on  $c_{x,\text{viable}}$ . Due to error propagation, the maximal error on  $\mu$  determined for an interval of 12 h is 0.01  $\text{h}^{-1}$ . Thus, the deviation of an average of 0.002  $\text{h}^{-1}$  (FB1) and 0.003  $\text{h}^{-1}$  (FB2), respectively, is negligible. Even for larger intervals like the whole growth phase of the fed-batches, the maximal error on  $\mu$  is still 0.002  $\text{h}^{-1}$  for the 75 h interval of  $\mu$ -control in FB1 and 0.001  $\text{h}^{-1}$  for the 88 h interval in FB2.

One might thus question the approach of a  $\mu$ -control strategy for bioprocesses with such low specific growth rates. Opposed to that, investigations such as the one carried out by Douma et al. (2010), describing the influence of  $\mu$  on the productivity, underline the importance of controlled constant specific growth rates. With the control strategy developed here, we aimed to find a compromise by regulating  $\mu$  indirectly via the control of a biomass trend ( $c_{x,\text{tar}}$ ).

## 4.2. Benefits of the method

### *4.2.1. Advantages of dielectric spectroscopy: viable biomass*

The proposed method is applicable for viable biomass estimation in the growth and the decline phase. Hence, it is adaptable to changes in physiology and morphology of cells due to the shift from hyphal elements to pellets and finally to cell degradation at the end of the bioprocess. The advantage of the dielectric spectroscopy only measuring the volume of viable biomass was exploited. By using viable biomass, e.g. for mechanistic model building, instead of taking total biomass measurements, the errors caused by taking a significant amount of dead, inactive biomass into account ought to be avoided.

### *4.2.2. Application in decline phase and high viscosities*

Despite deviations in the decline phase due to physiological changes, where substrate accumulation, metabolite production and a strong decrease of the maximum growth rate could be observed, the prediction of viable biomass concentration was successful with an average error of 1 g/l (7%). This accuracy is comparable to the offline determination of viable biomass based on DCW. Moreover, the error is only half as high as the one of the at-line estimation of viable biomass based on wet weight determination. Prior investigations of dielectric spectroscopy for biomass prediction in filamentous bioprocesses stated this decline phase as their weak point (Neves et al. 2000; Rønneest et al. 2011; Sarra et al. 1996).

Especially for this late process phase, where the combination of high biomass concentration and significant hyphal background leads to immense viscosities, a method applicable online is of great advantage. The combination of broth viscosity with the occurrence of partially large hyphal aggregates hinders representative sample taking/preparation and pipetting is prone to error. Thus, analytical results are inaccurate. For elucidation, a picture of the cultivation broth in the last hours of the process is shown in Figure A.4 in the appendix.

### *4.2.3. Robustness and flexibility*

Further benefits of dielectric spectroscopy are reflected in the method presented here. Little process knowledge is necessary for the control strategy based on permittivity measurements. The method is robust to process changes like  $pO_2$ , spore inoculum concentrations or the feeding strategy and is thus easily transferable to other processes and process conditions. The development of this method for other strains/organisms, different processes and other probes/frequencies only requires some prior cultivations with different trends of viable biomass concentrations where  $\Delta C_{ap}$  is measured and  $c_{x,viable}$  is determined.

Furthermore, the regulation of  $\mu$  by biomass trend control showed to be feasible for processes with high fluctuations in the biomass yield, which can be seen as a great advantage to other  $\mu$ -control strategies (Jenzsch et al. 2006; Mou and Cooney 1983b).

Thus, the proposed control strategy in combination with the knowledge about  $\mu$ -profiles for optimal productivity ought to increase the product titer of penicillin processes and hence the rentability of the process. First investigations about optimal specific growth rates for increased specific penicillin production have been recently published (Douma et al. 2010; van Gulik et al. 2000).

## 5. Conclusion

- A method to measure viable biomass online, by applying dielectric spectroscopy in dual frequency mode, was developed. The model underlying the method for online biomass estimation distinguishes two process phases - growth and decline phase – and is applicable in both. In the final run an average error of only 1.4 g/l (13%) viable biomass was achieved in almost 160 h of cultivation.
- The online method was evaluated using an at-line procedure including viability measurements. To do so, the verification was done by measuring viable biomass. Hence, dead biomass was not neglected.
- The online viable biomass estimation enabled  $\mu$ -control during the growth phase with an average error of  $0.002 \text{ h}^{-1}$ . This  $\mu$ -control strategy copes with changing process conditions, even varying biomass yields. During the decline phase, the biomass growth showed to be impaired, which made  $\mu$ -control challenging.
- During the development process of this method, process parameters such as the spore inoculum concentration, the  $p\text{O}_2$ -level and the feeding strategy were varied. The application runs differed in their  $p\text{O}_2$  set-points (4% vs. >40%). The functionality of the developed control approach within these process parameter ranges shows its flexibility. Moreover, the method is applicable for typical physiological and morphological changes of the filamentous organism during fermentation.
- The method is ready to be applied for  $\mu$ -control in the growth phase of *Penicillium chrysogenum* bioprocesses and for an online biomass estimation throughout the growth and decline phase.

## 6. Acknowledgements

We thank the Austrian Federal Ministry of Science, Research and Economy in course of the Christian Doppler Laboratory for Mechanistic and Physiological Methods for Improved Bioprocesses for their financial support (grant number 171). Strains for the experiments were kindly provided by Sandoz GmbH (Kundl, Austria).

## 7. References

- Bizukojc M, Ledakowicz S (2010) The morphological and physiological evolution of *Aspergillus terreus* mycelium in the submerged culture and its relation to the formation of secondary metabolites. *World Journal of Microbiology and Biotechnology* 26:41-54. doi:10.1007/s11274-009-0140-1
- Dabros M, Dennewald D, Currie DJ, Lee MH, Todd RW, Marison IW, von Stockar U (2009) Cole-Cole, linear and multivariate modeling of capacitance data for on-line monitoring of biomass. *Bioprocess and biosystems engineering* 32 (2):161-173. doi:10.1007/s00449-008-0234-4
- Douma RD, Verheijen PJ, de Laat WT, Heijnen JJ, van Gulik WM (2010) Dynamic gene expression regulation model for growth and penicillin production in *Penicillium chrysogenum*. *Biotechnology and bioengineering* 106 (4):608-618. doi:10.1002/bit.22689
- Ehgartner D, Fricke J, Schroder A, Herwig C (2016) At-line determining spore germination of *Penicillium chrysogenum* bioprocesses in complex media. *Applied microbiology and biotechnology* 100 (20):8923-8930. doi:10.1007/s00253-016-7787-y
- Ehgartner D, Sagmeister P, Herwig C, Wechselberger P (2015) A novel real-time method to estimate volumetric mass biodensity based on the combination of dielectric spectroscopy and soft-sensors. *J Chem Technol Biotechnol* 90 (2):262-272. doi:10.1002/jctb.4469
- FDA (2006) Guidance for industry: Q9 Quality risk management. Maryland
- Fehrenbach R, Comberbach M, Petre JO (1992) On-line biomass monitoring by capacitance measurement. *J Biotechnol* 23 (3):303-314. doi:10.1016/0168-1656(92)90077-M
- Golabgir A, Ehgartner D, Neutsch L, Posch AE, Sagmeister P, Herwig C (2015) Imaging Flow Cytometry and High-Throughput Microscopy for Automated Macroscopic Morphological Analysis of Filamentous Fungi. In: van den Berg MA, Maruthachalam K (eds) *Genetic Transformation Systems in Fungi*, vol 2. *Fungal Biology*. Springer International Publishing, pp 201-210. doi:10.1007/978-3-319-10503-1\_17
- Golabgir A, Herwig C (2016) Combining Mechanistic Modeling and Raman Spectroscopy for Real-Time Monitoring of Fed-Batch Penicillin Production. *Chemie Ingenieur Technik* 88 (6):764-776. doi:10.1002/cite.201500101
- Haack MB, Lantz AE, Mortensen PP, Olsson L (2007) Chemometric analysis of in-line multi-wavelength fluorescence measurements obtained during cultivations with a lipase producing *Aspergillus oryzae* strain. *Biotechnology and bioengineering* 96 (5):904-913. doi:10.1002/bit.21170
- Hille A, Neu TR, Hempel DC, Horn H (2005) Oxygen profiles and biomass distribution in biopellets of *Aspergillus niger*. *Biotechnology and bioengineering* 92 (5):614-623. doi:10.1002/bit.20628
- Jenzsch M, Simutis R, Luebbert A (2006) Generic model control of the specific growth rate in recombinant *Escherichia coli* cultivations. *J Biotechnol* 122 (4):483-493. doi:10.1016/j.jbiotec.2005.09.013

- Manteca A, Alvarez R, Salazar N, Yague P, Sanchez J (2008) Mycelium differentiation and antibiotic production in submerged cultures of *Streptomyces coelicolor*. *Applied and environmental microbiology* 74 (12):3877-3886. doi:10.1128/AEM.02715-07
- Massimo C, Montague G, Willis M, Tham M, Morris A (1992) Towards improved penicillin fermentation via artificial neural networks. *Computers Chemical Engineering* 16 (4):283-291. doi:10.1016/0098-1354(92)80048-E
- Mishima K, Mimura A, Takahara Y, Asami K, Hanai T (1991) On-Line Monitoring of Cell Concentrations by Dielectric Measurements. *Journal of Fermentation and Bioengineering* 72 (4):291-295. doi:10.1016/0922-338X(91)90166-E
- Mou DG, Cooney CL (1983a) Growth monitoring and control in complex medium: a case study employing fed-batch penicillin fermentation and computer-aided on-line mass balancing. *Biotechnology and bioengineering* 25 (1):257-269. doi:10.1002/bit.260250119
- Mou DG, Cooney CL (1983b) Growth monitoring and control through computer-aided on-line mass balancing in a fed-batch penicillin fermentation. *Biotechnology and bioengineering* 25 (1):225-255. doi:10.1002/bit.260250118
- Neves A, Pereira D, Vieira L, Menezes J (2000) Real time monitoring biomass concentration in *Streptomyces clavuligerus* cultivations with industrial media using a capacitance probe. *Journal of Biotechnology* 84 (1):45-52. doi:10.1016/S0168-1656(00)00325-4
- Nielsen J, Johansen C, Villadsen J (1994) Culture fluorescence measurements during batch and fed-batch cultivations with *Penicillium chrysogenum*. *Journal of Biotechnology* 38 (1):51-62. doi:10.1016/0168-1656(94)90147-3
- Olsson L, Nielsen J (1997) On-line and in situ monitoring of biomass in submerged cultivations. *Trends in Biotechnology* 15 (12):517-522. doi:10.1016/S0167-7799(97)01136-0
- Paul GC, Syddall MT, Kent CA, Thomas CR (1998) A structured model for penicillin production on mixed substrates. *Biochemical Engineering Journal* 2 (1):11-21. doi:10.1016/S1369-703X(98)00012-6
- Pirt SJ, Righelato RC (1967) Effect of Growth Rate on the Synthesis of Penicillin by *Penicillium chrysogenum* in Batch and Chemostat Cultures. *Applied microbiology* 15 (6):1284-1290
- Posch AE, Koch C, Helmel M, Marchetti-Deschmann M, Macfelda K, Lendl B, Allmaier G, Herwig C (2013) Combining light microscopy, dielectric spectroscopy, MALDI intact cell mass spectrometry, FTIR spectromicroscopy and multivariate data mining for morphological and physiological bioprocess characterization of filamentous organisms. *Fungal genetics and biology : FG & B* 51:1-11. doi:10.1016/j.fgb.2012.11.008
- Posch AE, Spadiut O, Herwig C (2012) A novel method for fast and statistically verified morphological characterization of filamentous fungi. *Fungal genetics and biology : FG & B* 49 (7):499-510. doi:10.1016/j.fgb.2012.05.003
- Reichelt W, Thurrold P, Brillmann M, Kager J, Fricke J, Herwig C (2016) Generic biomass estimation methods targeting physiologic process control in induced bacterial cultures. *Engineering in Life Sciences* 16 (8):720-730. doi:10.1002/elsc.201500182
- Riesenberg D, Schulz V, Knorre WA, Pohl HD, Korz D, Sanders EA, Ross A, Deckwer WD (1991) High cell density cultivation of *Escherichia coli* at controlled specific growth rate. *J Biotechnol* 20 (1):17-27. doi:10.1016/0168-1656(91)90032-Q
- Rønnest NP, Stocks SM, Lantz AE, Gernaey KV (2011) Introducing process analytical technology (PAT) in filamentous cultivation process development: comparison of advanced online sensors for biomass measurement. *Journal of industrial microbiology & biotechnology* 38 (10):1679-1690. doi:10.1007/s10295-011-0957-0
- Sagmeister P, Wechselberger P, Herwig C (2012) Information Processing: Rate-Based Investigation of Cell Physiological Changes along Design Space Development. *PDA journal of pharmaceutical science and technology / PDA* 66 (6):526-541. doi:10.5731/pdajpst.2012.00889

- Sagmeister P, Wechselberger P, Jazini M, Meitz A, Langemann T, Herwig C (2013) Soft sensor assisted dynamic bioprocess control: Efficient tools for bioprocess development. *Chemical Engineering Science* 96:190-198. doi:10.1016/j.ces.2013.02.069
- Sarra M, Ison A, Lilly M (1996) The relationships between biomass concentration, determined by a capacitance-based probe, rheology and morphology of *Saccharopolyspora erythraea* cultures. *Journal of Biotechnology* 51 (2):157-165. doi:10.1016/0168-1656(96)01612-4
- Thompson M, Kramer M (1994) Modeling Chemical Processes Using Prior Knowledge and Neural Networks. *AIChE Journal* 40 (8):1328-1340. doi:10.1002/aic.690400806
- van Gulik WM, de Laat WT, Vinke JL, Heijnen JJ (2000) Application of metabolic flux analysis for the identification of metabolic bottlenecks in the biosynthesis of penicillin-G. *Biotechnology and bioengineering* 68 (6):602-618
- Wechselberger P, Sagmeister P, Herwig C (2013) Model-based analysis on the extractability of information from data in dynamic fed-batch experiments. *Biotechnology progress* 29 (1):285-296. doi:10.1002/btpr.1649

**Supplementary material**

**Controlling the specific growth rate via biomass trend regulation in filamentous fungi bioprocesses**

Daniela Ehgartner<sup>1,2</sup>, Thomas Hartmann<sup>1,2</sup>, Sarah Heinzl<sup>1,2</sup>, Manuela Frank<sup>1,2</sup>, Lukas Veiter<sup>1,2</sup>, Julian Kager<sup>2</sup>, Christoph Herwig<sup>1,2</sup> and Jens Fricke<sup>\*,1,2</sup>

\*to whom the correspondence should be addressed to

<sup>1</sup> CD Laboratory on Mechanistic and Physiological Methods for Improved Bioprocesses, TU Wien, Vienna, Austria

<sup>2</sup> Research Area Biochemical Engineering, Institute for Chemical, Environmental and Biological Engineering, TU Wien, Vienna, Austria

Corresponding author:

jens.fricke@tuwien.ac.at

Tel (Office): +43 1 58801 166462

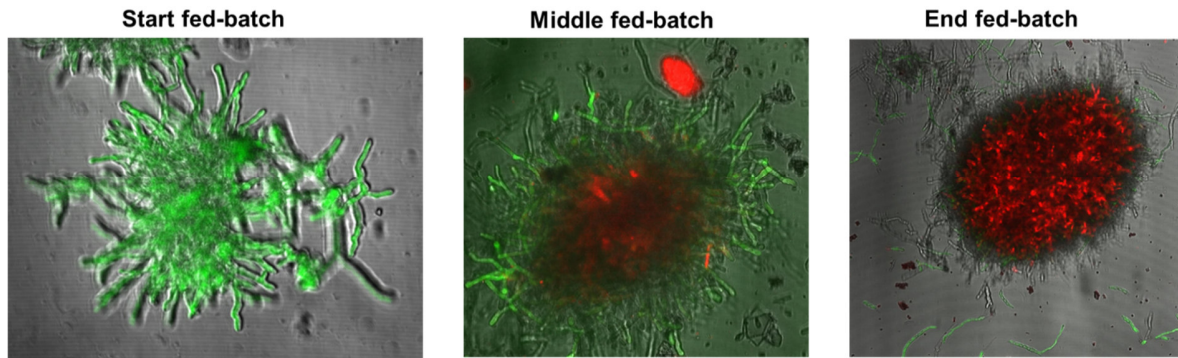


Figure A.1. Representing viability of pellets using confocal microscopy: beginning of fed-batch (after 27 h), middle of fed-batch (53 h) and end of fed-batch (125 h).

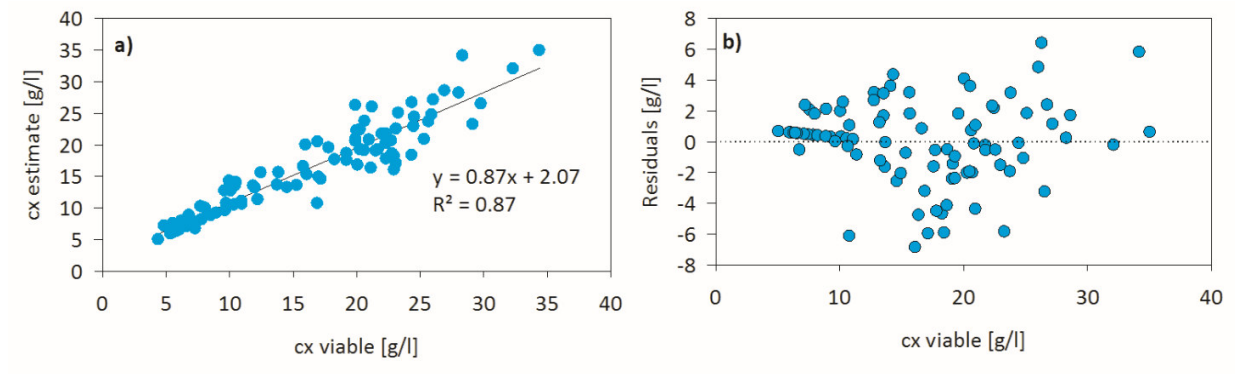


Figure A.2: Quality of the growth phase model. a)  $C_{x,viable}$  vs  $C_{x,estimate}$  for the growth phase model. b) Residuals of viable biomass estimation.

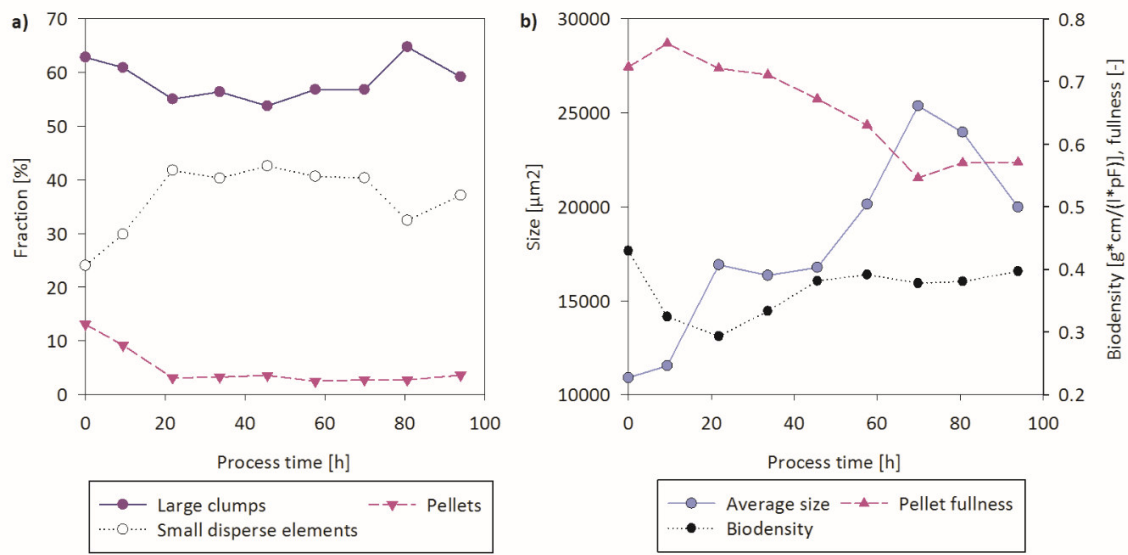


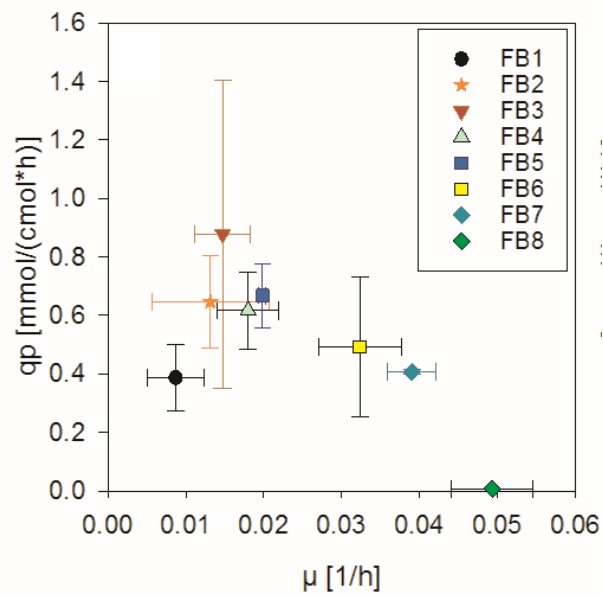
Figure A.3: Morphological data for FB1. a) Morphological fractions representing pellets, large clumps and small disperse elements. b) Single morphological parameter as the mean size of large elements and pellet average fullness are compared to biodensity representing the  $\Delta\text{Cap}$ -biomass-correlation.



Figure A.4: Cultivation broth at the end of fed-batch cultivation

## Production rate dynamics at constant growth conditions in a penicillin production process

Ehgartner, D., Hartmann, T., Heinzl, S., Herwig, C., & Fricke, J, Engineering in Life Sciences, submitted



**Production rate dynamics at constant growth conditions in a penicillin production process**

Daniela Ehgartner<sup>1,2</sup>, Thomas Hartmann<sup>1,2</sup>, Sarah Heinzl<sup>1,2</sup>, Christoph Herwig<sup>1,2</sup>, Jens Fricke<sup>1,2\*</sup>

\*to whom the correspondence should be addressed to

<sup>1</sup>CD Laboratory on Mechanistic and Physiological Methods for Improved Bioprocesses, TU Wien, Vienna, Austria

<sup>2</sup>Research Area Biochemical Engineering, Institute for Chemical, Environmental and Biological Engineering, TU Wien, Vienna, Austria

\*Corresponding author:

jens.fricke@tuwien.ac.at; Tel (Office): +43 1 58801 166462

Gumpendorferstrasse 1a / 166-4

1060 Wien, Austria

## Abstract

Economically, viable processes in biotechnology need high productivity, operating at high specific production rates. A connection between the specific growth rate ( $\mu$ ) and the specific penicillin production rate ( $q_p$ ) has been described in various studies, especially for chemostat and fed-batch cultures with a constant  $q_p$ . In this context, the question to be answered is: Are there similar influences of  $\mu$  on  $q_p$  in fed-batch cultures with dynamic  $q_p$ -trajectories and what are the mechanisms behind those?

In this contribution, the relation of  $\mu$  and  $q_p$  was investigated at constant  $\mu$  levels in fed-batch cultures even during highly dynamic  $q_p$ . Despite lacking constant  $q_p$ -phases, a connection between  $\mu$  and  $q_p$  could be described, which fits formerly published results. First,  $q_p$  started to increase parallel with  $\mu$  until it reached an optimum and decreased subsequently at higher  $\mu$ . Furthermore, it was found that whenever the maximal  $q_p$  was reached, a nearly equal amount of glucose had been metabolized. Thus, the time needed to reach maximal  $q_p$  and thus the starting point of  $q_p$ -decline, is a function of the average  $\mu$  of the fed-batch. The initially increasing  $q_p$  was associated with an adaption effect to the actual specific growth rate. Decline of  $q_p$  was proposed to be associated to NADPH supply from the mannitol cycle.

The here presented results enable predicting  $q_p$ -trajectories and thus are of use for planning and operating of fed-batch cultivations for optimal penicillin production.

**Keywords:** filamentous fungi, mannitol, penicillin, specific growth rate  $\mu$ , specific production rate  $q_p$

**Abbreviations:** DCW, dry cell weight; FB, fed-batch; PBS, phosphate buffered saline; PI, propidium iodide;  $q_p$ , specific penicillin production rate;  $Y_{x/glucose}$ , biomass yield from glucose;  $\mu$ , specific growth rate;

## 1. Introduction

Apart from good product quality, high product yields are favourable in biotechnological production of pharmaceuticals. A major step leading to high product titer is the adjustment of optimal process parameters for production in the upstream process. Concerning the production of penicillin with *Penicillium chrysogenum*, several studies identified the specific growth rate  $\mu$  as crucial variable influencing the specific production rate  $q_p$  [1-6]. This was shown for chemostat [1, 4, 5] as well as fed-batch cultures [1, 6]. At low  $\mu$ -values a positive correlation between  $\mu$  and  $q_p$  was found [1, 2, 4-6]. Dependent on the investigation, the level of the optimal specific growth rate varied. Van Gulik et al. (2000) published a maximal  $q_p$  of penicillin G at a specific growth rate of  $0.03 \text{ h}^{-1}$  for continuous cultures [5]. Contrary, the maximum  $q_p$  in the fed-batch cultures described by Ryu and Hospodka (1980) was reached at a  $\mu$  of  $0.015 \text{ h}^{-1}$  [4]. The maximum  $q_p$  found in fed-batch cultures conducted by Wittler and Schügerl (1992) was at a specific growth rate of  $0.018 \text{ h}^{-1}$  [6]. The maximal  $\mu$  investigated in the last-mentioned study was the one with maximal  $q_p$  ( $\mu=0.018 \text{ h}^{-1}$ ) and thus the maximal  $q_p$  ought to be found at higher growth rates. Therefore, the value of  $\mu = 0.018 \text{ h}^{-1}$  fits well with the findings of another study investigating fed-batches. Douma et al. (2010) described the maximal  $q_p$  in fed-batch cultures to be at approximately  $0.02 \text{ h}^{-1}$  [1, 6]. The trend of  $q_p$  at higher specific growth rate levels differs dependent on the contribution. While Douma et al. (2010) and van Gulik et al. (2000) found a negative correlation between  $\mu$  and  $q_p$  for chemostat and fed-batch cultures [1, 5], other investigations stated  $q_p$  to be independent of  $\mu$  [3, 4]. The two studies describing cultivations for penicillin V production (versus penicillin G in the other studies) did not investigate growth rates exceeding  $0.018 \text{ h}^{-1}$  [6] respective  $0.009 \text{ h}^{-1}$  [2]. However, different strain constructs lead to different maximum specific production rates and relationships of  $\mu$ - $q_p$ .

Data for the description of  $\mu$ - $q_p$ -curves were derived from different approaches: When continuous cultures were investigated, each steady state yielded one pair of  $\mu$  and  $q_p$  [3, 5]. Pirt and Righelato (1967) calculated the mean  $q_p$  of each steady state [3]. Contrary, van Gulik et al. (2000) used the maximal  $q_p$  in case the steady state was not stable [5]. Also, the results for fed-batch processes yielded from different approaches: either one cultivation revealed one  $\mu$ - $q_p$ -pair [6] or several  $\mu$ - $q_p$ -pairs (e.g. one from each biomass sample) [1].

Apart from late process phases, few information about the constancy of  $q_p$  concerning process time is found in the studies described above. An adaption time to C-limited conditions was mentioned [1]. Save for single, instable steady states [5],  $q_p$  is expected to be stable in the investigation period of continuous cultures. Deducing from exemplary fed-batches presented in several studies,  $q_p$  was constant over 80 h and more [4, 6].

A well-known phenomenon in penicillin production processes is the so called “strain degeneration” or “penicillin degradation”. Biomass was reported to (partially irreversibly) lose its ability to produce penicillin during C-limited cultivation. Thus, the  $q_p$  starts to decrease [7, 8]. Various authors described this phenomenon [7-10]. Studies investigating  $\mu$ - $q_p$ -relations were designed to avoid this decline in  $q_p$  in later process phases by choosing a stable strain or restricting cultivation length [1, 3, 5]. A first explanation for penicillin degradation was the occurrence of mutations concerning the penicillin production pathway, followed by an overgrowth of producing genotype by non-producing genotype [7]. More recent investigations denied this theory, as the degeneration phenomenon was too reproducible. Thus, changes in gene regulation were proposed as cause. Here, Douma et al. described degradation to be partly reversible, which stands in contrast to former studies. In these continuous processes  $q_p$ -trajectories were very dynamic. After the start of the C-limitation phase,  $q_p$  increased to reach a maximum value within 40-80 h and further decreased due to degeneration [8].

The here presented study aims to describe  $\mu$ - $q_p$ -relations for penicillin V producing fed-batch cultures even during highly dynamic  $q_p$ -trajectories without intervals of constant  $q_p$ . Thus,  $q_p$ -dynamics at constant  $\mu$  levels in fed-batch cultures were investigated and  $\mu$ - $q_p$ -curves were characterized. In a further step, the background and possible explanations of arising  $q_p$ -dynamics were examined in detail.

## **2. Materials and methods**

### **2.1 Strains and inoculum**

Spore suspensions of the P-14 *P. chrysogenum* candidate strain for penicillin production descending from the P-2 *P. chrysogenum* candidate strain [11] were kindly provided by Sandoz GmbH (Kundl, Austria) and used for all experiments.

### **2.2 Bioreactor cultivation**

Eight cultivations were performed in either of two Techfors S bioreactors (Infors HT, Bottmingen, Switzerland) - 10 l and 20 l maximal working volume. Initial batch and fed-batch volumes were 6.5 l for the 10-l bioreactor and 13 l for the bigger one. The stirrer was equipped with three six bladed Rushton turbine impellers, of which two were submersed and one was installed above the maximum liquid level for foam destruction.

Fermentation temperature was kept at 25°C via double jacket. Aeration was controlled at 1 vvm in batch and initial fed-batch with mass flow controllers (Vögtlin, Aesch, Switzerland). Dissolved oxygen

concentration was measured using a dissolved oxygen probe (Hamilton, Bonaduz, Switzerland) and controlled at a level higher than 40%, via adjustment of stirrer speed. pH was measured using a pH probe (Hamilton, Bonaduz, Switzerland). CO<sub>2</sub> and O<sub>2</sub> concentration were analyzed with an off-gas analyzer (M. Müller AG, Egg, Switzerland).

Dielectric spectroscopy was applied in dual frequency mode using a Biomass Monitor 220 (Aber Instruments, Aberystwyth, UK). Every minute the delta capacitance was recorded for the following frequencies: 100/15650 kHz. For further application, the signal was smoothed using a Savitzky-Golay-filter (first order, window of 60 data points).

The batch was carried out on complex bioreactor medium similar as described in Posch et al. (2013) [12]. The culture was inoculated with a spore inoculum concentration of 10<sup>8</sup> spores/l. During this phase pH was not controlled. The end of the batch was indicated by an increase in pH of 0.5.

After the batch, a fed-batch was performed on defined medium (similar as described elsewhere [12]). For this purpose, 10% of the batch broth were added to defined medium with 90% of the initial fed-batch volume. Initial fed-batch volumes were 6.5 l and 13 l, respectively. During fed-batch phase, pH was kept constant at  $6.5 \pm 0.1$  by addition of 20% (w/v) KOH or 15% (v/v) H<sub>2</sub>SO<sub>4</sub>, respectively. An initial constant feed of 1.01 ml/(l\*h) of 500 g/l glucose solution was only applied for 24 h, then  $\mu$ -control was started. The 24 h of (low) constant feed were necessary as sugars and metabolites like gluconate were transferred from the batch culture, prohibiting C-limited conditions at fed-batch start. Thus, C-limitation always refers to the initialization of  $\mu$ -control, 24 h after the start of fed-batch. The eight cultivations differed in their specific growth rate during  $\mu$ -control phase. Table 1 depicts the fed-batches and their respective specific growth rate.

Table 1: The fed-batch cultivations and their specific growth rate

FB ID	Average $\mu$ [h <sup>-1</sup> ]
FB1	0.009
FB2	0.013
FB3	0.015
FB4	0.018
FB5	0.020
FB6	0.032
FB7	0.040
FB8	0.049

For  $\mu$ -control, viable biomass was determined at-line (see sections 2.4 and 2.5). Further, a regression was calculated for the viable biomass concentrations of the last 24 h and the corresponding delta capacitance values (see Equation 1). This allowed the online prediction of the actual viable biomass based on the delta capacitance signal. The regression was actualized every 12 h, when a new biomass sample was taken.

$$c_{x,\text{viable}}(t) = b_0 + b_1 * dC(t) \quad (1)$$

In addition, the biomass yield  $Y_{x/\text{glucose}}$  was determined at-line for the last 12 h. This was necessary because of changing yields during the process. The biomass yield was crucial for the calculation of the feeding rate to achieve aimed levels of  $\mu$  which is shown in Equation 2.

$$F_{\text{glucose}}(t) = c_{x,\text{viable}}(t) * V_R * \mu_{\text{aim}} * \frac{1}{Y_{x/\text{glucose}}} * \frac{\rho_{\text{glucose}}}{c_{\text{glucose}}} \quad (2)$$

### 2.3 Calculations

Calculations of yields, rates and specific rates like the specific growth rate were calculated as stated elsewhere [13]. The filamentous fungus used in this study forms pellets, which partially contain high amounts of dead biomass. Thus, viability of the biomass was investigated at-line (see section 2.4) and viable biomass used as basis for calculation.

#### 2.4 At-line viability measurement

To investigate viability via propidium iodide (PI) staining, 200  $\mu\text{l}$  of sample were diluted 1:5 with phosphate buffered saline (PBS, see elsewhere [14]). In addition, 1 ml of sample was diluted 1:5 with PBS and microwave treated by leaving it for 30 s at 940 W in a M510 microwave oven (Philips, Amsterdam, Netherlands). One millilitre of the microwave treated sample was used for further investigation. In a next step, duplicates of all samples (including microwave treated and untreated samples) were centrifuged for 15 min at 500 rpm. 800  $\mu\text{l}$  of supernatant were removed and 800  $\mu\text{l}$  of PBS buffer were added. The pellet was resuspended and the washing step repeated. 100  $\mu\text{l}$  of the resuspended sample was pipetted into a microtiter well and 1  $\mu\text{l}$  of 200  $\mu\text{M}$  PI solution (Sigma Aldrich, St. Louis, Missouri/USA) was added. The PI was prepared by diluting a 20 mM PI stock solution in DMSO, 1:100 in PBS. After an incubation time of 20 min at room temperature in darkness, the measurement was performed in a Tecan well-plate reader (Tecan, Männedorf, Switzerland; ex./em. 535/600 nm). Each duplicate of the microwave treated and untreated sample was measured three times simultaneously using 96 well plates. Viability was calculated using Equation 3. To determine viable biomass concentration, the viability value was multiplied by the total biomass concentration (see section 2.5).

$$\text{Viability} = 1 - \frac{\text{Average of red fluorescence native sample}}{\text{Average of red fluorescence microwaved sample}} \quad (3)$$

#### 2.5 Total biomass concentration

Two methods to determine total biomass concentration were applied. For at-line determination of viable biomass, wet weight was measured. Due to lower measurement error (4% vs. 10%), total biomass for offline use was evaluated via dry cell weight (DCW) measurement.

Measurements were carried out in quadruplicates by transferring 5 ml of fermentation broth into weighed glass eprovettes and centrifuging them at 4800 rpm for 10 min at 4°C. The supernatant was removed and stored at -20°C for later analysis of sugars, metabolites and penicillin. The pellets were then resuspended in 5 ml of deionized water and the eprovettes were centrifuged again at the conditions mentioned above. The supernatant was discarded. For wet weight determination, the eprovettes were weighed and the biomass concentration calculated using a predefined regression to DCW. After wet weight determination, the eprovettes were dried at 105°C for at least 72 h and weighed again, resulting in DCW.

## 2.6 Light microscopy

Morphological analysis via scanning of microscopic images was conducted as described elsewhere [12]. Therefore, 900 images per sample were recorded by a Leitz wide field microscope (Leitz, Stuttgart, Germany). It was equipped with a five-megapixel microscopy CCD colour camera (DP25, Olympus, Tokio, Japan) and a fully automated x-y-z stage (Märzhäuser, Wetzlar, Germany). The software for image recording was analysis5 (Olympus, Tokio, Japan).

## 2.7 Sugar and metabolites

Gluconic acid, glucose and mannitol were quantified with ion chromatography. Analysis was carried out using a Dionex column (Thermo Fisher Scientific, Waltham, Massachusetts, US) at a column temperature of 30°C. For detection, a Dionex PAD detector in quadrupole potential mode (Thermo Fisher Scientific, Waltham, Massachusetts, US) was used. A gradient profile was applied combining three different solvents (MQ water, 0.1 N NaOH and 1 N NaOH).

## 2.8 Penicillin measurements

High performance liquid chromatography (HPLC) using a Thermo Scientific UltiMate 3000 system (Thermo Fisher Scientific, Massachusetts, United States) together with Chromeleon 7 Chromatography Data System (Thermo Fisher Scientific, Massachusetts, USA) was used for quantifying penicillin concentrations with a Zorbax Eclipse AAA C18 column (Agilent Technologies, Santa Clara, USA) with a buffer as described elsewhere [15].

A flow rate of 1.0 ml/min was applied and the required temperature of the column oven was 30°C. The UV/VIS detector for determining penicillin peaks via absorption was set to 210 nm.

# 3. Results

## 3.1 $q_p$ -trajectory

Similar as reported in a previous study [1], several  $\mu$ - $q_p$ -pairs from each of the eight cultivations were plotted in Figure 1A to describe the link between  $\mu$  and  $q_p$ . Although only data pairs from the C-limited phase with increasing  $q_p$  were used (see Figure 1B), no clear trend was observable.

A typical  $q_p$ -trajectory at constant  $\mu$  is shown in Figure 1B. Two phases were distinguishable in the  $q_p$ -trajectory:

- Phase 1: before  $q_p$ -maximum
- Phase 2: after  $q_p$ -maximum

These two phases were found in all fed-batches but FB1. In last mentioned,  $\mu$  as well as  $q_p$  were strongly fluctuating. Thus, a maximum of  $q_p$ , signalling the start of phase 2, could not be clearly identified. However, two possible maxima were identified at  $t=114$  h and at  $t=130$  h. FB1 is shown in Figure 1C.

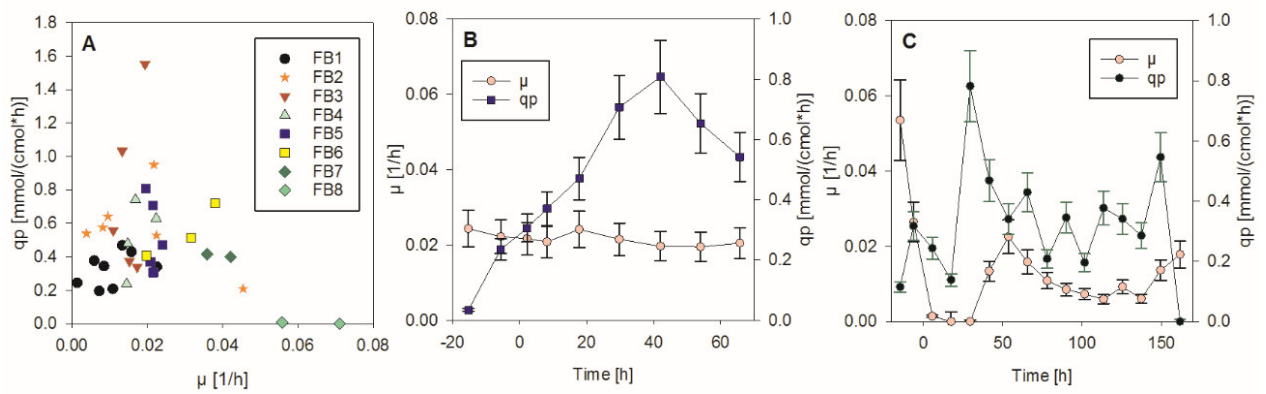


Figure 1: Specific growth rate and specific production rate. A)  $\mu$  vs.  $q_p$  for all samples in phase 1 of all cultivations. B-C)  $\mu$  and  $q_p$  over time since C-limitation for FB5 (B) and FB1 (C). The start of  $\mu$ -control (respectively C-limitation) is indicated as time point 0.

### 3.2 $q_p$ depends on $\mu$

Figure 1 depicted dynamic  $q_p$ -trajectories over process time and thus no clear trend of  $q_p$  was detected when several  $\mu$ - $q_p$ -pairs per cultivation were plotted. Hence, a different approach was investigated. Due to similar dynamics in  $q_p$  in all cultivations and constant  $\mu$  within each cultivation, it was deduced to choose one value for  $\mu$  and  $q_p$ , respectively. Therefor four different approaches as shown in Figure 2 are presented. First, average values of  $\mu$  and  $q_p$  during phase 1 were calculated for the eight cultivations. Figure 2A represents this investigation. Reproducibility was shown at an average  $\mu$ -value of  $0.019 \text{ h}^{-1}$  where FB4 and FB5 overlap.

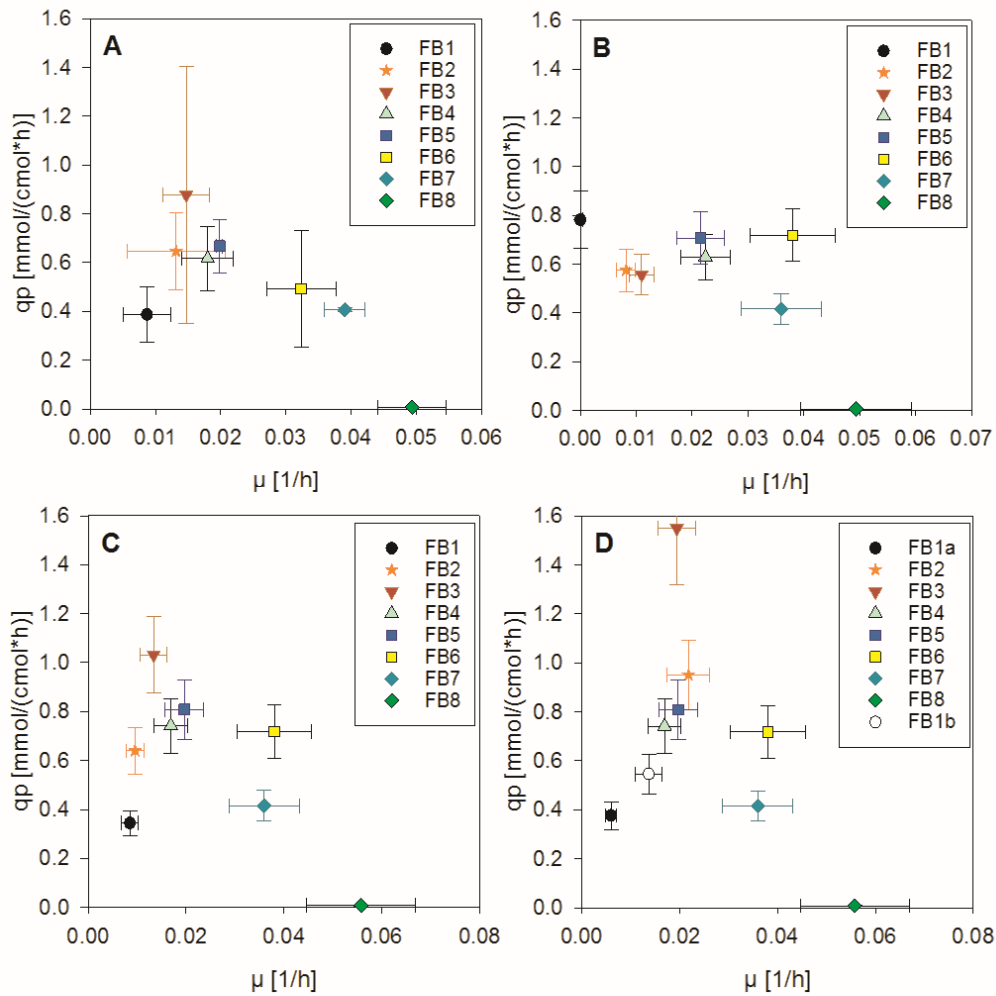


Figure 2:  $\mu$ - $q_p$ -relation. A) Average values for constant  $\mu$  during phase 1. B) after 30-34 h of C-limitation C) After consumption of 40-60 g glucose per initial biomass concentration since fed-batch start. D) At maximum  $q_p$

The dynamics of  $q_p$  (Figure 1B) suggest a dependency of  $q_p$  not only on  $\mu$  but also on time. Thus,  $\mu$ - $q_p$ -pairs for a constant time point since C-limitation are plotted in Figure 2B. A trend is observable although FB1 and FB6 do not fit into the trend curve. While the high  $q_p$ -value of FB6 may be explained by the lower  $\mu$  12 h earlier ( $0.031 \text{ h}^{-1}$  compared to  $0.042 \text{ h}^{-1}$  in FB7), the higher  $q_p$ -value in FB1 cannot be explained. However, the influence of earlier  $\mu$ -values in the cultivations on  $q_p$  might be due to adaptation of the organism. Like it was already shown for  $\mu$ - $q_p$ -relations based on average values (Figure 2A), FB4 and FB5 overlap quite well. The time point  $t=30\text{-}34 \text{ h}$  after C-limitation was chosen in the way to allow the organism to adapt to C-limited conditions and  $\mu$ -levels, but to set the time point before  $q_p$  starts to decrease for most fed-batches.

As alternative to process time, a parameter possibly more closely representing adaption of the organism was chosen in another approach: the consumed glucose. The respective  $\mu$ - $q_p$ -pairs are presented in Figure 2C. The value of 40-60 g consumed glucose per initial biomass concentration since fed-batch start was chosen with the same criteria as the 30-34 h mentioned before. The connection between  $\mu$  and  $q_p$  seems to be similar to the trend shown for average values in Figure 2A. Still, the absolute values are slightly different. Differences in FB6 and FB7 are the same as already mentioned when discussing Figure 2B.

Finally, the  $q_p$ -maxima of all cultivations were investigated concerning the dependency on  $\mu$ . Figure 2D shows a similar trend as Figure 2A and Figure 2C although the maximum shifted to higher  $\mu$ -values. The maximum  $q_p$  of FB3 (1.55 mmol/(c-mol\*h)) by far exceeds maxima of the other cultivations. Concerning FB1, two  $\mu$ - $q_p$ -pairs are represented, as the real  $q_p$ -maximum marking the start of  $q_p$ -decline could not be identified. Both data points fit into the trend curve.

### 3.3 Background of $q_p$ -dynamics

In section 3.2, time and consumed glucose, representing the period of adaption of the organism to constant process conditions, were analyzed. Consumed glucose was chosen as alternative to time as representor necessary to describe the adaption of the organism. This was applied as the start of phase 2, indicated by  $q_p$ -maximum, was not comparable according to the passed time. The  $q_p$ -maximum was reached within 20 h to 150 h after C-limitation (see Figure 3A). Contrary, the amount of consumed glucose as parameter representing the organisms' metabolism, respective the adaption of the metabolism, seemed more appropriate: The start of  $q_p$ -decrease for all cultivations was found within 40-60 g consumed glucose per initial biomass concentration (see Figure 3B). Only exception was again FB1. One of the defined possible  $q_p$ -maxima of FB1 lay within the range of 40-60 g, the other was found at more than 80 g consumed glucose per initial biomass.

The finding to describe dynamics in  $q_p$  with the metabolic workload of the organism was confirmed by the dependency of the start of  $q_p$ -decrease on the average  $\mu$  prior to this point (see Figure 3C): the lower the average  $\mu$ , the longer it takes to consume the same amount of glucose than cultivations with higher  $\mu$ . Interestingly, the glucose consumed seems to be the key parameter, independently of the usage of the metabolized substrate. Instead of a linear connection of average  $\mu$  and time until start of phase 2, the trend follows a negative power function. The reason therefor can be found in the biomass yield shown in Figure 3D. At low specific growth rates (until ca. 0.015 h<sup>-1</sup>) the biomass yield in C-limited culture positively correlated with  $\mu$ , as a regression analysis shows ( $p=0.006<0.05$ ). In higher  $\mu$ -ranges (above 0.015 h<sup>-1</sup>) the biomass yield was constantly high and hence did not correlate with  $\mu$  ( $p=0.28>0.05$ ).

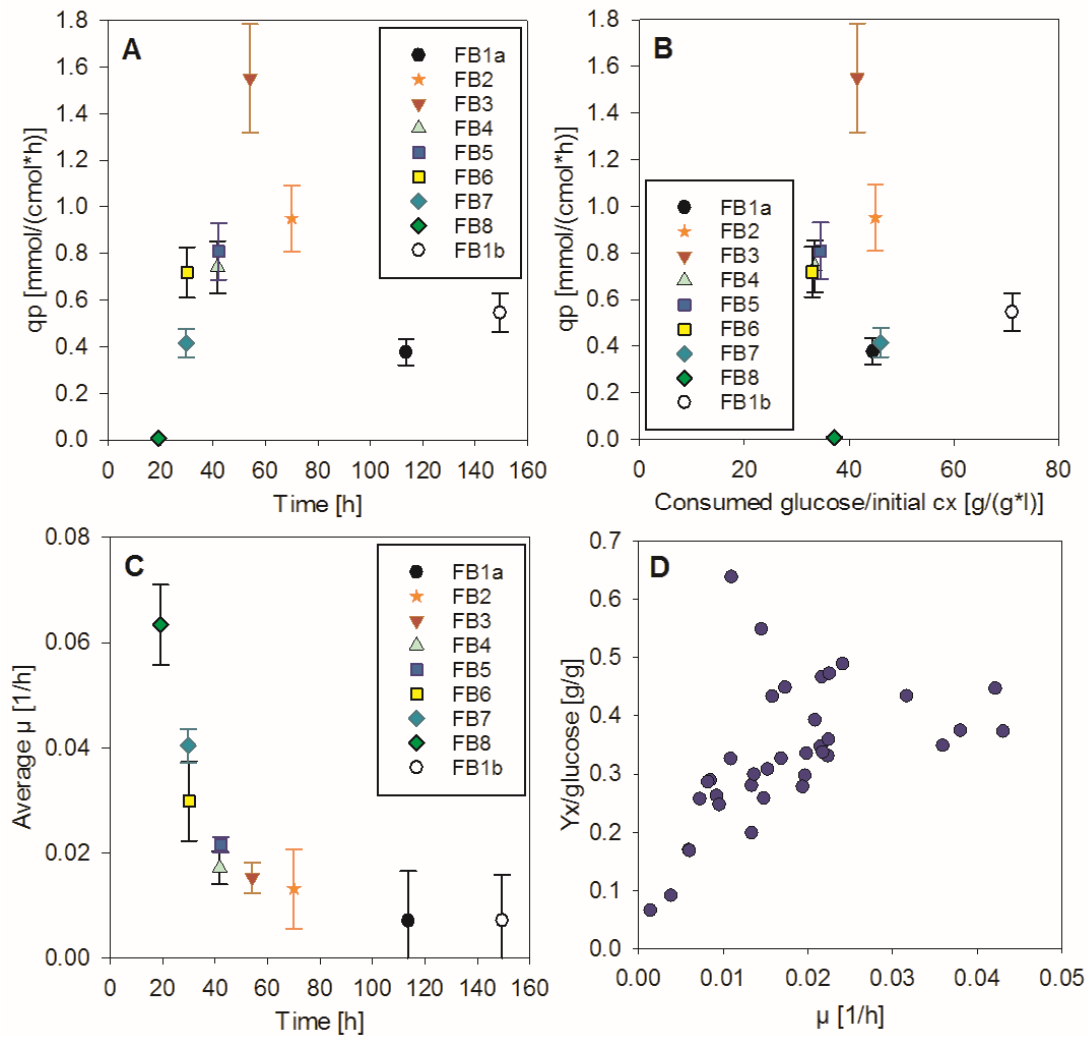


Figure 3:  $q_p$ -maximum. A) Time since C-limitation vs.  $q_p$ . B) Consumed glucose since start of fed-batch normalized by the initial biomass concentration. C) Time since C-limitation vs. average specific growth rate in C-limited phase. D) Biomass yield ( $Y_{x/glucose}$ ) for different  $\mu$ -levels.

### 3.4 Phenomena accompanying the decline of $q_p$

The  $q_p$ -maximum and the following decrease of  $q_p$  is a crucial event for penicillin production. Thus, it was investigated in more detail in order to increase understanding. The C-source utilization would be expected to be redirected from penicillin biosynthesis to biomass production. But no significant trends in the  $Y_{x/glucose}$  were observable.

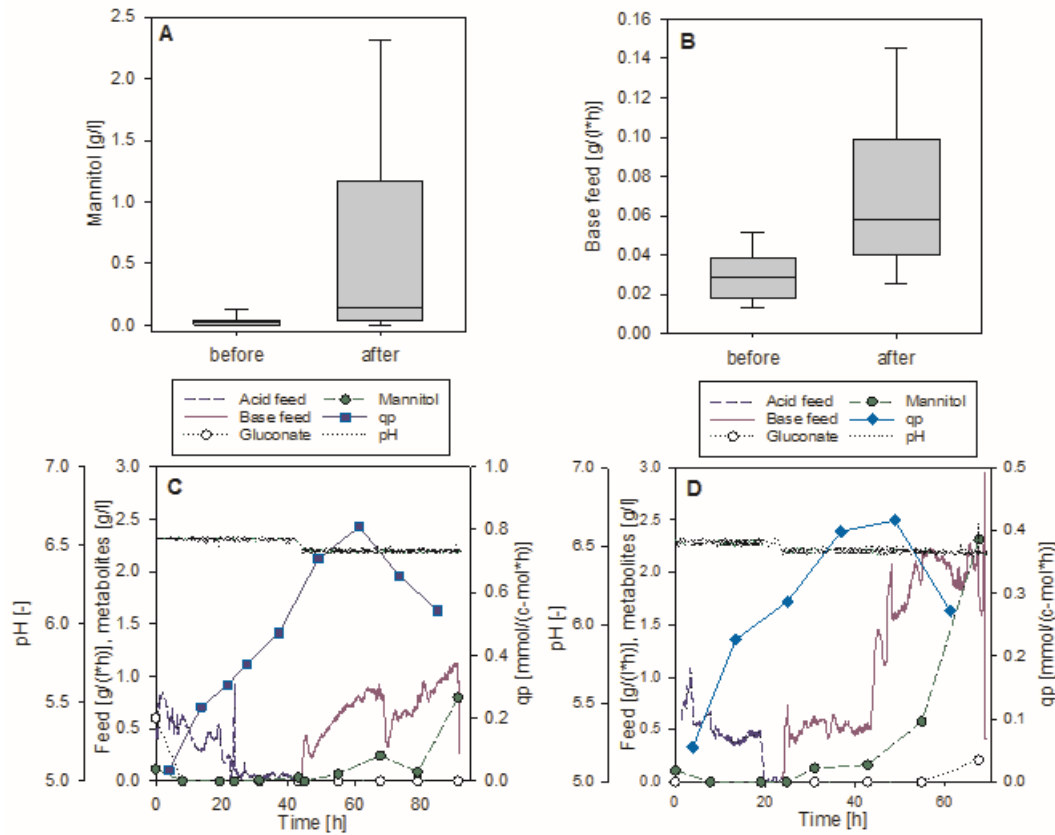


Figure 4: Increase of mannitol concentration and base consumption at start of phase 2. A-B) Boxplot for mannitol concentration (A) and normalized base consumption (per g biomass) (B) before and after maximal  $q_p$  of all cultivations except FB8. C) Mannitol, gluconate concentration, base and acid consumption and  $q_p$  during FB5. D) Mannitol, gluconate concentration, base and acid consumption and  $q_p$  during FB7.

However, two other phenomena were observed: First, around the start of phase 2 mannitol began to accumulate in the medium. A paired t-test comparing mannitol concentrations 18 h before and 18 h after the  $q_p$ -maximum of all cultivations except FB8 (glucose accumulated during cultivation) revealed a significant increase of accumulated mannitol in the medium ( $p=0.047 < 0.05$ ), which is shown in Figure 4A. Exemplary mannitol concentration trends for two cultivations are shown in Figure 4C and Figure 4D. To not use the same sampling points used for the calculation of  $q_p$ -maximum, the samples before and after these were taken resulting in  $\pm 18$  h.

A further physiological change was the increase of base consumption around the start of phase 2: The paired t-test for comparing normalized base consumption (g base/g biomass) before and after  $q_p$ -maximum could be stated as significant ( $p=0.01 < 0.05$ ; Figure 4B). Here, the base consumption was normalized to the actual total biomass to not wrongly misinterpret increasing base demand by raising

biomass concentrations. For illustration in Figure 4C and Figure 4D, base consumption was only normalized to the reactor volume but not to the biomass concentration, as biomass values are only accessible in 12-h-interval. Figure 4C and Figure 4D exemplarily illustrate pH regulation. In the first phase of fed-batch, acid needs to be added for the control of pH at a set-point of 6.5. During phase 1 the metabolism changes and base needs to be added to maintain a constant pH. Parallel to the increase of mannitol concentration in the medium, the base consumption partially increases abruptly.

Apart from physiological parameters, the morphology was investigated. No significant changes in morphology were observed. Nonetheless, large clumps and pellet roughness suddenly seemed to increase with the start of phase 2 (data not shown). However, the effect did not prove to be significant.

## 4 Discussion

### *Comparison to former investigations*

The penicillin V producing *Penicillium chrysogenum* strain in the here described fed-batch cultures showed highly dynamic  $q_p$ -trajectories even though  $\mu$  was set to a constant level. This is contrary to previous findings, where  $q_p$  was assigned directly to the specific growth rate [1, 2, 4, 5]. Taking several  $\mu$ - $q_p$ -pairs per cultivation, as it was done for other fed-batch cultivations describing the connection of  $\mu$  and  $q_p$  [1], resulted in a cloud of data points rather than a clear trend curve. Thus, other approaches similar to already published ones, like usage of the maximal  $q_p$  or the average per cultivation/steady state, were applied [3, 5]. In addition, one  $\mu$ - $q_p$ -pair per cultivation for one point in time and one metabolic variable were chosen. These approaches resulted in the same findings, which supports the most recent data on  $\mu$ - $q_p$ -correlation reported for continuous cultures and fed-batches [1, 5].

At low specific growth rate levels,  $\mu$  and  $q_p$  are positively correlated. After reaching the optimal specific production rate,  $q_p$  decreases with increasing  $\mu$ -values. Douma et al. (2010) described this behavior by a rate-limiting enzyme, namely the isopenicillin-N synthase [1]. This enzyme is crucial for the building of penicillin V and penicillin G [1, 16]. The optimal specific growth rate for penicillin production differs between chemostat and fed-batch cultures due to the dynamic conditions in latter [1]. Thus, a comparison of the here described results to those from chemostat cultures is not favorable. Comparing the results to the most recent study conducted for fed-batches reveals a similar optimal  $\mu$ . Dependent on the approach for data investigation, the optimum found in this study was between  $0.012 \text{ h}^{-1}$  and  $0.02 \text{ h}^{-1}$ . Latter was the

optimum found by Douma et al. (2010) [1]. Differences could be explained by variation in penicillin (penicillin V vs. penicillin G), the strain or the cultivation strategy (media etc.). Moreover, the here conducted study applied viability measurements to neglect dead (non-producing and non-growing, hence metabolically inactive) biomass to not falsify  $\mu$ -values and  $q_p$ -values. The distinction of viable and dead biomass is crucial, especially for cultures growing hyphal pellets [2, 6]. However, the specific (viable) growth rate found in our study was lower compared to former contributions from e.g. Douma et al. (2010) [1]. This seems to be contradictive as the viable  $\mu$  has to be higher due to referring to a lower amount of biomass.

#### *Deriving optimal specific growth rates*

The definition of an optimal specific growth rate seems to be difficult as it is strongly depending on the operators' goal. From an industrial point of view, the optimal  $\mu$ -level is the one, where product titer and cost are in best relation. This means consideration of a high time-space-yield without reaching too high biomass concentrations (via high specific growth rates). The latter leads to high viscosities and hence impaired mass transfer as well as higher power input for stirring [17-19]. Further, the average  $\mu$  during fed-batch influences the percentage of pellets (counterpart to dispersed hyphae and aggregates) as it is shown in Figure S1 of the supporting information. Higher relative pellet concentrations promise a better mass and heat transfer as well as lower power input levels for stirring [20].

It has to be mentioned that the reason for different  $q_p$ -optima at specific growth rates between  $0.012 \text{ h}^{-1}$  and  $0.02 \text{ h}^{-1}$ , are slight fluctuations of the specific growth rate in the fed-batch with the highest  $q_p$  (FB3, see Figure S2 in the supporting information and Figure 2 in the manuscript). The initial  $\mu$  was almost  $0.02 \text{ h}^{-1}$ , slowly decreased to  $0.011 \text{ h}^{-1}$  and again slowly increased to reach  $0.02 \text{ h}^{-1}$ , before the decline of  $q_p$  began. In average, the  $\mu$  in this fed-batch was  $0.015 \text{ h}^{-1}$ . These slight differences in specific growth rate around the optimal level for penicillin production might be an alternative to constant growth rates resulting in higher penicillin titers. Still, the level of  $\mu$  seems of great importance, as also FB2 and FB6 show slight fluctuations in  $\mu$ -levels over process time without resulting in elevated  $q_p$  (see Figure 2A).

Herewith, a profile including different (controlled)  $\mu$ -levels ought to be advantageous to a constant  $\mu$  all over the fed-batch. A possible experimental design could be to start with a higher specific growth rate of  $0.02 \text{ h}^{-1}$  to quickly reach higher  $q_p$ -phases of the cultivation (consumed glucose is the important factor in approaching  $q_p$ -maximum – the more glucose is consumed, the closer the  $q_p$ -maximum is). In a next step,  $\mu$  should be decreased to  $0.012 \text{ h}^{-1}$  in order to achieve higher  $q_p$ , elongate the period of production until

$q_p$ -declines and to avoid too high biomass concentrations. However, further investigations are necessary to better approach this attempt.

*Adaption: Increasing  $q_p$*

Dynamic  $q_p$ -trajectories have already been observed before. These were explained by the time the organism needs to adapt [8]. Enzymes of the penicillin production pathway are repressed during C-unlimited conditions in batch. After the beginning of C-limitation, time is needed for these enzymes to adapt and to reach maximal levels. Further, the rate-limiting enzyme (isopenicillin-N synthase) showed to be dependent on the specific growth rate. Enzyme levels need time scales from minutes to hours to adapt. Thus,  $q_p$  is dynamic due to dynamic conditions in the fed-batch and always lacks behind, respective needs time for adaption [1]. Douma et al. (2010) raised the issue of dynamic conditions in the fed-batch (vs. steady state in continuous cultures), arguing with the inconstancy of  $\mu$  in their fed-batches. As  $\mu$  was found to be the trigger for changing enzyme levels in the penicillin pathway, the enzymes gradually needed to adapt [1].

Hereby the question arose: Are conditions in fed-batches with constant  $\mu$  really that dynamic? In the fed-batches conducted within this contribution, many process variables were kept constant: dissolved oxygen tension  $pO_2$ , air inflow, nitrogen and phenoxyacetate levels,  $\mu$  and even the reactor volume, as glucose was added in a highly-concentrated form and sample was taken regularly. Process variables which were less constant in these fed-batch cultivations were trace element and metabolite concentration, penicillin concentration, biomass concentration, (and hence viscosity), viability and morphology. In case, the specific growth rate is supposed to be the only trigger for  $q_p$ , the steadily increasing  $q_p$  must be interpreted as a long adaption period taking decades of hours.

As neither enzymatic levels were measured nor flux analysis conducted, the here presented study cannot explain mechanisms behind the dynamics in  $q_p$  and their dependence on  $\mu$  in more detail. However, the adaption of the organism, independent of dynamic conditions (e.g. viscosity, metabolite concentration, changes in morphology), to a  $q_p$ -maximum could be described in this contribution. This adaption under fed-batch conditions seems to be not directly influenced by time but rather by metabolic throughput represented by consumed glucose. This is an important finding as the penicillin production period ought to be elongated using this knowledge.

*Decline of  $q_p$* 

The phase of an increasing  $q_p$  can be explained by adaption processes. How about the decline phase? Penicillin degeneration is a widely-known phenomenon and was reported to occur as early as after 40-80 h of C-limited cultivation [8]. It was found in cultures with penicillin V [7], penicillin G [8] and other antibiotics [21]. Already 30 years ago strain degeneration was reported for Panlab strains with decreasing yields after each slant-to-slant transfer [11]. Working with a penicillin V producing strain, originating from the Panlab strain line, makes the occurrence of penicillin degradation probable.

The start of this phase 2 can be presumed to be the maximal  $q_p$ -point. This goes in line with previous investigations [8]. We observed accumulation of mannitol and increased base consumption, which seems to happen simultaneously with the start of  $q_p$ -decline phase. A decline in  $q_p$  at stable process parameters suggests some kind of change in the organism, possibly originating in the metabolism. Hence, the occurrence of mannitol in the medium could be connected to the event of starting  $q_p$ -decrease. Mutations in the penicillin gene cluster, as previous investigations reasoned as cause for the  $q_p$ -decrease [7], seem thereby to be unlikely, as the begin of  $q_p$ -decline is a function of consumed glucose. Thus, a directed regulation of gene expression is more probable but needs to be investigated as no enzymatic assays were performed as mentioned earlier.

The accumulation of mannitol could be connected to the penicillin producing pathway by the need of cofactors for amino acid generation (e.g. NADPH) [5, 10]. NADPH was found to be the limiting factor for cysteine production, one of the three precursor amino acid for penicillin besides L- $\alpha$ -aminoadipic acid and valine [22]. The mannitol cycle supplies NADPH by the usage of NADH and ATP. Thus, for the delivery of NADPH, mannitol is simultaneously synthesized and again metabolized [23]. Therefore, the extracellular accumulation of mannitol could represent a reduced NADPH supply, as mannitol is produced but not metabolized, omitting the crucial step for NADPH generation. Whether the accumulation of mannitol happens due to decreased concentrations of mannitol dehydrogenase, the enzyme responsible for the conversion of mannitol to fructose [23], or the accumulation of the polyol is used as energy storage or done for other reasons [24], cannot be clearly answered.

A last point concerns the morphology after start of  $q_p$ -decline. Earlier, changes in colony morphology had been observed on agar plates [9]. However, the here applied morphology measurement via microscopy did not reveal significant changes. Still, morphological changes could be reasonable due to a switch away from penicillin production freeing resources of the organism.

*Concluding remarks*

This contribution investigated the relation of  $\mu$  and  $q_p$ , even during highly dynamic  $q_p$ -trajectories at constant  $\mu$ -levels. Despite lacking constant  $q_p$ -phases, a connection between  $\mu$  and  $q_p$  could be described which fits to results published earlier.

Trends of  $q_p$ -trajectories were described as follows: With the begin of a C-limited phase,  $q_p$  started to increase until it reached a maximum and decreased. The increase of  $q_p$  was associated with an adaption effect to the actual specific growth rate. Furthermore, it was found that the maximal  $q_p$  was reached after metabolizing a certain amount of glucose. Thus, the time needed to reach maximal  $q_p$  and hence the point of  $q_p$ -decline, is a function of the average  $\mu$  of the fed-batch. Decline of  $q_p$  was proposed to stand in relation with NADPH supply from the mannitol cycle.

The here presented findings enable not only the prediction of the  $q_p$ -maximum but even more allow to plan and operate the penicillin production process in the way to achieve maximal output. Different  $\mu$ -profiles ought to be conducted, resulting in short adaption times of the filamentous organism. Further, a prolonged production at high  $q_p$ -levels and avoidance of disturbing occurrences like high broth viscosities, leading to raised power input levels and decreased mass transfer, could be achieved.

### Acknowledgement

We thank the Austrian Federal Ministry of Science, Research and Economy in course of the Christian Doppler Laboratory for Mechanistic and Physiological Methods for Improved Bioprocesses for financial support (grand number 171). Strains for the experiments were gratefully provided by Sandoz GmbH (Kundl, Austria).

### Conflict of interest

The authors declare no financial or commercial conflict of interest.

### Nomenclature

$b_0$  [g/l] Offset of the delta capacitance correlation with biomass

$b_1$  [(g\*cm)/(l\*pF)] Slope of the same correlation

$c_{\text{glucose}}$  [g/l] Concentration of glucose feed

$c_{x,\text{viable}}$  [g/l] Viable biomass concentration

$dC$  [pF/cm] delta Capacitance

$F_{\text{glucose}}$  [g/h] Glucose feeding rate

$q_p$  [mmol/(c-mol\*h)] Specific penicillin production rate

$V_R$  [l] Reactor volume

$Y_{x/\text{glucose}}$  [g/g] Biomass yield

### Greek symbols

$\rho_{\text{glucose}}$  [g/l] Density of the glucose feed

$\mu$  [h<sup>-1</sup>] Specific growth rate

---

$\mu_{aim}$  [h<sup>-1</sup>] Aimed specific growth rate

## 5 References

1. Douma, R.D., Verheijen, P.J., de Laat, W.T., Heijnen, J.J., et al., Dynamic gene expression regulation model for growth and penicillin production in *Penicillium chrysogenum*. *Biotechnol. Bioeng.* 2010, *106*, 608-18.
2. Kluge, M., Siegmund, D., Diekmann, H., Thoma, M., A model for penicillin production with and without temperature shift after the growth phase. *Appl. Microbiol. Biotechnol.* 1992, *36*, 446-51.
3. Pirt, S.J., Righelato, R.C., Effect of Growth Rate on the Synthesis of Penicillin by *Penicillium chrysogenum* in Batch and Chemostat Cultures. *Appl. Microbiol.* 1967, *15*, 1284-90.
4. Ryu, D.D.Y., Hospodka, J., Quantitative Physiology of *Penicillium chrysogenum* in Penicillin Fermentation. *Biotechnol. Bioeng.* 1980, *22*, 289-298.
5. van Gulik, W.M., de Laat, W.T., Vinke, J.L., Heijnen, J.J., Application of metabolic flux analysis for the identification of metabolic bottlenecks in the biosynthesis of penicillin-G. *Biotechnol. Bioeng.* 2000, *68*, 602-18.
6. Wittler, R., Schügerl, K., Interrelation between penicillin productivity and growth rate. *Appl. Microbiol. Biotechnol.* 1985, *21*, 348-355.
7. Christensen, L.H., Henriksen, C.M., Nielsen, J., Villadsen, J., et al., Continuous cultivation of *Penicillium chrysogenum*. Growth on glucose and penicillin production. *J. Biotechnol.* 1995, *42*, 95-107.
8. Douma, R.D., Batista, J.M., Touw, K.M., Kiel, J.A., et al., Degeneration of penicillin production in ethanol-limited chemostat cultivations of *Penicillium chrysogenum*: A systems biology approach. *BMC Syst. Biol.* 2011, *5*, 132.
9. Künkel, W., Berger, D., Risch, S., Wittmann-Bresinsky, B., Genetic instability of industrial strains of *Penicillium chrysogenum*. *Appl. Microbiol. Biotechnol.* 1992, *36*, 499-502.
10. van Gulik, W.M., Antoniewicz, M.R., de Laat, W.T., Vinke, J.L., et al., Energetics of growth and penicillin production in a high-producing strain of *Penicillium chrysogenum*. *Biotechnol. Bioeng.* 2001, *72*, 185-193.
11. Lein, J., The Panlabs penicillin strain improvement program. *Biotechnol Ser* 1986.
12. Posch, A.E., Spadiut, O., Herwig, C., A novel method for fast and statistically verified morphological characterization of filamentous fungi. *Fungal. Genet. Biol.* 2012, *49*, 499-510.
13. Sagmeister, P., Wechselberger, P., Herwig, C., Information Processing: Rate-Based Investigation of Cell Physiological Changes along Design Space Development. *PDA J. Pharm. Sci. Technol.* 2012, *66*, 526-41.
14. Ehgartner, D., Fricke, J., Schroder, A., Herwig, C., At-line determining spore germination of *Penicillium chrysogenum* bioprocesses in complex media. *Appl. Microbiol. Biotechnol.* 2016, *100*, 8923-30.
15. Posch, A.E., Spadiut, O., Herwig, C., Switching industrial production processes from complex to defined media: method development and case study using the example of *Penicillium chrysogenum*. *Microb. Cell Fact.* 2012, *11*, 88-101.
16. Jorgensen, H., Nielsen, J., Villadsen, J., Mollgaard, H., Analysis of penicillin V biosynthesis during fed-batch cultivations with a high-yielding strain of *Penicillium chrysogenum*. *Appl. Microbiol. Biotechnol.* 1995, *43*, 123-30.
17. Chain, E.B., Gualandi, G., Morisi, G., Aeration studies. IV. Aeration conditions in 3000-liter submerged fermentations with various microorganisms. *Biotechnol. Bioeng.* 1966, *8*, 595-619.

18. Petersen, N., Stocks, S., Gernaey, K.V., Multivariate models for prediction of rheological characteristics of filamentous fermentation broth from the size distribution. *Biotechnol. Bioeng.* 2008, *100*, 61-71.
19. Riley, G.L., Tucker, K.G., Paul, G.C., Thomas, C.R., Effect of biomass concentration and mycelial morphology on fermentation broth rheology. *Biotechnol. Bioeng.* 2000, *68*, 160-72.
20. Znidarsic, P., Pavko, A., The morphology of filamentous fungi in submerged cultivations as a bioprocess parameter. *Food Technol. Biotechnol.* 2001, *39*, 237-252.
21. Gravius, B., Bezmalinovic, T., Hranueli, D., Cullum, J., Genetic instability and strain degeneration in *Streptomyces rimosus*. *Appl. Environ. Microbiol.* 1993, *59*, 2220-8.
22. Nasution, U., van Gulik, W.M., Ras, C., Proell, A., et al., A metabolome study of the steady-state relation between central metabolism, amino acid biosynthesis and penicillin production in *Penicillium chrysogenum*. *Metab. Eng.* 2008, *10*, 10-23.
23. Hult, K., Gatenbeck, S., Production of NADPH in the mannitol cycle and its relation to polyketide formation in *Alternaria alternata*. *Eur. J. Biochem.* 1978, *88*, 607-12.
24. Witteveen, C.F., Visser, J., Polyol pools in *Aspergillus niger*. *FEMS Microbiol. Lett.* 1995, *134*, 57-62.

**Supplementary material**

**Production rate dynamics at constant growth conditions in a penicillin production process**

Daniela Ehgartner<sup>1,2</sup>, Thomas Hartmann<sup>1,2</sup>, Sarah Heinzl<sup>1,2</sup>, Christoph Herwig<sup>1,2</sup> and Jens Fricke<sup>\*,1,2</sup>

\*to whom the correspondence should be addressed to

<sup>1</sup> CD Laboratory on Mechanistic and Physiological Methods for Improved Bioprocesses, TU Wien, Vienna, Austria

<sup>2</sup> Research Area Biochemical Engineering, Institute for Chemical, Environmental and Biological Engineering, TU Wien, Vienna, Austria

Corresponding author:

jens.fricke@tuwien.ac.at

Tel (Office): +43 1 58801 166462

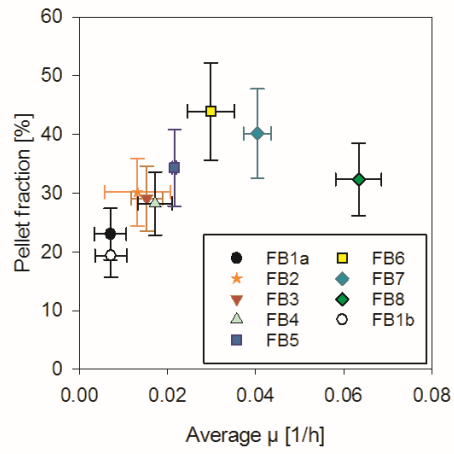


Figure S1: The average specific growth rate influencing morphology at the start of phase 2 – average  $\mu$  vs. pellet fraction

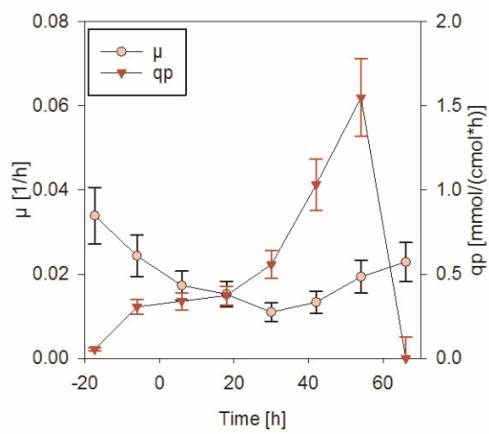


Figure S2:  $q_p$  and  $\mu$  over time in FB3. Time point 0 reflects the start of  $\mu$ -control.

### 3 Conclusions & future perspectives

Penicillin production is a complex process with changing morphology, viability and physiology. One parameter shown to directly influence the specific penicillin production rate is the specific growth rate. Dependent on the contributed study, this link between  $\mu$  and  $q_p$  varied [1-6]. Thus, the knowledge about  $\mu$ - $q_p$ -interlinks in combination with tools for process analytic and control could be the key for the optimization of the penicillin producing process.

The here presented thesis aimed to develop an analytical and process-technological toolbox and to apply these tools for the description of  $\mu$ - $q_p$ -interlinks in processes with dynamic  $q_p$ -trajectories, providing the basis for robust bioprocesses with optimized penicillin production.

Five different tools were developed and assigned to three fields of function. In the following, the methodologies are shortly summarized and interlinks to their applicability given. In addition, their importance, concerning the description of  $\mu$ - $q_p$ -interlinks and the provision of robust bioprocesses with optimized penicillin production, is underlined.

#### 1) Spore-tools

Two methods approaching the so-called spore quality were developed (tool I and tool II). In processes with either of scientific (investigation of interlinks of variables in fed-batch) or industrial (robust process with optimizing penicillin production) goals, a common starting point for the fed-batch phase is important. This issue is served with reproducible and robust cultivations, beginning with a common starting point of all batches.

The here presented tools showed to be faster and easier alternatives to the CFU determination. In the flow cell of the flow cytometer metabolically active cells are distinguished from other cell populations via fluorescence measurement. Furthermore, the morphology of the spore is detected, whereby round spores can be differentiated from germinated spores (see Figure 3.1).

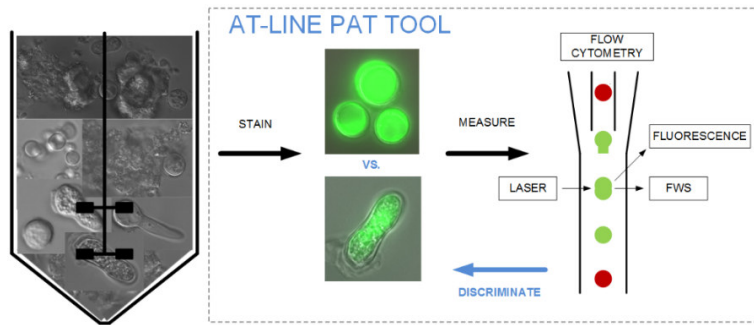


Figure 3.1: Scheme of tool I and tool II measuring metabolically active spore concentration and spore germination by combining viability staining and flow cytometry.

I propose a combination of tool I (measurement of metabolically active spores) and tool II (measurement of spore germination) for the determination of viable spore concentration in combination with bioreactor cultivations. Three different approaches are possible, which is shown in Figure 3.2. One possibility would be a 30 h shake flask culture where spore germination of metabolically active spores is measured and thereby the viable spore concentration determined. The bioreactor is then inoculated with the volume of the spore inoculum needed due to the viable spore concentration measurements.

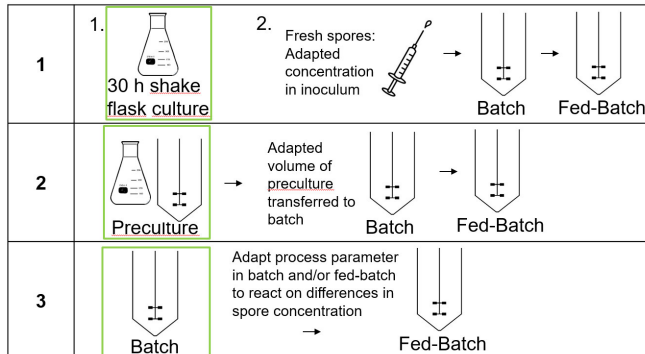


Figure 3.2: Proposed applications of tool I and tool II.

In the cultivations presented in this thesis (manuscripts 4-6), the fed-batch was in focus. In such experiments, tool I and tool II are of minor yet important application. The potential of these is surely bigger and could further be exploited in investigations of the batch phase like the influence of changing media components, strain development et cetera.

## 2) Measuring morphology using a large particle flow cytometer

Tool III and tool IV, using flow cytometry, are faster alternatives to our former state-of-the-art method, the morphological analysis via image analysis based on microscopy [7]. While tool IV applies

the same image analysis as the microscopy method does, tool V aims to use the same concept of morphology but shows another approach for accessing morphological parameters. A comparable information content to the state-of-the-art method was gained and supplemental morphological parameters for the description of the pellet core were found. In addition, both flow cytometry methods are faster, at-line applicable and allow higher throughput than image analysis via microscopy. Transferability to other processes is given for all three morphological analysis methods.

In the here presented studies (manuscripts 5-6), morphology was not applied as key factor. If anything, there where physiological variables in the focus of investigation like the specific growth rate and the penicillin productivity. Nevertheless, the morphology is an important variable with complex interactions to the filamentous bioprocess, and thus important to bear in mind. Therefore, morphology of all fed-batch samples in the here presented studies was analyzed. As manuscripts 5 and 6 show, morphological parameters are often in focus for the description of phenomena like the change of biomass-permittivity-correlation or the begin of declining  $q_p$ . Concerning the interaction of  $\mu$  and  $q_p$ , morphology was investigated as well (data not shown) but without finding significant connections. A higher number of fed-batches than presented in manuscript 6 would be necessary to better investigate parameters as complex as morphological ones. In addition,  $\mu$ -profiles instead of one constant  $\mu$  per fed-batch could be interesting, and better exclude the effect of time on the morphology.

Although no significant link between morphology and  $q_p$  was found, it could be an important factor in future applications. From an industrial point of view, the optimal process is the one, where product titer and cost are in best relation. This means consideration of a high time-space-yield without reaching too high biomass concentrations (e.g. via high specific growth rates). The latter leads to high viscosities and hence impaired mass transfer as well as higher power input for stirring [8-10]. Further, the average  $\mu$  during fed-batch influences the percentage of pellets (counterpart to dispersed hyphae and aggregates) as it is shown in manuscript 6. Higher relative pellet concentrations promise a better mass and heat transfer as well as lower power input levels for stirring [11].

### **3) Online control of fungal growth**

Process control is of utter importance – in industry as well as in process development. The control of the specific growth rate was crucial for the study presented in manuscript 6, as the interlink of  $\mu$  and  $q_p$  was investigated. Tool V presented in manuscript 5 is a  $\mu$ -control method based on online viable

biomass estimation via permittivity measurements, which in addition is capable of adapting to changing biomass-permittivity-relations and to varying biomass yield. It is a  $\mu$ -control strategy fully running online without needing interference of the operator. Therefore, it is of great advantage to its prototype method applied for  $\mu$ -control in the study shown in manuscript 6. The methods are based on the same approach, but the former application needed regular sampling and at-line analysis of viable biomass to adjust the biomass-permittivity-correlation and to adapt the biomass yield. An advantage of the at-line method applied in manuscript 6 is the direct transferability to new processes/strains. However, the online method (tool V) only needs few prior cultivations for model building before it is applicable on a new process/strain.

Online  $\mu$ -control is a crucial method when bioreactor cultivations aiming optimized penicillin productivity ought to be conducted. Based on the findings presented in manuscript 6, the specific growth rate is one of the key parameters in such processes. Hence, an online  $\mu$ -control for the conductions of the optimal  $\mu$ -profile in the fed-batch is of utter importance for a robust bioprocess with optimized productivity.

An overview of the toolbox' application during the penicillin producing process is presented in Figure 3.3. Spore inoculum quality (tool I) and spore germination measurements (tool II) for the determination of viable spore concentration can be applied at the begin of the batch to adjust inoculated spore suspension volume. The inoculation of every single cultivation presented in this thesis was based on beforehand conducted spore viability measurements and the tools were already transferred for application in industrial environment, underlining the importance of these tools for reproducible and robust processes.

After the end of batch phase, the fed-batch starts with the inoculation of batch broth into the fed-batch medium and the begin of glucose feed. At this point of the process, hyphal aggregates are already found in the bioreactor. Development of these hyphal aggregates and the formation of pellets is one important link between spore inoculum concentration and the fed-batch [12-14], hence linking tools I-IV. Morphological investigation of the fungi and further analytics to investigate physiology were conducted for each biomass sample to investigate  $\mu$ - $q_p$ -relations as well as physiological and morphological changes connected to the  $q_p$ -trajectory.

For the experiments described in manuscript 6, viable biomass was online estimated and  $\mu$  was controlled via adjustment of the feed (tool V). Tool V showed to be a robust method, independent of

changing process parameters and variables like spore inoculum concentration and fungal morphology (see manuscript 5).

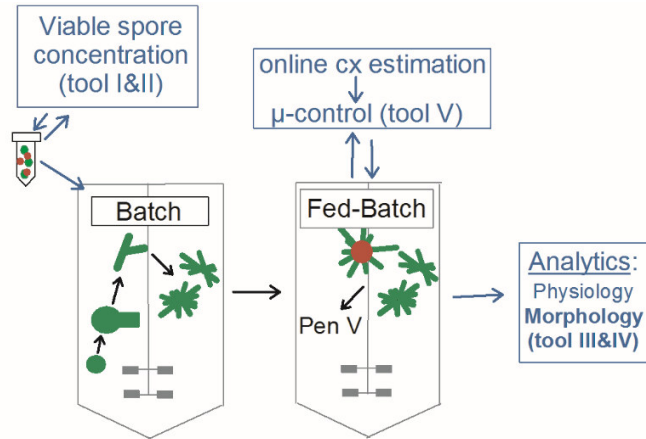


Figure 3.3: Application of the tools in the bioprocess. Description of spore sub-populations and viable spore concentration determination are conducted at/before the start of the batch to adjust spore inoculum volume (tool I&II). Morphology is analyzed during fed-batch using two different methodologies (tool III&IV). The specific growth rate is controlled by adjusting the glucose feed based on online viable biomass measurements (tool V) to enable a constant  $\mu$  at set levels.

The application of the here presented tools (manuscripts 1-5) illustrated in Figure 3.3 in combination with the description of the  $\mu$ - $q_p$ -relation, the  $q_p$ -trajectories and further important variables like consumed glucose in manuscript 6, allowed the achievement of the goal of this thesis: *Development of an analytical and process-technological toolbox and its application for the description of  $\mu$ - $q_p$ -interlinks in processes with dynamic  $q_p$ -trajectories to provide the basis for robust bioprocesses with optimized penicillin production.*

In combination with the achievement of the goal, the hypothesis was verified: *The application of an analytical and process-technological toolbox enables the description of  $\mu$ - $q_p$ -trajectories and thus provides the basis for robust bioprocesses with optimized penicillin production.*

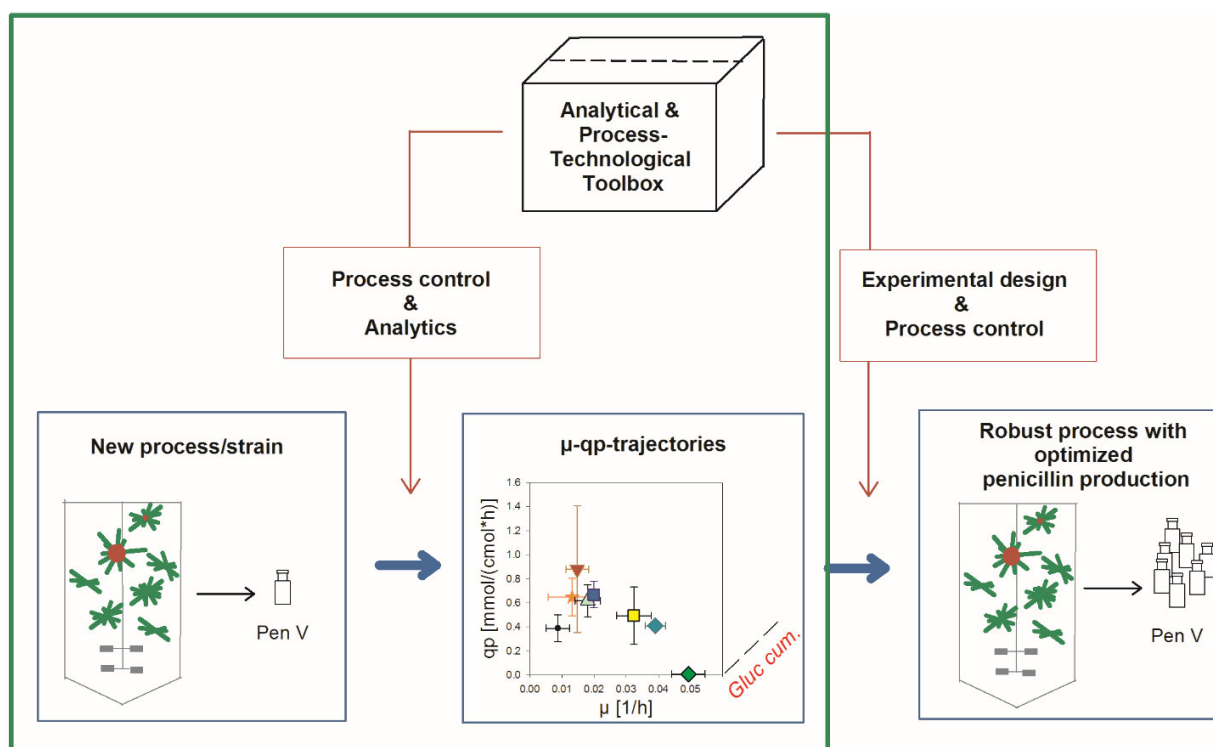


Figure 3.4: Overview of the applications of the analytical and process-technological toolbox for the descriptions of  $\mu$ - $q_p$ -trajectories. The green box highlights the contribution of the here presented thesis. It provides the basis for further usage of this knowledge in combination with the toolbox towards robust processes with optimized penicillin production.

Goal achievement and verification of the hypothesis are illustrated in Figure 3.4. The green box highlights the frame of this thesis: For a *Penicillium chrysogenum* strain,  $\mu$ - $q_p$ -relations were investigated and further variables influencing  $q_p$ -trajectories identified. The application of viable spore concentration measurements, morphological investigations and  $\mu$ -control in manuscript 6 underlined the importance of the newly developed analytical and process-technological toolbox.

These findings in combination with the toolbox provide the basis for further studies towards robust bioprocesses with optimized penicillin production. Knowledge about optimal specific growth rate levels can be used to develop an experimental design including  $\mu$ -profiles for optimal production (concerning titer and costs). Approaching different  $\mu$ -levels ought to be advantageous to a constant  $\mu$  all over the fed-batch. Like for example starting with a specific growth rate of  $0.02 \text{ h}^{-1}$  to faster reach a higher  $q_p$  (consumed glucose is the important factor in approaching  $q_p$ -maximum – the more glucose is consumed, the closer the  $q_p$ -maximum is). In a next step,  $\mu$  could be decreased to  $0.012 \text{ h}^{-1}$  in order to achieve higher  $q_p$ , elongate the period of production until  $q_p$  declines and to avoid too high biomass concentrations.

## References

1. Douma, R.D., Verheijen, P.J., de Laat, W.T., Heijnen, J.J., et al., Dynamic gene expression regulation model for growth and penicillin production in *Penicillium chrysogenum*. *Biotechnol Bioeng* 2010, 106, 608-18.
2. Kluge, M., Siegmund, D., Diekmann, H., Thoma, M., A model for penicillin production with and without temperature shift after the growth phase. *Appl Microbiol Biotechnol* 1992, 36, 446-51.
3. Pirt, S.J., Righelato, R.C., Effect of Growth Rate on the Synthesis of Penicillin by *Penicillium chrysogenum* in Batch and Chemostat Cultures. *Appl Microbiol* 1967, 15, 1284-90.
4. Ryu, D.D.Y., Hospodka, J., Quantitative Physiology of *Penicillium chrysogenum* in Penicillin Fermentation. *Biotechnol Bioeng* 1980, 22, 289-298.
5. van Gulik, W.M., de Laat, W.T., Vinke, J.L., Heijnen, J.J., Application of metabolic flux analysis for the identification of metabolic bottlenecks in the biosynthesis of penicillin-G. *Biotechnol Bioeng* 2000, 68, 602-18.
6. Wittler, R., Schügerl, K., Interrelation between penicillin productivity and growth rate. *Appl Microbiol Biotechnol* 1985, 21, 348-355.
7. Posch, A.E., Spadiut, O., Herwig, C., A novel method for fast and statistically verified morphological characterization of filamentous fungi. *Fungal Genet Biol* 2012, 49, 499-510.
8. Chain, E.B., Gualandi, G., Morisi, G., Aeration studies. IV. Aeration conditions in 3000-liter submerged fermentations with various microorganisms. *Biotechnology and Bioengineering* 1966, 8, 595-619.
9. Petersen, N., Stocks, S., Gernaey, K.V., Multivariate models for prediction of rheological characteristics of filamentous fermentation broth from the size distribution. *Biotechnol Bioeng* 2008, 100, 61-71.
10. Riley, G.L., Tucker, K.G., Paul, G.C., Thomas, C.R., Effect of biomass concentration and mycelial morphology on fermentation broth rheology. *Biotechnol Bioeng* 2000, 68, 160-72.
11. Znidarsic, P., Pavko, A., The morphology of filamentous fungi in submerged cultivations as a bioprocess parameter. *Food Technology and Biotechnology* 2001, 39, 237-252.
12. Posch, A.E., Herwig, C., Physiological description of multivariate interdependencies between process parameters, morphology and physiology during fed-batch penicillin production. *Biotechnol Prog* 2014, 30, 689-99.
13. Posch, A.E., Koch, C., Helmelt, M., Marchetti-Deschmann, M., et al., Combining light microscopy, dielectric spectroscopy, MALDI intact cell mass spectrometry, FTIR spectromicroscopy and multivariate data mining for morphological and physiological bioprocess characterization of filamentous organisms. *Fungal Genet Biol* 2013, 51, 1-11.
14. Tucker, K.G., Thomas, C.R., Inoculum effects on fungal morphology: Shake flasks vs agitated bioreactors. *Biotechnology techniques* 1994, 8, 153-156.